HYPERTHERMOPHILIC HYDROGEN PRODUCTION FROM CATTLE MANURE BY TWO-STAGE DARK FERMENTATION AND MICROBIAL ELECTROLYSIS CELL

A THESIS SUBMITTED TO
THE GRADUATE SCHOOL OF NATURAL AND APPLIED SCIENCES
OF
MIDDLE EAST TECHNICAL UNIVERSITY

BY

BERİVAN TUNCA

IN PARTIAL FULFILLMENT OF THE REQUIREMENTS
FOR
THE DEGREE OF MASTER OF SCIENCE
IN
ENVIRONMENTAL ENGINEERING

AUGUST 2023

Approval of the thesis:

HYPERTHERMOPHILIC HYDROGEN PRODUCTION FROM CATTLE MANURE BY TWO-STAGE DARK FERMENTATION AND MICROBIAL ELECTROLYSIS CELL

submitted by **BERİVAN TUNCA** in partial fulfillment of the requirements for the degree of **Master of Science** i**n Environmental Engineering, Middle East Technical University** by,

Prof. Dr. Halil Kalıpçılar
Dean, Graduate School of **Natural and Applied Sciences**   _____

Prof. Dr. Bülent İçgen
Head of the Department, **Environmental Engineering**   _____

Assoc. Prof. Dr. Yasemin Dilşad Yılmazel Tokel
Supervisor, **Environmental Engineering, METU**   _____

Examining Committee Members:

Prof. Dr. Tuba Hande Bayramoğlu
Environmental Engineering, METU   _____

Assoc. Prof. Dr. Yasemin Dilşad Yılmazel Tokel
Environmental Engineering, METU   _____

Assoc. Prof. Dr. Harun Koku
Chemical Engineering, METU   _____

Assoc. Prof. Dr. Eda Çelik Akdur
Chemical Engineering, Hacettepe University   _____

Assist. Prof. Dr. Hale Demirtepe
Environmental Engineering, İzmir Institute of Technology   _____

Date: 24.08.2023

I hereby declare that all information in this document has been obtained and presented in accordance with academic rules and ethical conduct. I also declare that, as required by these rules and conduct, I have fully cited and referenced all material and results that are not original to this work.

Name Last name : Berivan Tunca

Signature :

ABSTRACT

HYPERTHERMOPHILIC HYDROGEN PRODUCTION FROM CATTLE MANURE BY TWO-STAGE DARK FERMENTATION AND MICROBIAL ELECTROLYSIS CELL

Tunca, Berivan
Master of Science, Environmental Engineering
Supervisor: Assoc. Prof. Dr. Yasemin Dilşad Yılmazel Tokel

August 2023, 152 pages

The objective of this study is to implement an efficient two-stage DF and MEC system operation to produce hydrogen from unpretreated cattle manure (UCM) at hyperthermophilic temperatures. In the first part of this thesis, the DF of UCM at high loadings (up to 50 g volatile solids (VS)/L) by hyperthermophilic cellulolytic bacterium *Caldicellulosiruptor bescii* was studied in batch reactors operated at 75 ºC. To increase the yield and the rate of H_2 production, the impact of intermittent gas sparging and adaptation of inoculum were investigated. The results revealed that adaptation strategy has a superior effect on biohydrogen production. The highest hydrogen yield was achieved with the adapted culture as 161.3 mL H_2/g VS_{added} at 15 g VS/L UCM and the maximum hydrogen production rate was 7.77 mL H_2/mL/h at 25 g VS/L of UCM.

In the second part of the thesis, bioelectrochemical hydrogen production from fermentation effluent, rich in acetate, was studied in MEC at 80 ºC using hyperthermophilic electro-active archaea. The experimental work included the selection of inoculum for hyperthermophilic MECs and electrode material for biofilm formation. Further, the utilization of DF effluent in single chamber MECs were studied to enhance the hydrogen production by *Geoglobus acetivorans* and finally adaptation strategy similar to the first part was used for performance

enhancement. Hydrogen production rate (0.52 ± 0.07 m^3 H$_2$/m^{3}d) was successfully increased by 11.5 times via the use of adapted culture compared to the acetate-grown wild type culture (and 0.05 ± 0.02 m^3 H$_2$/m^{3}d). A variety of biofilm imaging analyses such as confocal laser scanning and scanning electron microscopy were conducted to study the viability of the adapted culture biofilm. This study demonstrates the promising potential of a two-stage hyperthermophilic DF and MEC process for hydrogen production from UCM, achieving a significant hydrogen yield of 506.8 mL H$_2$/g VS$_{added}$.

Keywords: Dark fermentation (DF), microbial electrolysis cell (MEC), culture adaptation, biohydrogen production, lignocellulosic biomass

ÖZ

İKİ AŞAMALI KARANLIK FERMANTASYON VE MİKROBİYAL ELEKTROLİZ HÜCRESİ İLE SIĞIR GÜBRESİNDEN HİPERTERMOFİLİK HİDROJEN ÜRETİMİ

Tunca, Berivan
Yüksek Lisans, Çevre Mühendisliği
Tez Yöneticisi: Doç. Dr. Yasemin Dilşad Yılmazel Tokel

Ağustos 2023, 152 sayfa

Bu çalışmanın amacı, hipertermofilik sıcaklıklarda ön işlem görmemiş sığır gübresinden (İSG) hidrojen (H_2) gazı üretmek için verimli bir iki aşamalı KF ve MEH sistemi geliştirmektir. Bu tezin ilk bölümünde, İSG'nin karanlık fermantasyonu hipertermofilik selülolitik *Caldicellulosiruptor bescii* bakterisi ile yüksek organik yüklerde (50 g uçucu katı madde (UKM)/L'ye kadar), 75 ºC'de çalıştırılan kesikli reaktörler işletilerek incelenmiştir. H_2 üretim verimi ve hızını artırmak için, aralıklı gaz serpmenin etkisi ve inokulumun adaptasyonu araştırılmıştır. Sonuçlar, adaptasyon stratejisinin biyohidrojen üretimi üzerinde üstün bir etkiye sahip olduğunu ortaya koymuştur. En yüksek hidrojen verimi, 15 g UKM/L İSG konsantrasyonunda 161,3 mL H_2/g $UKM_{eklenen}$ olarak adapte edilen kültürden elde edilmiştir ve maksimum hidrojen üretim hızı, 25 g UKM/L İSG ile edilen 7,77 mL H_2/mL/saat olarak kaydedilmiştir.

Tezin ikinci bölümünde, asetat açısından zengin fermantasyon çıkış suyundan biyoelektrokimyasal hidrojen üretimi, hipertermofilik elektro-aktif arke kullanılarak MEH'de 80 ºC'de incelenmiştir. Deneysel çalışma hipertermofilik MEH'ler için inokulum ve biyofilm oluşumu için elektrot malzemesi seçimi ile başlamıştır. *Geoglobus acetivorans* tarafından hidrojen üretimini arttırmak için tek odacıklı

MEH'lerde KF çıkış suyunun kullanımı incelenmiş ve son olarak performansın arttırılması için tezin ilk kısmına benzer şekilde adaptasyon stratejisi kullanılmıştır. Hidrojen üretim hızı ($0,52 \pm 0,07$ m^3 H$_2$/m^{3}gün), asetatla yetiştirilen kültüre (ve $0,05 \pm 0,02$ m^3 H$_2$/m^{3}gün) kıyasla adapte edilmiş kültür kullanılarak başarıyla 11,5 kat artırılmıştır. Adapte olan biyofilm konfokal lazer taramalı ve taramalı elektron mikroskobu gibi farklı görüntüleme analizleri ile incelenmiştir. Bu çalışmada elde edilen 506,8 mL H$_2$/g UKM$_{eklenen}$ H$_2$ verimi önemli derecede yüksek olup, İSG'den hidrojen üretimi için iki aşamalı hipertermofilik KF ve MEH operasyonunun umut vadeden potansiyelini göstermektedir.

Anahtar Kelimeler: Karanlık fermantasyon (KF), mikrobiyal elektroliz hücresi (MEH), kültür adaptasyonu, biyohidrojen üretimi, lignoselülozik biyokütle

To my family and my beloved

ACKNOWLEDGMENTS

TABLE OF CONTENTS

LIST OF TABLES

LIST OF FIGURES

FIGURES

xix

xx

LIST OF ABBREVIATIONS

ABBREVIATIONS

ADP	Adenosine diphosphate
AEM	Anion exchange membrane
ARB	Anode respiring bacteria
ATP	Adenosine triphosphate
BES	Bioelectrochemical system
CCR	Carbon catabolite repression
CEM	Cation exchange membrane
COD	Chemical oxygen demand
CV	Cyclic voltammetry
DET	Direct electron transfer
DF	Dark fermentation
EAB	Electrochemically active (electro-active) bacteria
EET	Extracellular electron transfer
HER	Hydrogen evolution reaction
MEC	Microbial electrolysis cell
MES	Microbial electrosynthesis
MET	Mediated electron transfer
MFC	Microbial fuel cell
NADH	Nicotinamide adenine dinucleotide
PEM	Proton exchange membrane
PFL	Pyruvate-formate-lyase
SS	Stainless steel
TS	Total solid
UCM	Unpretreated cattle manure
VFA	Volatile fatty acid
VS	Volatile solid
WW	Wastewater

CHAPTER 1

INTRODUCTION

1.1   Background information

The global population and economic development increase has put a tremendous demand on energy supply. By the year 2030, the increase in energy demand is expected to rise by 50%, which has set limits on fuel sources and become unable to meet the demand in the industrial and public markets (IEA, 2022). Over the years, the dependency on fossil fuels to meet the energy demand has led to the overuse of non-renewable resources, resulting in adverse environmental effects and climate change. Therefore, the danger of relying solely upon fossil fuels has promoted the search for alternatives that can eventually replace fossil fuels and meet rising energy demands. Renewable energy sources have been promising alternatives to restrain carbon emissions and greenhouse gases released due to the use of fossil fuels. Traditional renewable energy sources include solar, wind, hydropower, and geothermal energy. However, the alternatives are not limited to these traditional sources; biofuel production from waste materials has gained attention over the years and has become a promising alternative energy source (Saha et al., 2022).

Biofuels can be defined as fuels derived from biomass, which represent clean, biodegradable, sustainable, renewable and cost-efficient energy sources. Among different biofuels, hydrogen (H_2) has been promoted as a future energy carrier because of its emission-free nature and high energy content. Hydrogen can be generated from both renewable and non-renewable sources (Boodhun et al., 2017). At present, global hydrogen generation is dependent on the technologies using non-renewable sources such as steam reforming of natural gas, catalytic decomposition, and partial oxidation of heavy hydrocarbons (Megia et al., 2021). These methods are associated with environmental pollution, and they have an energy-intensive nature.

As a result, hydrogen production from renewable energy sources, including biomass, via biological production processes become strong alternatives to traditional hydrogen generation methods (Łukajtis et al., 2018). The biological hydrogen production can take place through four different technologies as photo-fermentation, dark fermentation (DF), biophotolysis and microbial electrolysis cell (MEC) (H. S. Lee et al., 2010). Among these technologies, DF has high hydrogen production rates and applicable to various feedstocks including organic wastes such as food waste, agricultural residues and animal manure and do not require complicated reactor designs (Łukajtis et al., 2018). Yet, the main drawback of DF is the low hydrogen production yield since theoretical maximum hydrogen yield from glucose is only 4 mol H_2 per 1 mol of glucose (Thauer et al., 1977). This implies that the use of complex substrates can be resulted in even lower yields. The main reason for this situation is the formation of by-products, mainly volatile fatty acids (VFAs) such as acetate, or incomplete substrate degradation. To overcome lower hydrogen yields, different alternatives such as two-stage systems including DF linked to photo fermentation, anaerobic digestion or microbial electrolysis cells (MECs) have been studied (Sekoai et al., 2018). VFAs as by-products of DF can be used as a feedstock in MECs to produce hydrogen at higher yields (Bakonyi et al., 2018). It has been reported that the theoretical maximum yield of 12 mol H_2 per mol of glucose and 4 mol of H_2 per mol of acetate is possible when 100% conversion of electrons equivalents are used for hydrogen production in MECs (Bakonyi et al., 2018). The highest productivities have been shown in MECs when acetate was used as a substrate (Muddasar et al., 2022). Since acetate is the major by-product in DF operation of some feedstocks, coupling DF and MEC systems is a promising strategy to enhance hydrogen production yield from complex substrates.

MEC is a novel bioelectrochemical reactor type that is used to produce hydrogen from renewable biomass and wastewaters in a process known as electrohydrogenesis (Saravanan et al., 2020). The basic working principle of MECs depends on the activities of electro-active microorganisms colonized on the anode that can perform extracellular electron transfer to a solid electrode enabling the current production,

which leads to the hydrogen evolution reaction on the cathode with some external voltage applied (Kadier et al., 2014). The exoelectrogens play the key role in the hydrogen production via MEC; therefore, the choice of inoculum is a significant factor to increase hydrogen generation (Kadier et al., 2016). Exoelectrogenic microorganisms have been found in various environments, and includes both bacteria and archaea. Most of the identified exoelectrogens have been isolated at mesophilic temperatures (25-35°C) since MECs were generally operated at mesophilic temperatures (Logan et al., 2019). However, there are also a few exoelectrogenic microbes that originate from extreme environments such as high temperatures (Sekar et al., 2017; Yilmazel et al., 2018), high salinity (Carmona-Martínez et al., 2013), or extreme pH environment (Badalamenti et al., 2013; Malki et al., 2008).

Using non-sterile feedstocks without any pretreatment is a necessity to commercialize the biohydrogen production (Gilroyed et al., 2008; Hussy et al., 2005). DF can be performed at either moderate (25-50 °C) or elevated temperatures (≥ 50 °C) at which the hydrogen productivity is higher (Ljunggren et al., 2011). Along with that, DF operation at elevated temperatures offers several advantages, such as (i) waste stabilization, (ii) higher solubilization of feedstock, and (iii) lower risk of contamination by hydrogen consuming microorganisms (Dessì et al., 2018; Yilmazel & Duran, 2021). In addition, the effluent of high temperature DF consists of high amount of acetate. Hyperthermophilic MECs can play a significant role as a post-treatment of high-temperature DF effluent which can be utilized by exoelectrogens as a feedstock for hydrogen production. There are only a few studies using MEC as a secondary stage after a thermophilic DF operation (Khongkliang et al., 2017, 2019a), using the effluent after DF of starch processing wastewater and palm oil mill wastewater. Khongkliang et al. (2019) resulted in a significant increase in hydrogen production yield (3 times) and offered a better waste removal strategy (4 times increase in COD removal) using two-stage DF and MEC process compared to only DF operation. Kas and Yilmazel (2022) showed for the first time the applicability of a stable current production along with hydrogen generation using DF

effluent at hyperthermophilic temperatures. However, the hydrogen production rate and current generation is decreased in the previous work by Kas and Yilmazel (2022) when the feed was switched to DF effluent. It was suggested that there is a need for an acclimation process for MEC inoculum to use DF effluent effectively (Kas & Yilmazel, 2022).

The adaptation of inoculum can be a powerful technique to develop phenotypic traits of interest in industrial microbial strains (Dragosits & Mattanovich, 2013). There are several methods to adapt microbial communities to different feedstocks. Most common adaptation procedure is that microorganisms are subjected to a specific stress to enhance the necessary mutations that will improve fitness (Dragosits & Mattanovich, 2013). Although this is a promising strategy, little to no research has been conducted to examine the possible enhancement in hydrogen production via two-stage hyperthermophilic operation by adapting hyperthermophilic pure cultures to complex feedstocks (Sandberg et al., 2019).

1.2 Aim of the study

The aim of this thesis is to enhance the biohydrogen production from unpretreated cattle manure (UCM) using a two-stage hyperthermophilic DF and MEC operation. For this purpose, different strategies were investigated to increase the performance of DF and MEC processes. Cattle manure was selected as a substrate for DF since it is rich in organic content and its generation has significantly increased because of high demand to agricultural activities, yet, improper manure management results in various environmental problems.

The experimental study was divided into two major parts as (i) enhancement of fermentative hydrogen production and (ii) use of DF effluent as a feedstock for bioelectrochemical hydrogen production. In the first part of this thesis, the efforts were focused on the industrially relevant use of hyperthermophilic cellulolytic bacterium *Caldicellulosiruptor bescii* for biohydrogen production from cattle

manure without any pretreatment. To this purpose, non-sterile UCM (15-50 g VS/L) was fed to the biohydrogen production reactors maintained at 75 °C. Further, two different strategies, namely intermittent gas sparging and adaptation of inoculum to substrate, were used to enhance the performance of fermentative biohydrogen production. In the second part, the efforts were focused on the use of DF effluent in MECs to further increase in hydrogen production during hyperthermophilic operation. In the second part of the thesis, experiments were designed to select the most suitable inoculum, the electrode material and to investigate the adaptability of inoculum to DF effluent (Figure 1.1).
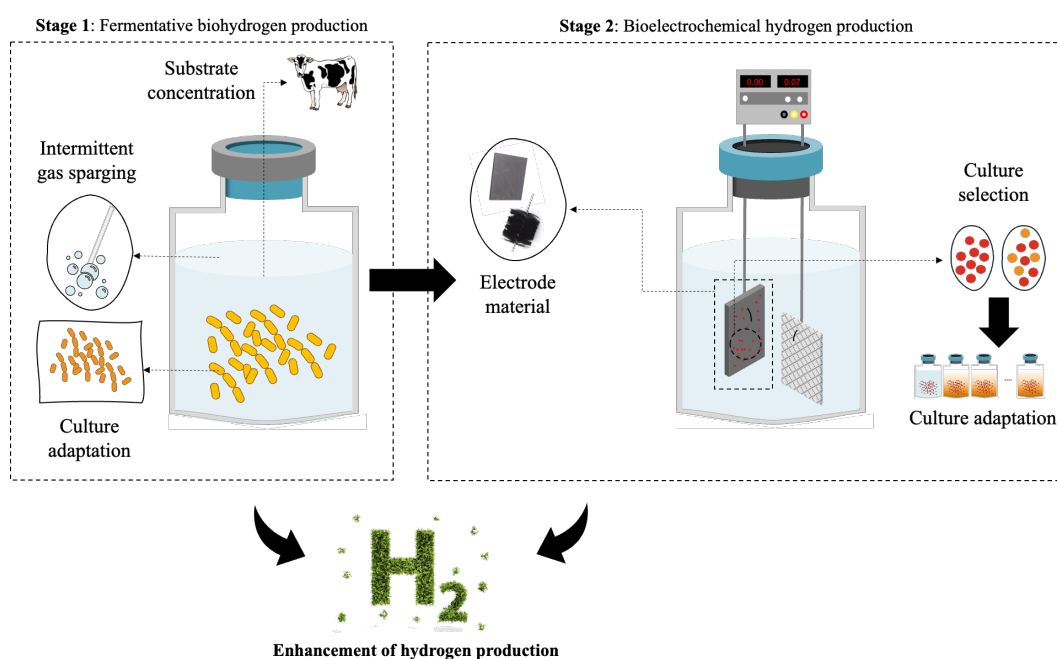
Figure 1.1 Aim of the study

1.3   Scope of the study

This thesis consists of two parts (total of 8 sets) in which the first part included five experimental sets and the second part included three experimental sets. First part regards the DF operation and the second part is on MECs.

DF operation

In the first set, the degradability of unpretreated cattle manure by *C. bescii* was assessed in batch DF reactors. In Set 2, 3 and 4, biohydrogen production potential at higher concentrations of cattle manure was investigated via different enhancement strategies. Set 5 was conducted for further assessment of the impact of culture adaptation on fermentative biohydrogen production by conducting carbon balance.

MEC operation

In the first set, hyperthermophilic pure culture and enriched co-cultures were examined to select the inoculum used in Mini-MECs with an active volume of 5 mL. The selected culture was used as an inoculum for Set 2 of the second part where the utilization DF effluent in single chamber MEC (active volume of 65 mL) was investigated. In the last set of the part 2, two-chamber MEC operation, *i.e.,* separated by a membrane, was conducted to gain better knowledge on the utilization of DF effluent in MEC system.

CHAPTER 2

LITERATURE REVIEW

2.1   Biohydrogen production

Hydrogen (H_2) is presented as the most suitable renewable energy source for future that can replace fossil fuel-based energy. It has a high calorific value (142 kJ/g) and high energy yield as 122 kJ/g, which is about 3 times higher than any hydrocarbon fuels (Łukajtis et al., 2018). Further, hydrogen is the cleanest energy carrier since its combustion only produces water vapor as a by-product and does not emit any greenhouse gases to the atmosphere (Łukajtis et al., 2018).

Hydrogen is an important industrial material which is widely used for different purposes such as petrochemical production, oil and fat hydrogenation, fertilizer production, metallurgical applications, and manufacturing processes for electronic and aerospace industry (Amin et al., 2023). The current global demand of hydrogen is about 70 million tons per year which will exceed 200 million tons in the next decade (Osman et al., 2022). However, significant portion of current hydrogen demand (96%) is supplied by using fossil fuel-based hydrogen generation technologies which produce significant carbon emissions. Only 4% of this demand is provided via water electrolysis; however, it is significantly energy intensive process associated with its high cost (Łukajtis et al., 2018). Biohydrogen is one of the most promising low-carbon alternative fuel, which is produced from renewable and sustainable biomass and environmentally friendly processes. Biological hydrogen generation processes can be divided into four main categories: biophotolysis, photo-fermentation, dark fermentation and bioelectrochemical hydrogen production (Figure 2.1).
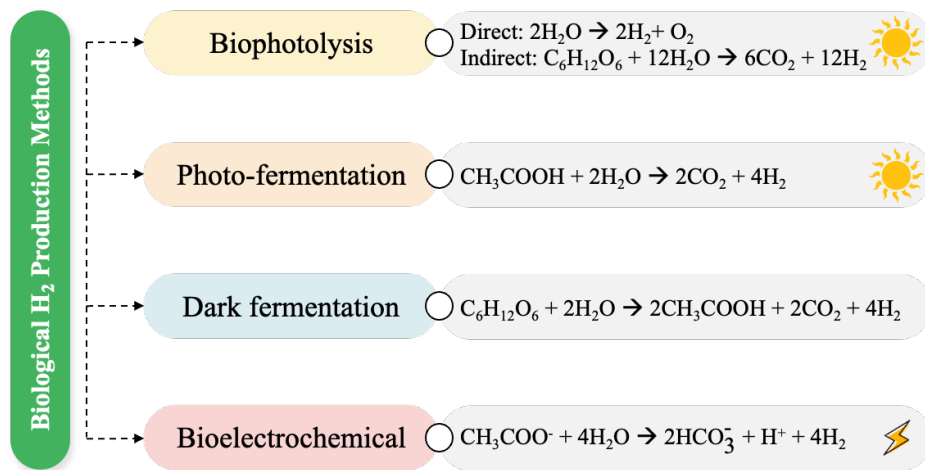
Figure 2.1 Biological hydrogen production processes (Adopted from Osman et al., 2020)

2.1.1 Biophotolysis

Hydrogen production via biophotolysis relies on green algae using solar energy to proceed water splitting photosynthesis and the transfer of electrons to produce H_2. Biophotolysis is divided into two main subcategories as direct and indirect photolysis. In direct photolysis, the light energy is directly utilized for the activity of hydrogenase enzyme to generate H_2 (Equation 2-1) (Hallenbeck, 2012).

$$2H_2O \xrightarrow{\text{light energy}} 2H_2 + O_2 \qquad \text{(Equation 2-1)}$$

In indirect photolysis, hydrogen production is conducted via two-stage process as carbohydrate synthesis in the presence of light (Equation 2-2) and carbohydrate fermentation to produce hydrogen (Equation 2-3) (Hallenbeck, 2012).

$$6H_2O + 6CO_2 \xrightarrow{\text{light energy}} C_6H_{12}O_6 + 6O_2 \qquad \text{(Equation 2-2)}$$

$$C_6H_{12}O_6 + 6H_2O \rightarrow 12H_2 + 6CO_2 \qquad \text{(Equation 2-3)}$$
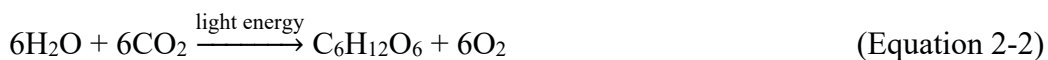
Biophotolytic hydrogen generation suffers from many drawbacks. For direct photolysis, hydrogenases are significantly susceptible to the presence of oxygen; therefore, these enzymes are strongly inhibited during the photosynthesis due to

oxygen evolution. Further, there are several competing metabolic pathways present for photosynthetic electrons such as Calvin-Benson cycle and nitrogen assimilation (Nikkanen et al., 2021). In addition, due to low rates and high cost of photobioreactors, hydrogen generation via indirect photolysis is significantly limited (Osman et al., 2020). Moreover, the hydrogen yield, calculated as the ratio of hydrogen energy produced to the solar energy used in the process, is considerably low in both direct and indirect biophotolysis and it does not exceed about 10% (Cheonh et al., 2022).

2.1.2   Photo-fermentation

The principle of photo-fermentation is based on the activities of purple non-sulfur photosynthetic bacteria which use light energy and convert organic acids to H_2 and CO_2 (Equation 2-4) (Cheonh et al., 2022).

$$CH_3COOH + 2H_2O \xrightarrow{\text{light energy}} 2CO_2 + 4H_2 \qquad \text{(Equation 2-4)}$$
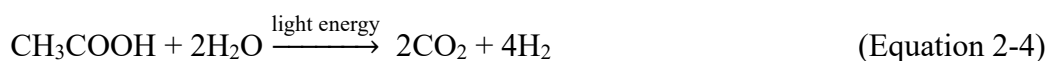
In photo-fermentation, microorganisms can use light energy from the sun or from an artificial light source. Sun is an economical energy source; however, it allows biohydrogen production only at daytime. On the other hand, using artificial light sources such as tungsten lamps can also allow the production of hydrogen at night. Yet, this requires additional investment and operating costs. Besides that, the main drawback of photo-fermentation is the need for sufficient ATP supply since the amount of energy necessary to produce biohydrogen by nitrogenase is significant. Also, biohydrogen production yield in continuous photo-fermentation is considerably low due to the significant washout of bacteria from the continuous bioreactor (Cheonh et al., 2022; Hallenbeck, 2012).

2.1.3   Dark fermentation

Dark fermentative biohydrogen production is defined as the biodegradation of organic matters by anaerobic microorganisms in the absence of light and oxygen. DF can be carried out by either obligate or facultative anaerobic fermentative microorganisms such as *Clostridia*, *Enterobacter*, *Thermotoga*, and *Caldicellulosiruptor* strains (Łukajtis et al., 2018). The theoretical yield of dark fermentative H_2 can be estimated based on the metabolic pathway used by fermentative microorganisms. In general, there are two major routes for molecular hydrogen formation: (i) through reoxidization of nicotinamide adenine dinucleotide (NADH) pathway, and (ii) through the pyruvate-formate-lyase (PFL) pathway (Cabrol et al., 2017). For both pathways, the first step is the conversion of glucose to pyruvate followed via generation of acetyl-CoA and either reduced ferredoxin or formate (Figure 2.2). The first pathway is mainly used by obligate anaerobes which enables the production of 4 mol H_2 from the fermentation of 1 mol of glucose (Cabrol et al., 2017). The details of energetics and metabolic pathways of DF are explained in the following sections.

Dark fermentative hydrogen generation can take place in four different temperature ranges: mesophilic (25-40 ºC), thermophilic (40-65 ºC), extremely thermophilic (65-80 ºC) and hyperthermophilic ($\geq$ 80 ºC). During DF, there are other by-products generated by microorganisms along with the hydrogen such as organic acids (acetic acid, lactic acid, butyric acid or propionic acid) or alcohols like ethanol. DF has significant advantages over other biological hydrogen methods which can be summarized as (i) higher hydrogen production rate, (ii) no light requirement, (iii) simplicity of the process, (iv) lower net energy input and (v) low value wastes as potential feedstocks. Also, a simple reactor design is sufficient for DF operations. On the other hand, by-product generation other than H_2 is the greatest drawback for dark fermentation since the generation of these products causes low volumetric hydrogen yield. Even though the organics acids or alcohols produced during DF have a considerable market value, the concentration of these products is too low for an

economically viable downstream process, and they require separation/purification application (Łukajtis et al., 2018).

2.1.3.1 Energetics of dark fermentation

The hydrogen production is governed by the thermodynamics of the process. Theoretically, the complete oxidation of glucose into H_2 results 12 mol of H_2 per mol of glucose (Equation 2-5), and the free energy change of this reaction is negative (Thauer et al., 1977).

$$C_6H_{12}O_6 + 6H_2O \rightarrow 12H_2 + 6CO_2 \quad \Delta G^{0'} = -6.18 \text{ kcal/mol} \qquad \text{(Equation 2-5)}$$
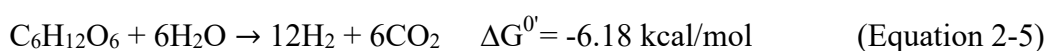
However, there is no microorganism that mediates the complete degradation of organic matter to H_2 and CO_2 as given in Equation 2-5. When it is a microbial process, the fermentation process must be coupled with the ATP synthesis from ADP and inorganic phosphate to ensure that the cell can sustain its life (Thauer et al., 1977). During the hydrogen generation, ATP synthesis can be achieved via the phosphorylation mechanism (Thauer et al., 1977). The energy requirement for ATP synthesis under physiological conditions is between 10-12 kcal/mol (Thauer et al., 1977). Therefore, at least 10-12 kcal/reaction should be produced during H_2 formation to achieve ATP synthesis. In a living cell, it is not possible to occur this assuming equilibrium condition. The energy need for ATP synthesis has to be even larger (about 15 kcal/mol) under irreversible conditions (Thauer et al., 1977). The free energy change of only 6 kcal/mol is the reason why complete degradation of glucose to H_2 and CO_2 cannot be achieved via microbial conversion (Thauer et al., 1977).

The maximum theoretical amount of H_2 via fermentation was determined by Thauer et al. (1977) as a maximum yield of 4 mol H_2 from 1 mol of glucose by following reaction (Equation 2-6):

$$C_6H_{12}O_6 + 2H_2O \rightarrow 2CH_3COO^- + 2H^+ + 2CO_2 + 4H_2 \quad \Delta G^{0'} = -51.6 \text{ kcal/mol}$$
$$\text{(Equation 2-6)}$$
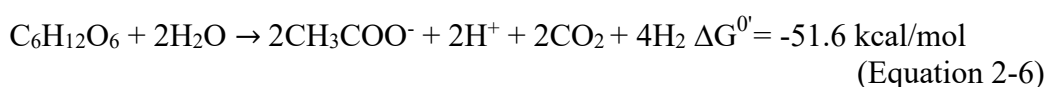
The generation of 4 mol H_2 per 1 mol of glucose is defined as ''Thauer limit'' which is only possible through acetate generation as a sole metabolic by-product. Consequently, homogenous acetate generation has not been achieved in DF at mesophilic temperatures. The hydrogen yields for mesophilic dark fermentation were reached only to 2 mol H_2 per 1 mol glucose (Table 2.1).

2.1.3.2   Metabolic pathways of dark fermentation

As previously mentioned, hydrogen production follows two main pathways in the presence of specific coenzymes as (i) through the reoxidation of nicotinamide adenine dinucleotide (NADH) pathway or (ii) through the pyruvate-formate-lyase (PFL) pathway (Cabrol et al., 2017). In both pathways, glucose is first converted to pyruvate, which results acetyl-CoA and either reduced ferredoxin or formate (Figure 2.2). The first pathway occurs through the conversion of pyruvic acid to acetyl-CoA via the activity of pyruvate-ferredoxin (Fd) oxidoreductase, which achieved in the case of obligate and thermophilic anaerobes (Equation 2-7).

Pyruvate + CoA + 2Fd(ox) → Acetyl-CoA + 2Fd(red) + CO_2 (Equation 2-7)

Obligate and thermophilic anaerobes have the ability to reoxidate the NADH formed during the glycolysis to generate extra hydrogen molecules via two other hydrogenases (NADH-dependent and bifurcating NADH-Fd_{red}-dependent hydrogenase). Hence, 4 mol of H_2 per mol glucose can be achieved from the fermentation if all the NADH are reoxidated (Cabrol et al., 2017; Gopalakrishnan et al., 2019).

In PFL pathway, formate is splitted into CO_2 and H_2 via formate hydrogen lyase complex, consisting of a nickel-iron (NiFe) hydrogenase, which is followed by facultative anaerobes (Equation 2-8) (Gopalakrishnan et al., 2019).

Pyruvate + CoA → Acetyl-CoA + Formate   (Equation 2-8)

Microorganisms that can only follow PFL pathway do not have access to NADH for hydrogen formation; therefore, the hydrogen yield through PFL pathway is theoretically limited to 2 mol H_2 per mol of glucose (Cabrol et al., 2017).
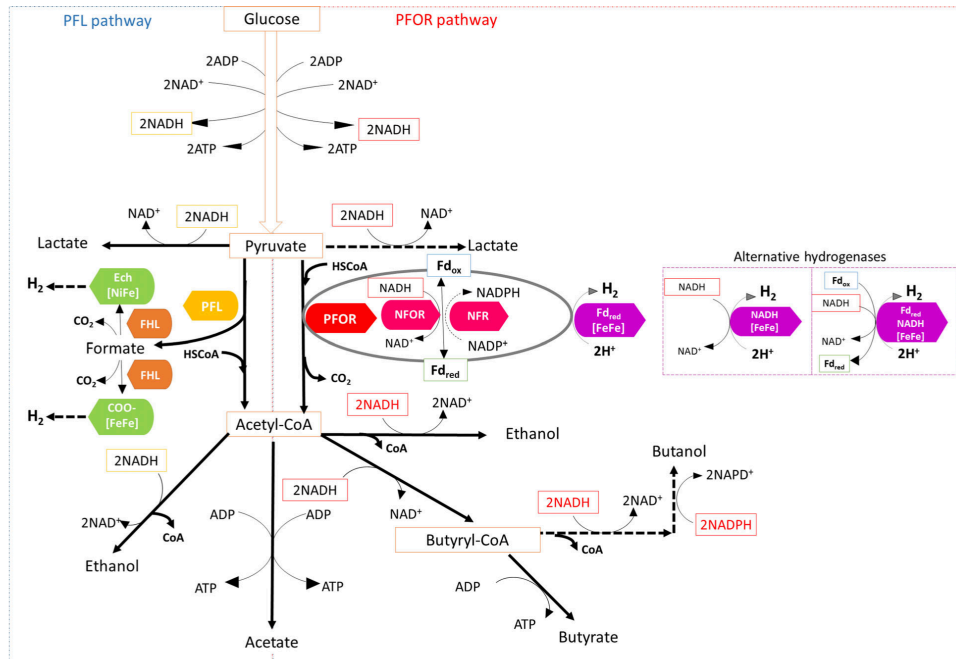
Figure 2.2 Fermentation pathways for H_2 generation from glucose, under anaerobic conditions (Cabrol et al., 2017)

2.1.3.3   Fermentative hydrogen producing microorganisms

Under anaerobic conditions, a wide range of microorganisms can produce H_2 through different metabolic pathways. In the absence of oxygen, anaerobic microorganisms need to search for an alternative terminal electron acceptor (Cabrol et al., 2017). There can be different electron acceptors and H_2 is generated when an electron is transferred to the proton as an electron acceptor (Gopalakrishnan et al., 2019). Dark fermentative microorganisms are generally classified based on their sensitivity to the presence of oxygen as obligate and facultative anaerobes, and also based on their temperature requirements (Gopalakrishnan et al., 2019). Depending on the temperature requirements, microorganisms are divided into four main domains as

mesophiles (25-40 ºC), thermophiles (40-65 ºC), extremophiles (65-80 ºC) and hyperthermophiles ($\geq$ 80 ºC). Table 2.1 shows the maximum hydrogen yield achieved by different microorganisms from a hexose, where (hyper)thermophiles have been reported to reach the maximum theoretical yield of H_2 (4 mol H_2/mol glucose) because of the smaller thermodynamic barrier and following homogenous acetate formation pathway (Gopalakrishnan et al., 2019). In addition, dark fermentative hydrogen production at elevated temperatures has several advantages over mesophilic operation: (i) higher reaction rates, (ii) stabilization of wastes, (iii) higher tolerance to high hydrogen partial pressure and (iv) lower risk of contamination by hydrogen consuming methanogens (Gupta et al., 2016). The further details of an ideal hydrogen producing microorganisms are given in the following section.

Table 2.1 Hydrogen production yields reported in dark fermentation studies using hexoses

Microorganism	T_{opt} (ºC)	Substrate	Operation type	H_2 Yield[*]	Reference
• Mesophilic					
Enterobacter aerogenes	40	Glucose	Batch	1.0	(Tanisho et al., 1987)
Escherichia coli SR15	37	Glucose	Fed-batch	1.8	(Yoshida et al., 2005)
Enterobacter cloacae	37	Starch	Fixed bed	1.4	(N. Kumar & Das, 2001)
Clostridium butyricum	30	Glucose	Continuous	2.0	(Kataoka et al., 1997)
Clostridium beijerinckii RZF-1108	35	Glucose	Batch	2.0	(Zhao et al., 2011)
• (Hyper)Thermophilic					
Thermotoga neapolitana	77	Glucose	Batch	3.9	(Munro et al., 2009)
Thermotoga maritima	80	Glucose	Batch	4.0	(Schröder et al., 1994)
Caldicellulosiruptor saccharolyticus	70	Glucose	Batch	3.4	(Mars et al., 2010)
Caldicellulosiruptor owensensis	70	Glucose	Batch	4.0	(Zeidan & van Niel, 2010)

[*]: Yield is given as mol of H_2 produced per mol of hexose consumed.

2.1.3.4 The ideal microorganism for dark fermentative hydrogen production

Search for ideal hydrogen producing microorganisms for DF has been continued for several decades which requires important consideration of several parameters. The most crucial aspect is the hydrogen production rate and yield since the rate is directly linked to enhanced efficiency and productivity. As previously mentioned, thermophiles are presented as promising alternatives compared to mesophiles for enhanced hydrogen production via DF (Elsharnouby et al., 2013). Although the most thermophiles present significant characteristics for biohydrogen production, there are specific features which an ideal hydrogen producer should have. There is no such microorganism that possess all the characteristics identified to date. In their review, Pawar and van Niel (2013) suggested a combination of these features in detail and proposed a summary in a Venn diagram for the microorganisms identified as a thermophilic hydrogen producers based on these characteristics (Figure 2.3). The features proposed by Pawar and van Niel (2013) can be listed as: (A) thermophilic, (B) consists of vectors/tools for genetic modifications, (C) has Fd-dependent hydrogenases, (D) is not auxotrophic to any amino acids, (E) has capability of use a wide range of biomass, (F) has an ability to metabolize multiple sugars simultaneously (absence of carbon catabolite repression), (G) can shift the metabolism to the production of useful by-products under stress conditions, (H) shows a tolerance to high osmotic stresses due to high substrate/by-product concentrations, and (I) is tolerant to oxygen. Further, the higher resistance to growth inhibitors in renewable feedstocks and lower need for expensive media to grow are important features to possess by an ideal hydrogen producer for scaled-up biohydrogen technology. Among all hydrogen producers, the genera of *Caldicellulosiruptor* are the closest to being ideal hydrogen producing microorganisms (Figure 2.3).
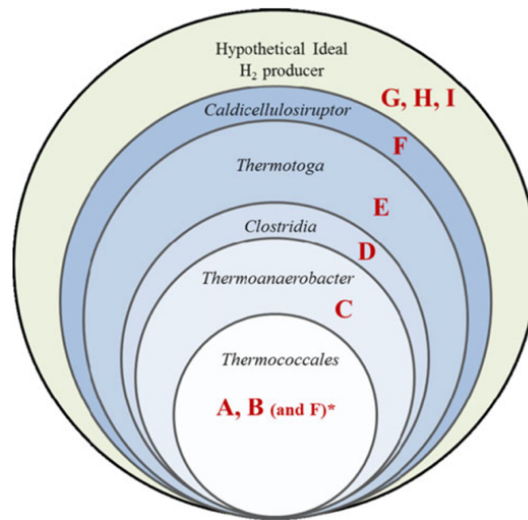
Figure 2.3 A Venn diagram for the comparison between distinguished thermophilic hydrogen producers with respect to the desirable features of an ideal H_2 producer (Asterisk, note : property F is also present in *Thermococcales* and is indeed absent from other genera as depicted; adopted from Pawar & Van Niel, 2013)

2.1.3.4.1   The genus of *Caldicellulosiruptor*

The species belong to the genus of *Caldicellulosiruptor* are gram-positive, extremely thermophilic/hyperthermophilic, anaerobic, cellulolytic/hemicellulolytic bacteria that have low GC content. According to the GenBank of National Center for Biotechnology Information (NCBI) data base, the classification of the *Caldicellulosiruptor* genus is given in Table 2.2.

Table 2.2 The classification of the *Caldicellulosiruptor* genus

Phylum	Firmicutes
Class	*Clostridia*
Order	*Thermoanaerobacterales*
Family	*Thermoanaerobacterales* Family III *Incertae Sedis*
Genus	*Caldicellulosiruptor*

Starting with *Caldicellulosiruptor saccharolyticus*, there are 14 species identified in the genus of *Caldicellulosiruptor* to date from six different countries (L. L. Lee et al., 2020). In general, the dominance of the *Caldicellulosiruptor* genus has been observed in terrestrial hot springs at elevated temperature ranges (65-80 ºC), yet,

there are species belong to the genus of *Caldicellulosiruptor* isolated from pond sediment and compost (Table 2.3).

Table 2.3 Identified species belonging to the genus of *Caldicellulosiruptor*

Specie	Source	Isolation temperature	Reference
C. acetigenus	Geothermal area, Iceland	65-68 °C	(Onyenwoke et al., 2006)
C. bescii	Hot spring, Russia	72-85 °C	(Yang et al., 2010)
C. changbaiensis	Hot spring sediment, China	80-83 °C	(Bing et al., 2015)
C. danielii	Hot spring, New Zealand	-	(L. L. Lee et al., 2015)
C. hydrothermalis	Geothermal spring, Russia	55-65 °C	(Miroshnichenko et al., 2008)
C. kristjanssonii	Hot spring biomat, Iceland	78 °C	(Bredholt et al., 1999)
C. kronotskyensis	Geothermal spring, Russia	55-65 °C	(Miroshnichenko et al., 2008)
C. lactoaceticus	Hot spring sediment/biomat, Iceland	74 °C	(Mladenovska -Indra et al., 1995)
C. morganii	Hot spring, New Zealand	63 °C	(L. L. Lee et al., 2015)
C. naganoensis	Hot spring, Japan	75-85 °C	(Taya et al., 1988)
C. obsidiansis	Hot spring, USA	66 °C	(Hamilton-Brehm et al., 2010)
C. owensensis	Freshwater sediment, USA	75 °C	(Huang et al., 1998)
C. saccharolyticus	Geothermal spring pool, New Zealand	70 °C	(Rainey et al., 1994)
C. sp. F32	Biocompost, China	-	(Ying et al., 2013)

The members of the *Caldicellulosiruptor* genus are recognized by their superior ability to degrade and convert plant biomass resulting enhancement of biomass conversion and rate of decomposition along with H_2 production (L. L. Lee et al., 2020). For example, Yang et al. (2010) demonstrated that *C. bescii* can effectively utilize untreated plant biomass, including potential bioenergy plants such as poplar and switchgrass. This ability of the *Caldicellulosiruptor* species is a unique characteristic. In general, microorganisms can secrete either free, individual cellulases or large multi-protein complexes, *i.e.*, cellulosomes. The members of *Caldicellulosiruptor* lack a cellulosome, and instead they contain 'free acting' cellulases that are not part of the cellulosome complex (Blumer-Schuette et al., 2010; Schwarz, 2001). The members of *Caldicellulosiruptor* genus can simultaneously degrade both pentoses (C_5) and hexoses (C_6) since they lack carbon catabolite repression (CCR) mechanism (L. L. Lee et al., 2020). This is a critical feature of the

Caldicellulosiruptor genus in which enables the development of an industrially relevant strains.

In the last decade, the studies on the *Caldicellulosiruptor* genus have been dramatically increased owing to their ability to efficient use of lignocellulosic materials. The focus of the research has been directed to understand the mechanisms of the biodegradation of simple sugars to produce hydrogen and the capacity of the species, *i.e.*, volumetric productivity and yield. *C. saccharolyticus* is the most comprehensively examined specie from the genus of *Caldicellulosiruptor*. The studies showed that *C. saccharolyticus* is able to produce hydrogen with significant yield as 3.3 mol H_2/mol hexose which is about 83% of Thauer limit (van Niel et al., 2002). Another study using *C. saccharolyticus* revealed that the bacterium could reach to 4 mole H_2 per mole of hexose at lower concentrations and about 88% of Thauer limit at higher concentrations during continuous-mode cultivation (De Vrije et al., 2007). Zeidan and van Niel (2009) investigated different *Caldicellulosiruptor* species (*C. saccharolyticus*, *C. owensensis*, *C. kristjanssonii*) as both pure cultures and co-cultures for effective use of mixed sugars with high hydrogen yield. As pure cultures, three species showed high hydrogen yields in the range of 2.7-3.0 mol H_2/mol hexose. Co-culture of *C. kristjanssonii* and *C. saccharolyticus* showed a superior performance by reaching up to 3.8 mol H_2 per mole hexose with a high volumetric productivity (17 mmol per liter per hour). Other than studies using simple sugars, there are several studies examined the degradability of lignocellulosic materials such as switchgrass and hydrogen production by different *Caldicellulosiruptor* species. Ivanova et al. (2009) examined the use of different feedstocks without any chemical pretreatment which are sweet sorghum, sugarcane bagasse, wheat straw, maize leaves and silphium by *C. saccharolyticus* and the outcomes of the study illustrated that the best feedstock is wheat straw with the highest yield of 3.7 mol H_2/mol glucose consumed. Talluri et al. (2013) examined the biodegradation of unpretreated switchgrass by *C. saccharolyticus* in batch-type reactors and the result of the study showed 11 mmol H_2/g switchgrass consumed. In their recent study, Abreu et al. (2019) studied the co-fermentation of garden and food

wastes by *C. saccharolyticus*. By using the mixture of 90% garden waste and 10% food waste, they reached to the maximum hydrogen yield of 46 mL H_2/g feedstock in batch operation.

2.1.3.4.2 *Caldicellulosiruptor bescii*

Caldicellulosiruptor bescii, formerly *Anaerocellum thermophilum*, is one of the most thermophilic cellulolytic members of the *Caldicellulosiruptor* genus with a growth temperature range of 42-90 ºC (T_{opt} 78-80 ºC, at pH 7.2) (L. L. Lee et al., 2020; Yang et al., 2010). *C. bescii* is an obligate anaerobe with a rod-shaped morphology, having important fermentative characteristics to degrade various carbohydrates such as cellobiose, crystalline cellulose and xylose which mainly present in lignocellulosic biomasses (Yang et al., 2010). Up to now, there are several studies on the metabolic pathways followed by *C. bescii*, yet, the complete mechanism of the strain is not fully understood (L. L. Lee et al., 2020). The major fermentation products generated by *C. bescii* are CO_2, H_2, lactate and acetate (Yang et al., 2010).

C. bescii has a significant potential for industrial applications since the carbon catabolite repression mechanism is absent which enables to metabolize multiple sugars simultaneously (L. L. Lee et al., 2020). It is an ideal characteristic for a microorganism considering industrial operations since having a natural ability to co-utilize the sugars enables economically viable process and allows the flexible feedstock selection (Pawar & Van Niel, 2013). A comparative analysis showed among others in the same genus (*C. bescii, C. kronotskyensis, and C. saccharolyticus*), *C. bescii* is better suited to solubilize both unpretreated switchgrass (about 40%) and microcrystalline cellulose (about 77%) as it showed superior performance on the solubilization of the lignocellulosic feed (Zurawski et al., 2015). It was also shown that *C. bescii* can grow with industrially relevant loads (50-200 g/L) of unpretreated switchgrass (Basen et al., 2014; Straub et al., 2019). In their recent study, Straub et al. (2019) showed a considerable enhancement in the deconstruction of unpretreated switchgrass (50 g/L) by *C. bescii* in continuous

operation. The focus of most studies in the literature was on the lignocellulosic biomass degradation capacity of *C. bescii* and not on hydrogen production (Conway et al., 2017; Straub et al., 2019; Zurawski et al., 2015). Yet, the promising findings about *C. bescii* have led to use this microorganism as the inoculum in dark fermentative biohydrogen production from organic wastes. For example, the co-culture of *C. saccharolyticus* and *C. bescii* were used for biohydrogen production from garden waste and food waste which resulted a maximum yield of 98.3 L H_2/kg VS added (A. Abreu et al., 2016). When the same system was operated with single cultures, the highest H_2 yield was reported as 84.6 L H_2/kg VS added which was obtained by *C. bescii* (A. Abreu et al., 2016). Furthermore, as a proof of concept, the studies demonstrated that *C. bescii* can degrade sterilized wastewater biosolids up to 2.5 g VS/L (Yilmazel et al., 2015) and sterilized cattle manure at 2.5 g VS/L as the sole carbon source for hydrogen production (Yilmazel & Duran, 2021). The hydrogen yields with wastewater biosolids, and cattle manure were both higher than other studies reported in the literature (Yilmazel et al., 2015; Yilmazel & Duran, 2021).

2.1.4   Bioelectrochemical hydrogen production

Bioelectrochemical hydrogen production, *i.e.*, electrohydrogenesis, is an integration of microbial metabolism with electrochemistry (Ferraren-De Cagalitan & Abundo, 2021). This relatively new technology is operated with a specific reactor type named as MEC which is a bioelectrochemical system (BES) to generate hydrogen. The general principle of BESs is dependent on the use of electro-active microorganisms that can transfer electrons to a solid electrode (exoelectrogens) or that receive electrons from the electrode (electrotrophs) (Logan et al., 2019). An MEC included two electrodes as an anode and a cathode. The basic principle of bioelectrochemical hydrogen production in an MEC is that exoelectrogenic microorganisms convert organic matter to CO_2, electrons (e^-), and protons (H^+) (Figure 2.4) (Ferraren-De Cagalitan & Abundo, 2021). The electrons transferred to the anode electrode and the

protons are released to the electrolyte solution. Then, electrons move to the cathode electrode from anode through an external electrical circuit which combine with free protons to generate H_2 in the absence of oxygen. The thermodynamics of the electrohydrogenesis process in an MEC is explained below.
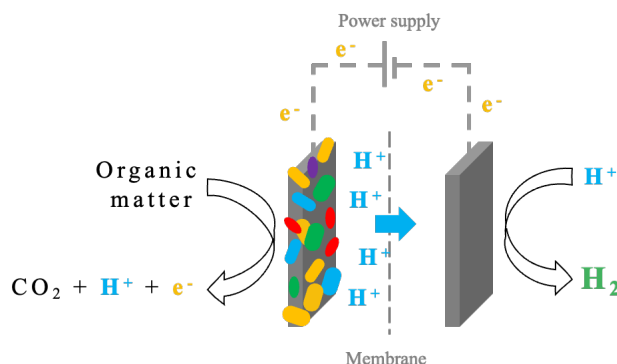
Figure 2.4 Schematic illustration of bioelectrochemical hydrogen production in an MEC

Bioelectrochemical hydrogen production can be achieved from various organic matters such as acetate, glucose and glycerol which are highly presented in wastewaters or organic wastes (Rozendal et al., 2006). Acetate is used as a model substrate in MEC studies (Logan et al., 2019). The overall reaction happening in MEC system can be explained by Equation 2-9.

$$CH_3COO^- + 4H_2O \rightarrow 2HCO_3^- + H^+ + 4H_2 \qquad \text{(Equation 2-9)}$$
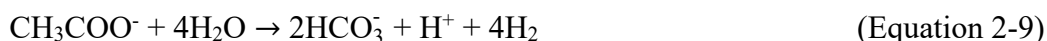
In anode and cathode parts, bioelectrochemical oxidation of acetate and hydrogen production occur as following Equation 2-10 and Equation 2-11, respectively. The bioelectrochemically oxidation of acetate on anode gives a potential of about -0.279 V and hydrogen evolution reaction (HER) at the cathode needed a potential of about -0.414 V (Logan et al., 2008).

$$CH_3COO^- + 4H_2O \rightarrow 2HCO_3^- + 9H^+ + 8e^- \quad E_{anode} \cong -0.28 \text{ V} \qquad \text{(Equation 2-10)}$$

$$8H^+ + 8e^- \rightarrow 4H_2 \qquad\qquad\qquad\qquad E_{cathode} \cong -0.42 \text{ V} \qquad \text{(Equation 2-11)}$$

$$E_{cell} = E_{cathode} - E_{anode} \cong -0.14 \text{ V} \qquad\qquad\qquad \text{(Equation 2-12)}$$

Equation 2-12 expresses the theoretical overall cell potential to generate hydrogen in an MEC system. Thus, hydrogen generation in MEC is a non-spontaneous and there should be external voltage to make it happen (Bora et al., 2022). In practice, the applied potential must be higher than 0.14 V to drive the HER at the cathode to account for losses in the system. Mostly, this value should be much higher, at least 0.5 V, due to electrode overpotentials and ohmic losses (H. Wang & Ren, 2013). Yet, this value is still much lower than the potential required for water electrolysis (1.8-2.0 V), which is used in large scale to generate H_2 (H. Wang & Ren, 2013).

Bioelectrochemical hydrogen production is a relatively new-developed concept for biohydrogen production, and it offers several advantages over other biohydrogen production methods: (i) use of several biodegradable organic compounds as a substrate, (ii) significantly higher hydrogen production rate about fivefold higher compared to other biohydrogen production methods, and (iii) reduction of solid production and lower sludge handling cost (Kadier et al., 2019; Saravanan et al., 2020). Yet, there are several parameters and components affecting the capacity of hydrogen generation in an MEC system which will be described in the following sections in detail.

2.1.4.1 Reactor components

There are several parts of MEC system, and the components are significant for the operation performance. In general, the fundamental components for the MEC are the reactor type along with electrode material, separator, microorganisms, and feedstocks used in the system (Krieg et al., 2014). The knowledge on the components and their interactions with each other is essential since these have significant impacts on the overall performance of hydrogen generation.

2.1.4.1.1 Reactor types

The reactor design is an important component to determine the efficiency of MEC system as well as the system cost. MECs can be investigated under two main categories based on the presence or absence of the membrane in the reactors as (i) two-chamber MEC and (ii) single chamber MECs (Figure 2.5) (Bora et al., 2022).
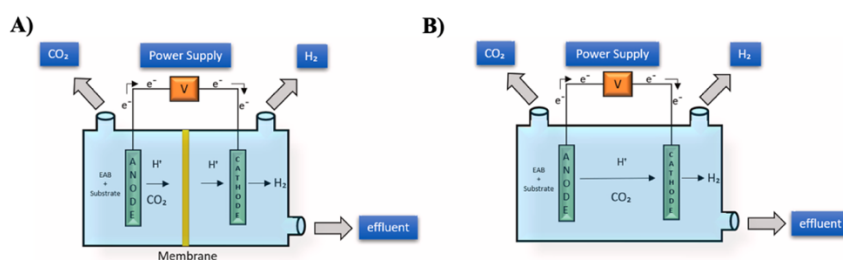
Figure 2.5 Reactor types for MEC (A) Two-chamber and (B) Single chamber (Adopted from Ferraren-De Cagalitan & Abundo, 2021)

Two-chamber MECs

Two-chamber MECs consists of two compartments including anode and cathode with an ion-exchange membrane to separate the compartments (Figure 2.5). This reactor type enables high purity of hydrogen production in cathode chamber and high substrate degradation in anode chamber by electroactive microorganisms (Krieg et al., 2014). The minimization of hydrogen diffusion to anode chamber from cathode part is very important to ensure higher hydrogen yield (Krieg et al., 2014). There are various types of membranes used in two-chamber MECs and the common types are proton exchange membrane (PEM), anion-exchange membrane (AEM) and cation-exchange membrane (CEM). Up to now, there are different two-chamber MECs were implemented as in the shape of bottle-type, dual-chamber disc-shaped, rectangular-shaped, H-type, and cube or cylindrical type (Bora et al., 2022). The first design of two-chamber MEC for hydrogen generation was investigated by Liu et al. (2005). In the study, two-chamber bottle-type MEC including carbon cloth electrodes and connected with PEM was used (Liu et al., 2005). Later, different

configurations of two-chamber MEC have been developed as two-chambers composed of one chamber for liquid and another chamber for gas equipped with a gas dispersion electrode and membrane electrode assembly to reduce the mass transfer resistance (Rozendal et al., 2007).

Although two-chamber MEC offers high-purity hydrogen gas generation, there are several drawbacks of this configuration like pH gradient between the chambers, high material cost of the membrane, and significant membrane resistance. For instance, the faster transfer rates of cations other than protons across the cation membranes results a pH decrease in the anode part which leads to increase in internal resistance of the system. Thus, a single change of pH may cause a possible loss of 0.006 V in the system (Bora et al., 2022).

Single chamber MEC

A single chamber MEC is composed of anode and cathode electrodes presented in the same chamber including the electrolyte solution (Figure 2.5) (Murugaiyan et al., 2022). There is no membrane in single chamber MECs which decrease any potential losses caused by the membrane resistance, in addition, reduces the fabrication cost; thereby, increasing the current density and hydrogen production rate. In general, the current densities obtained in single chamber MECs were higher than those reported in the studies using two-chamber MECs. A membrane-free MEC design was investigated using different features such as ammonia-treated anodes, high surface area graphite brush anodes, and shorter electrode distance to decrease the potential losses linked with the membranes (Bora et al., 2022).

On the other hand, single chamber MECs also have disadvantages such as the consumption of hydrogen in mixed culture studies (Muddasar et al., 2022). In general, exoelectrogens surpass methanogens for acetate on an MEC anode, yet the studies reported a significant methane production combined with considerable decrease in hydrogen production rates in single chamber MECs after a few weeks

operation using mixed culture (D. Call & Logan, 2008; Hu et al., 2008). In order to prevent that, different strategies investigated such as intermittent exposure of cathodes to air to inhibit methanogens, operating the system at low pH range to suppress the methanogenic activity and physical/chemical pretreatment of inoculum source (Hu et al., 2008).

2.1.4.1.2   Electrode materials

One of the important components is the electrode material which has a great impact on the performance of the system. Electrodes can act as an electron acceptor or donor in an MEC system. The choice of the electrode material is an important factor in which the redox processes at the electrodes and interactions of microorganisms/biocatalysts with electrodes should be considered (Krieg et al., 2014). The electrode materials are generally characterized as carbon-based electrodes, metal-based electrodes, and composite electrodes. Because of the higher biocompatibility and corrosion resistance, carbon-based electrodes have been highly preferred in bioelectrochemical applications (Gautam et al., 2023). In case of bioelectrochemical hydrogen production, biofilm is formed on anode and HER occurs at the cathode. The important characteristics to decide on anode materials can be summarized as its cost-effectiveness, corrosion-resistance, biocompatibility, good electrical conductivity and non-toxic behavior (Gautam et al., 2023). In addition to these, it is important that anode should have larger surface area for biofilm formation, high surface to volume ratio, and low over potential (Gautam et al., 2023). For cathode material, the main features can be summarized as high HER potential, low cost, non-corrosive, and non-toxic nature (Gautam et al., 2023). The details of anode and cathode materials are discussed in the following sections.

Anode electrode

Most research in MECs has used carbon-based materials as anode electrode because of its high conductivity, biocompatibility, adaptability in morphologies, considerably low overpotentials and low costs (Liu et al., 2010). At high potentials and the presence of oxygen, carbon materials have a tendency to corrode in water electrolysis system; however, they have a high stability under the anaerobic anodic process in MECs (Liu et al., 2010). In addition, carbon materials having high surface area have been utilized as an anode in MECs to increase the biofilm density attached to the surface by that enhance anodic current generation (Liu et al., 2010). There are several examples for these materials such as graphite brushes, graphite granules, carbon cloth, graphite felt, and carbon paper (Table 2.4).

Although there are significant advantages, the use of graphite brushes and granules have two major challenges linked with the low electrical conductivity and mechanical strength (Liu et al., 2010). At first, loosely packed materials might be disconnected due to the electrolyte flow or biofilm development (Liu et al., 2010). The core structure may maintain the conductivity during operation, but the deficiency of contact between brush fibers might result an increase the electrode resistance (Feng et al., 2010). The second challenge is the risk of a large distance between anode and cathode on scale-up applications due to the low proton concentration which leads to higher internal resistance (Liu et al., 2010). To further enhancement on the anode performance, different techniques were examined to modify electrode surfaces such as using self-assembled monolayers into graphite electrodes to drive the electron transfer to the anode surface. An increase on the performance was also showed by high-temperature treatment of the carbon-based anodes in other bioelectrochemical systems which may be applied to MECs (W. Chen et al., 2018; Feng et al., 2010).

Cathode electrode

In MECs, a cathode is generally composed of metal catalysts and catalyst supporting materials similar to the cathode of water electrolysis (Liu et al., 2010). The purpose of the catalyst is to decrease the activation energy by that reducing the cathodic activation overpotential along with enabling the improvement of the HER kinetics at the cathode surface (Liu et al., 2010). Among numerous catalysts, platinum is a well-established catalyst for this reaction and mostly preferred in MEC systems to increase the performance of hydrogen production (Table 2.4). However, the high cost of the platinum and sulphide poisoning bring important challenges to scale-up applications of the MEC system (Gautam et al., 2023). Thus, most research has been directed to find new materials without any precious metal catalyst and showing high-performance for HER.

Table 2.4 Reactor components and hydrogen production performance reported in MEC studies

Anode	Cathode	Substrate	E_{app} (V)	Q_{H2}*	Reference
• **Two-chamber operation**					
Carbon cloth	Carbon cloth	Synthetic WW	1.1	0.28	(Almatouq & Babatunde, 2017)
Graphite felt	Ti/Pt mesh	Acetate	0.5-1.0	0.02-0.33	(Rozendal et al., 2007)
Graphite granules	Carbon cloth/Pt	Acetate	0.6	1.1	(Cheng & Logan, 2007)
Graphite brush	Carbon cloth/Pt	Alkaline WAS	0.6	0.91	(Lu et al., 2012)
Graphite brush	Carbon felt	Acetate	-	0.41	(Zikmund et al., 2018)
• **Single chamber operation**					
Graphite brush	Carbon cloth/Pt	Acetate	0.8	3.12	(D. Call & Logan, 2008)
Carbon cloth	Carbon cloth/Pt	Acetate	0.6	2.3	(Hu et al., 2008)
Graphite fiber brush	Carbon cloth/Pt	Cellobiose	0.5	0.96	(Lalaurette et al., 2009)
Graphite fiber brush	SS mesh	Acetate	0.9	0.59	(Selembo et al., 2009)
Graphite brush	SS brush	Acetate	0.6	1.7	(D. F. Call et al., 2009)

*: m^3 $H_2/m^3/d$; WW: wastewater; WAS: waste activated sludge; SS: stainless steel

In recent, there are some low-cost cathode catalysts, like nickel oxide, nickel alloys and stainless steel, were suggested as a replacement of platinum in MECs (Liu et al., 2010). Additionally, there are different application to increase the surface area of the cathode by coating or placing a physical support to provide an extra surface for metal particles to disperse. Owing to its high conductivity and lower interference with the catalysts, carbon has been utilized as one of the most common support materials. Jeremiasse et al. (2011) showed that copper cathodes coated with nickel-molybdenum and cobalt-molybdenum alloys resulted high catalytic activity and hydrogen evolution rate as high as 50 m^3 H_2/m^3.day. Table 2.4 demonstrates the different types of materials as alternative cathode catalysts to platinum for hydrogen generation in MEC. These studies emphasize that non-precious metal catalysts such as alloys of stainless steel, generate comparable results to those obtained by using Pt catalyst. Although these materials are not superior to Pt catalyst, stainless steel and nickel alloys can be efficiently used with proper optimization for H_2 generation in an economical manner (Parkhey & Gupta, 2017).

2.1.4.2   Electro-active microorganisms

Electro-active microorganisms can electrically interact with each other and their environment including anaerobic soils and sediments, digesters and the surface of corroding metal (Lovley & Holmes, 2022). These microorganisms, as microbial electrocatalysts, have an ability to mediate a redox potential difference between solid electrodes and microbes, resulting a spontaneous electron transfer to the electrode or electron uptake from the electrode (Thapa et al., 2022). Based on their mechanisms, electro-active microorganisms can be divided into two categories as (i) exoelectrogens which can donate electrons to solid electrode and (ii) electrotrophs that can accept electrons from an electrode (Lovley & Holmes, 2022). Hydrogen production is achieved via exoelectrogens which are located on anode in MECs; therefore, the focus of this section is directed to exoelectrogenic microorganisms.

Exoelectrogens are microorganisms that generate electrical energy by oxidizing organic matter and facilitate extracellular electron transfer (EET) to an electron acceptor outside of their cells (Bora et al., 2022). These microorganisms are also referred as electricigens, anode respiring bacteria (ARB) and electrogenic bacteria. The capacity of exoelectrogens on the anode to facilitate electron transfer from substrate to the anode (current generation) has a direct impact on hydrogen production performance of MEC. The mechanism of electron transfer by exoelectrogens are still being studies which occurs in two possible EET mechanisms have been reported so far: (i) Direct electron transfer (DET) via outer membrane cytochromes or highly conductive nanowires, and (ii) Mediated electron transfer (MET) by using soluble electron shuttles (Figure 2.6) (Bora et al., 2022). The DET via outer membrane cytochromes and MET mechanisms were first revealed based on the search of how dissimilatory metal-reducing bacteria utilize solid minerals during their respiratory electron transport process (Myers & Myers, 1992; Rabaey & Verstraete, 2005). Later, DET via conductive bacterial nanowires was reported by providing a proof that bacteria can synthesize nanowires having an ability of transferring electric current across the wire diameter and along their length (El-Naggar et al., 2008; Reguera et al., 2005).
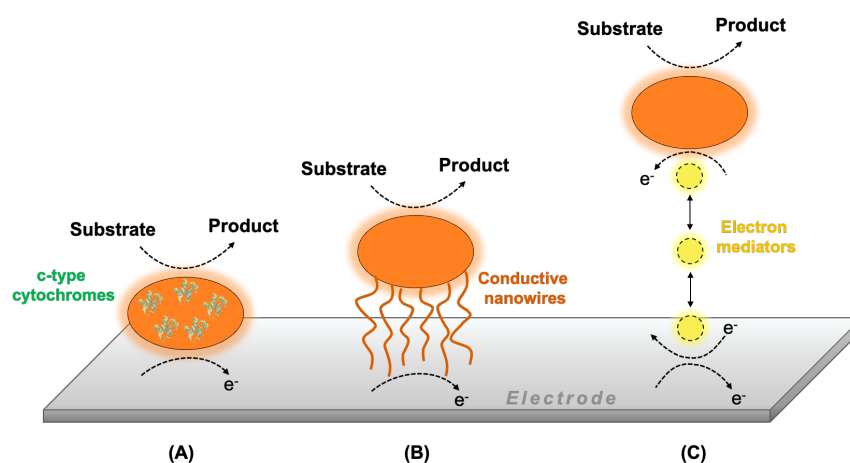
Figure 2.6 Electron transfer mechanism on electrode (A) DET over membrane-bound c-type cytochromes (B) DET via microbial conductive nanowires (long-range electron transfer) (C) long-range electron transfer via external electron carriers

There are several exoelectrogens discovered up to date such as metal-reducing bacteria as *Geobacter sulfurreducens*, *Desulfuromonas acetoxidans*, *Shewanella putrefaciens*, *Rhodoferax*, and *Geothrix* (Bora et al., 2022). Electro-active microorganisms have been identified in numerous environments including wastewaters, sewage sludge, ocean and marine sediments. The environmental conditions have a great impact on the community type of microorganisms present in the MECs. These species and other exoelectrogens were mostly isolated at mesophilic temperatures (Wrighton et al., 2008) but thermophilic or hyperthermophilic microorganisms have been also known to possess exoelectrogenic abilities (Fu, Fukushima, et al., 2015; Kobayashi et al., 2017; Lusk, Khan, et al., 2015; Marshall & May, 2009; Mathis et al., 2008; Parameswaran et al., 2013; Pillot et al., 2018; Narendran Sekar et al., 2017; Yilmazel et al., 2018; Yu et al., 2017; Kas & Yilmazel, 2022).

2.1.4.2.1 Thermophilic and hyperthermophilic exoelectrogens

The use of thermophiles and hyperthermophiles as inoculum in BESs have the potential to enhance the electrocatalytic rates over mesophiles enabling an enhanced oxidation currents and biohydrogen yields (Rathinam et al., 2019). Further, a wide range of feedstocks including lignocellulosic biomass can be effectively oxidized and converted to hydrogen at higher yields compared to mesophilic temperatures. In addition, theoretically hydrolysis rate of organic wastes will be enhanced at elevated temperatures. For this purpose, thermophilic or hyperthermophilic microorganisms that have stable protein and membrane structures even at high temperatures could be used in BESs which would provide important benefits for industrial applications such as higher reaction rates, minimal risk of contamination and maintaining anaerobic conditions with the lower solubility of oxygen in high temperatures (Sekar et al., 2017). The studies showed that both thermophilic/hyperthermophilic bacteria and archaea have the ability to perform extracellular electron transfer (Fu et al., 2013; Lusk, Khan, et al., 2015; Narendran Sekar et al., 2017; Yilmazel et al., 2018; Kas &

Yilmazel, 2022). On the other hand, there is a limited number of studies investigating thermophilic/hyperthermophilic BESs compared to the abundance of mesophilic BES applications. Only a limited portion of these studies directed their focus on microorganisms with a recognized role in electron transfer, and the understanding of the factors influencing the operation is limited. As dissimilatory iron-reducing microorganisms have been proposed to be involved in EET (B. H. Kim et al., 1999), this approach has been found to be applicable to most exoelectrogens to date (Logan et al., 2019), including thermophilic bacteria *Thermincola ferriacetica* (Lusk et al., 2015; Parameswaran et al., 2013) and hyperthermophilic archaea *Ferroglobus placidus* (Hafenbradl et al., 1996; Yilmazel et al., 2018), *Geoglobus ahangari* (Kashefi et al., 2002; Yilmazel et al., 2018), *Geoglobus acetivorans* (Kas & Yilmazel, 2022) and *Pyrococcus furiosus* (Sekar et al., 2016, 2017).

Thermophilic/hyperthermophilic exoelectrogenic bacteria

The membrane characteristics of bacteria have an important role on electrochemical activity, and this can be examined under two main categories based on the structure of membrane (i) gram-negative and (ii) gram-positive (Matsunaga & Nakajima, 1985). The difference between gram-positive and gram-negative bacteria can be explained that gram-positive bacteria have a thicker cell wall composed of peptidoglycan and an external lipoteichoic acid layer that helps biofilm formation on electrodes; therefore, different characteristics are expected in the electron transfer mechanisms between two groups (Ehrlich, 2008; Modestra & Mohan, 2014). In case of gram-negative bacteria, it is suggested to secrete permeable metabolic products, because of the thin peptidoglycan layer and selective outer membrane (Modestra & Mohan, 2014).

Thermophilic and hyperthermophilic exoelectrogenic bacteria in BESs are summarized in Table 2.5. Previous studies on different BES configurations proposed that gram-positive bacteria play an interface role rather than a direct participation in EET (Rabaey et al., 2007), and shuttle mediators are required to perform EET for

gram-positive bacteria due to their thick non-conductive envelope (Modestra & Mohan, 2014). However, the ability of the gram-positive *Thermincola* genus to produce current without electron shuttles has been reported in thermophilic BES studies (Lusk, Khan, et al., 2015; Marshall & May, 2009; Mathis et al., 2008; Wrighton et al., 2008). Chen et al. (2018) suggested that improving of the cell permeability in the peptidoglycan layer could increase the electron transport, as the non-conductive features and formate-acetate transfer across thick cell wall could negatively affect the process.

Table 2.5 Thermophilic and hyperthermophilic electro-active bacteria reported in BESs

Exoelectrogenic bacteria	Isolation/inoculum source	BES type	T (°C)	References
Thermincola ferriacetica	From a terrestrial hydrothermal spring	MEC	60	(Lusk et al., 2016, 2018; Marshall & May, 2009; Parameswaran et al., 2013)
Thermincola potens	MFC reactors inoculated with thermophilic AD sludge	MFC	55	(Wrighton et al., 2008)
Thermoanaerobacter pseudethanolicus	Algal-bacterial mat in Octopus Spring	MEC	60	(Lusk et al., 2015)
Calditerrivibrio nitroreducens	Terrestrial hot spring	MFC	55	(Fu et al., 2013)
Calditerrivibrio nitroreducens related specie	Thermophilic digester sludge from a WWTP	MFC	55	(Fu et al., 2013)

Thermophilic/hyperthermophilic electro-active archaea

In addition to the bacterial domain, thermophilic and hyperthermophilic archaea have also been studied in BESs. Exoelectrogenic archaea can donate electrons to an anode electrode similar to bacteria (Logan et al., 2019). To date, only a small number of hyperthermophilic archaea have been studied in BESs (Table 2.6). Hyperthermophilic archaea have a significant potential in numerous biotechnological applications owing to the extremozymes acting as biocatalysts

(Egorova & Antranikian, 2005). Despite these characteristics, laboratory-scale BES studies using hyperthermophilic archaea have not yielded significant results in terms of current generation. However, this may be due to the limited number of studies using hyperthermophilic archaea and the fact that the process is not yet fully understood. *Pyrococcus furiosus* was used in two-chamber MFCs operating at 90 ºC for the first report of hyperthermophilic archaea in BES operation (Narendran Sekar et al., 2017). Experiments with actively growing pure culture of *P. furiosus* resulted in well-defined current peaks ranging between 0.1-2.0 A/m^2 (Narendran Sekar et al., 2017). SEM images of the anode materials were used to observe the biofilm formation and the recovery time of the peak currents due to medium replenishment was analyzed using cyclic voltammetry (CV) analysis. The lack of redox peaks in the CV analysis of the spent medium was attributed to the DET capability of *P. furiosus* (Sekar et al., 2017). However, potential electron mediators such as cysteine and sodium sulfide were present in the growth medium and may cause MET (Yilmazel et al., 2018). Hence, the DET capability remains unclear.

Table 2.6 Hyperthermophilic electro-active archaea used in BESs

Exoelectrogenic archaea	Isolation/inoculum source	BES type	T (°C)	References
Pyrococcus furiosus	Geothermally heated marine sediment	MFC	90	(Sekar et al., 2017)
Ferroglobus placidus	Submarine hydrothermal vent	MEC	85	(Yilmazel et al., 2018)
Geoglobus ahangari	Hydrothermal system at a depth of 2000 m	MEC	80	(Yilmazel et al., 2018)
Geoglobus acetivorans	Hydrothermal system at a depth of 4100 m	MEC	80	(Kas & Yilmazel, 2022)
Archaeoglobales	Deep-sea hydrothermal vents	MEC	80	(Pillot et al., 2018)
Thermococcales	Deep-sea hydrothermal vents	MEC	80	(Pillot et al., 2018)

Ferroglobus placidus and *Geoglobus ahangari*, hyperthermophilic archaea, were used in single chamber MECs at temperatures of 85 °C and 80 °C, respectively (Yilmazel et al., 2018). Due to the absence of stress-related enzymes that model

exoelectrogen possesses, both hyperthermophilic archaea showed a considerably low current generation (Yilmazel et al., 2018). Of the various pressures affecting on the anode surface, proton transfer and pH alteration were expressed as a potential underlying reasons for low current generation, similar to the difficulties observed during *Thermincola ferriacetica* operations (Lusk et al., 2016, 2018).

Members of *Archaeoglobales* and *Thermococcales* orders that showed taxonomic similarity to *Geoglobus ahangari* (99% and 95%, respectively) enriched from the deep-sea hydrothermal vents showed higher current density reaching a maximum of 5.9 A/m^2 within a microbial organization similar to trophic chain (Pillot et al., 2018). It was suggested that rather than a pure culture BES application, mixed culture inoculation with conditions that enriches the exoelectrogens would improve the current generation due to the syntrophic activities of electroactive microorganisms (Pillot et al., 2018). Yeast extract included in the media was expected to be converted into acetate by heterotrophic microorganisms (Pillot et al., 2018); however, its presence might have induced MET through flavin-type compounds (Sayed et al., 2012). Therefore, the extent of the current production that could be attributed to DET mechanisms is unclear. Pillot et al. (2020) investigated the potential of current production by the mixed culture of hydrothermal chimneys in a hyperthermophilic MFC (80 °C) supplementing with different carbon sources. The experiments showed that the use of acetate, pyruvate and H$_2$ enable the current production directly, yet the indirect production was also observed when MFC fed with yeast extract and peptone through the H$_2$ and acetate production via fermentation. The study demonstrated that the *Archaeoglobales* sp. were presented all over the carbon fibers of the anode, which were mainly affiliated to *Geoglobus* sp. (98.6% similarity with *Geoglobus ahangari*). However, Yılmazel et al. (2018) showed that *Geoglobus ahangari* was unable to produce current using H$_2$, and Pillot et al. (2020) suggested that there might be several new exoelectrogens belonging to *Geoglobus* genus. A recent study was proved that there was another exoelectrogenic archaea, called *Geoglobus acetivorans*, belonging to *Geoglobus* genus in a hyperthermophilic MEC. Kas & Yılmazel (2022) conducted a single chamber Mini-MEC experiments using

pure culture of *G. acetivorans* fed with 10 mM acetate. They reached a peak current of 1.53 ± 0.24 A/m^2 which was significantly high current generation by a pure culture hyperthermophilic microorganism.

The genus of Archaeoglobales

Pure cultures of *Ferroglobus placidus, Geoglobus ahangari* and *Geoglobus acetivorans* are hyperthermophilic archaea belonging to the *Archaeoglobales* genus (Hafenbradl et al., 1996; Kashefi et al., 2002; Slobodkina et al., 2009).

These hyperthermophilic archaea were utilized in single-chamber Mini-MECs at temperatures of 85 °C for *F. placidus* and 80 °C for *G. ahangari* and *G. acetivorans*, (Yilmazel et al., 2018; Kas & Yilmazel, 2022). The current densities were reported as 0.68 ± 0.11 A/m^2 for *Ferroglobus placidus* and 0.57 ± 0.10 A/m^2 for *Geoglobus ahangari* (Yilmazel et al., 2018). While not definitely proven, there was a strong possibility that both hyperthermophilic archaea have the capability for DET via c-type cytochromes. This assumption was based on the presence of multiple genes encoding putative c-type cytochrome proteins (30 in *F. placidus* and 21 in *G. ahangari*), as indicated in studies by Manzella et al. (2015) and Smith et al. (2015). In addition, the biofilm on anode showed a protein concentration 3 times higher than the medium, which was linked to electron transfer proteins, including c-type cytochromes (Yilmazel et al., 2018). Kas & Yilmazel (2022) reported that *G. acetivorans* can produce higher current density in single chamber Mini-MECs at 80 °C. The maximum current production was 1.53 ± 0.24 A/m^2 which was significantly higher than other hyperthermophilic exoelectrogens. On the other hand, it was also proved that *G. acetivorans* has the ability to utilize H$_2$ as a sole electron donor in a single chamber MEC, *i.e.,* internal hydrogen cycling, which may contribute to the high current generation in this study. Therefore, two-chamber MEC operation should be performed to understand the effect of hydrogen cycling to current generation by *G. acetivorans*.

35

Geoglobus acetivorans

Geoglobus acetivorans SBH6 is an obligate anaerobic, hyperthermophilic, ferric iron reducing archaeal specie isolated from a hydrothermal vent at a depth of 4100 m (Slobodkina et al., 2009). *G. acetivorans* is the one of the two members of *Geoglobus* genus (Kashefi et al., 2002; Slobodkina et al., 2009) and both species are dependent on dissimilatory iron reduction. This specie can utilize various substrates including acetate, aromatic compounds or molecular hydrogen with this Fe(III) reduction (Mardanov et al., 2015).

This specie shares significant similarities with *G. ahangari* (97% identical in 16S rRNA genes) (Manzella et al., 2015) and with *F. placidus* share more than half (57%) of the *c*-type cytochrome sequences used in dissimilatory Fe(III) reduction (Smith et al., 2015). Additionally, this specie was known to possess pili-like appendages for binding to insoluble iron particles during dissimilatory iron reduction (Mardanov et al., 2015). Owing to these similarities and considerably high current generation compared to other hyperthermophilic BESs, pure culture of *G. acetivorans* were studied in this thesis as it provided a high potential to show exoelectrogenic activity in hyperthermophilic MECs.

2.2 Two-stage operation of thermophilic dark fermentation and microbial electrolysis cell
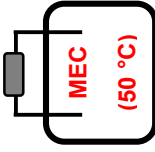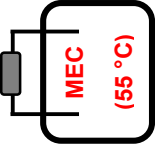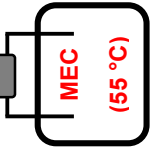
The integration of dark fermentative and microbial electrohydrogenesis processes has shown potential to significantly enhance the production of hydrogen from organic waste (Ndayisenga et al., 2021). The system can be implemented as a two-stage process. The first stage involving DF converting carbohydrate-rich substrates such as agricultural residues into H_2, CO_2, VFAs using dark fermentative bacteria, and the effluent of fermentation process is fed to the second stage of bioelectrochemical hydrogen production via MEC to generate additional biohydrogen along with higher waste treatment efficiency.

With the additional electrical voltage, MEC system can overcome the thermodynamic limitations of fermentative hydrogen production, and thereby achieve hydrogen production from fermentative dead-end products (Ndayisenga et al., 2021). Additional to that, integrating DF with MEC can enhance the stability and the efficiency of the DF (Ndayisenga et al., 2021). Although DF-MEC operation has significant advantages, research in this area is still new for biohydrogen production. Therefore, there are very few studies available in the literature, particularly concerning thermophilic and hyperthermophilic operations (Khongkliang et al., 2017, 2019; Lalaurette et al., 2009). Table 2.7 represented two-stage operation of DF-MEC system at thermophilic temperatures.

The first investigation involved a two-stage DF and MEC system that utilized *Clostridium thermocellum* as the fermentative bacterium for the corn-stover lignocellulose and cellobiose feeds (Lalaurette et al., 2009). The electrodes employed in MEC reactors were subjected to a 2-month acclimation process in MFC reactors. This was accomplished by using a wastewater inoculum that utilize a synthetic fermentative effluent or using the compounds in synthetic effluent as single substrates in 5 different MFC sets (Lalaurette et al., 2009). The MEC using a synthetic effluent produced the highest current density, reaching 0.146 A/m^2 (Lalaurette et al., 2009). The overall H$_2$ yield of the DF and MEC integrated system showed a considerable increase, reaching to 9.95 mol H$_2$/mol glucose (Lalaurette et al., 2009). Based on the findings, it could be argued that treating recalcitrant lignocellulosic materials with a combination of DF and MEC at thermophilic temperatures could be an effective alternative. In another integrated system study, cassava starch processing wastewater was fed into a DF reactor, which relied on *Thermoanaerobacterium thermosaccharolyticum* PSU-2 pure culture fermentative bacterium as inoculant (Khongkliang et al., 2017). MEC reactors were fed with the DF effluent and inoculated with a thermophilic mixed culture enriched from peatland soil (Khongkliang et al., 2017). A comparison was made between a single chamber MEC and a continuous two-stage system, with a potential application of 0.6 V. The results showed that the MEC reactor in the integrated system (205 ml H$_2$/g COD)

performed slightly better than the single-stage MEC (185 ml H_2/g COD). Additionally, hydrogen generated at the DF stage was 260 mL H_2/g COD bringing the total system yield of the integrated system for cassava starch wastewater to 465 mL H_2/g COD (Khongkliang et al., 2017). A similar configuration of the DF-MEC integrated system was utilized to treat palm oil mill wastewater effluent (Khongkliang et al., 2019). External voltages ranging from 0.2 V to 0.9 V were applied at 55 °C (Khongkliang et al., 2019). The hydrogen yield increased from 73 ml H_2/g COD produced only from DF up to 236 ml H_2/g COD with the DF-MEC integrated system, utilizing an external voltage application of 0.7 V (Khongkliang et al., 2019). As a results, the use of two-stage DF and MEC operation can be advantageous, especially for the treatment of lignocellulosic biomass which has a complex and recalcitrant structure that cannot be completely treated with using a single bioprocess.

Table 2.7 The studies using two-stage DF and MEC operation at thermophilic temperatures

	1st Stage	2nd Stage	Outcomes
(Lalaurette et al., 2009)	**DF (55 °C)** • *Clostridium thermocellum* ▪ Corn-stover cellobiose & corn-stover	**MEC (50 °C)** • DF-effluent acclimated MFC inoculum	○ Highest current density is observed with synthetic effluents that did not include any potential electron mediators. ○ Y_{DF}: 1.6 mol H_2/mole glucose, while implementing MEC increased the overall yield more than 6 times compared to only DF.
(Khongkliang et al., 2017)	**DF (55 °C)** • *Thermoanaerobacterium thermosaccharolyticum* PSU-2 ▪ Cassava starch processing wastewater	**MEC (55 °C)** • Peat soil sample	○ MEC in the integrated system performed better than solo MEC operation. ○ Hydrogen yield for integrated system increased more than 2.5 times.
(Khongkliang et al., 2019)	**DF (55 °C)** • Enriched thermophilic anaerobic sludge ▪ Palm oil mill effluent	**MEC (55 °C)** • Peat soil sample	○ Hydrogen yield increased more than 3 times with the integrated system. ○ Too high and too low voltage applications resulted in lower H_2 production. Optimum voltage was around 0.7 V.

2.3 Enrichment of microorganisms for enhanced hydrogen production

Microbial cells are of special importance for biotechnological applications and used for biofuel production in different industrial processes (Dragosits & Mattanovich, 2013). One of the most important parameters for an industrial bioprocess is the efficiency of substrate utilization which may be governed by factors such as feedstock cost or increased biodegradation rates (Dragosits & Mattanovich, 2013). There are different strategies reported in the literature to enhance the bioconversion rates and the enrichment of microbial communities for better substrate utilization is commonly studied on biohydrogen generation. Based on the inoculum source, there are two enrichment methods are expressed in the literature as (i) acclimation of mixed cultures and (ii) adaptation of pure cultures.

2.3.1 Acclimation of mixed cultures

The acclimation of biohydrogen producing microbes to substrate is a promising strategy to enhance biohydrogen production rate and yield. In the literature, the acclimation of inoculum is achieved both using batch and continuous reactors. In general, batch acclimation strategy is preferred to retain the biohydrogen producers without washout during the acclimation. Batch acclimation can be achieved two different ways: (i) acclimation of inoculum to feedstock operating as batch mode reactor as one time operation for a longer period of time without any additional operation and (ii) acclimation of inoculum in batch mode reactors with serial transfer for shorter period. For continuous acclimation, as gradual increase in feedstock concentration fed to a continuous reactor up to achieving steady-state was followed in general in which inhibition due to high concentrations of substrate can be prevented. For instance, Makinen et al. (2012) examined biohydrogen production from simple sugars as glucose and xylose using hot spring culture as inoculum. The microbial community obtained from hot springs was acclimated initially on glucose for hydrogen production (Makinen et al., 2012). The outcomes of the study revealed

40

that biohydrogen production can be achieved using batch acclimation via serial transfer and they reported 0.54 mol H_2/mol glucose and 0.71 mol H_2/mol xylose (Mäkinen et al., 2012). Another study conducted by Kim & Kim (2012) investigated the batch acclimation via single batch mode operation of the reactor for 5 days of anaerobic digester sludge to glucose (10 g COD/L); then, the reactor operation was switched to a continuous flow using pretreated tofu processing wastewater as a feedstock (11.5 g sugar/L). The highest hydrogen yield was 1.78 mol H_2/mol sugar added which was very close to the yield obtained with simple sugars while using the acclimated culture as inoculum source (Kim & Kim, 2012). Cakır et al. (2010) studied biohydrogen production from acid-hydrolyzed wheat starch (18 g sugars/L) using acclimated anaerobic digester sludge which was achieved using serial growth cycles in batch reactors and each cycle was continued for 3 days. The acclimation of inoculum was achieved using glucose at a concentration of 60 g/L in batch operation at 55 ºC. The hydrogen yield of 333 mL H_2/mol sugar was achieved using acclimated culture which was 1.5 times higher compared to non-acclimated culture operation (Cakır et al., 2010).

In addition, the acclimation of mixed cultures has been investigated in bioelectrochemical systems by developing acclimated cultures on anode material which called as bioanode. The acclimation in MEC systems is commonly achieved by two approaches: (i) direct mode and (ii) indirect mode (Kumar et al., 2017). In direct mode, the acclimation procedure is directly started in MEC reactor; on the other hand, the latter (indirect) is composed of two steps procedure in which bare anode electrodes are first acclimated in MFC to develop bioanodes with highly abundant exoelectrogenic community (Kumar et al., 2017). Then, MFC-grown bioanodes are transferred to MEC reactor to start the operation (Kumar et al., 2017). Li et al. (2017) studied the indirect acclimation of mixed culture from cow dung compost using as an inoculum source to enhance the hydrogen production from corn stalk fermentation effluent in MEC. At first, fermentation effluent from a hydrogen producing bioreactor was inoculated into MFCs with the same operational conditions except the substrate which were selected as acetate and butyrate. After a reproducible

maximum voltage was obtained, acclimated bioanodes were put into MECs fed with corn stalk fermentation effluent as a substrate (Li et al., 2017). The results of the study revealed that acclimation has an important effect on the treatment of fermentation effluent for bioelectrochemical hydrogen production via MEC. Bioanodes acclimated with butyrate showed a significant enhancement in both COD removal efficiency (1.58-fold) and hydrogen generation (1.23-fold) compared to acetate acclimated bioanodes (Li et al., 2017).

2.3.2 Adaptation of pure cultures

Adaptation experiments with microorganisms are generally easy to establish and the common methods can be listed as (i) batch cultivation using serial dilution and (ii) chemostat cultures where all the conditions are kept as same except the interested condition such as feedstock type or concentration (Dragosits & Mattanovich, 2013). Lee et al. (2023) studied the adaptation of hyperthermophilic archaeon *Thermococcus onnurineus* NA1 to enhance biohydrogen production from food waste. In this study, batch cultivation via serial dilution as 100 times was achieved to adapt hyperthermophilic archaeon. In their study, adapted cells showed 10.8 and 14.7 times increase in cell density and sugar consumption compared to the parent strain in batch bioreactors. When the bioreactor fed with food waste, the adapted cultures revealed better performance than parent strain on hydrogen production rate which was about 3.5 times higher in the reactors with adapted culture (Lee et al., 2023). Recently, a bacterium *Rhodospirillum rubrum* was investigated to produce hydrogen using CO and acetate as carbon sources in dark fermentation (Rodríguez et al., 2021). To enhance the hydrogen production along with CO reduction, the strain was adapted to CO using fed-batch adaptation strategy. The authors stated that the adaptation to CO during bacterial growth enhanced the hydrogen production rate up to 27.2 mmol H_2/L.h while decreasing the operation time by 50% (Rodríguez et al., 2021).

Adaptation of pure cultures has gained an important attention in bioelectrochemical systems during the last decade since it is an easy-to-use method to develop beneficial phenotypic traits in industrial microbial strains (Sandberg et al., 2019). Adaptation of pure cultures is a relatively new approach in bioelectrochemical systems. In recent, Shi et al. (2021) studied the adaptation of *Sporomusa ovata*, which is a strict anaerobe, to molecular oxygen to improve the robustness of acetate production via microbial electrosynthesis (MES). A stepwise adaptation strategy in batch cultures was followed over 58 generations; then, the adapted strains showed a higher performance in MES system as converting electrical energy and carbon dioxide into acetate as 1.5 times faster compared to parent strain. The authors reported that the increase in oxygen tolerance of the strain results to enhancement of the performance and robustness of energy-storage bioprocess even in the presence of an inhibitor like oxygen (Shi et al., 2021).

2.4   Use of agro-industrial wastes as feedstocks for hydrogen production

Agro-industrial waste is defined as waste material produced as a result of different agro-industrial operations which includes animal manure and other wastes from farms, poultry houses and slaughterhouses; agricultural residues such as corn stover, wheat straw (Urbaniec & Bakker, 2015). Along with other agricultural biomass and forestry wastes, agro-industrial wastes are one of the main lignocellulosic biomasses (Soares et al., 2020). Lignocellulosic biomass is the most abundant raw materials having a complex structure of three main polymers as cellulose, hemicellulose and lignin (Soares et al., 2020). Cellulose and hemicellulose are the main desired polymers in the lignocellulosic materials for dark fermentation as they consist of glucose in case of cellulose and various hexoses and pentoses (i.e., xylose) for hemicellulose. On the other hand, lignin has a high resistance to biodegradation. Because of high sugar content, agro-industrial waste has a high potential as a feedstock for DF. Extensive research on fermentative hydrogen production of these biomasses has been carried out in recent years.

2.4.1 Plant biomass

The plant biomass includes straws, peels, cornstalks, sugarcane bagasse, leaves and grass that is not suitable for animal feeding. In addition, fast-growing energy plants rich is lignocellulosic structure such as energy poplar, miscanthus can be a valuable raw material as a substrate for hydrogen production (Łukajtis et al., 2018). Biodegradation of plant biomass has been interested by biotechnologists; however, the recalcitrance structure of the insoluble materials prevents the effective degradation of plant biomass to sugars. Hence, pretreatment of plant biomass has been utilized to decrease the resistance of raw materials and to release the sugars. Most studies on DF of plant biomass reported the application of different pretreatment methods to enhance hydrogen yield (Cui & Shen, 2012; Lin et al., 2017; Mankar et al., 2021). On the other hand, pretreatment processes are significantly energy intensive methods associated with high cost and lower efficiencies. In addition, the composition of plant biomass is highly heterogeneous from site to site. Therefore, the development of effective biohydrogen production from plant biomass has remained as a significant challenge. As an example of DF for unpretreated lignocellulosic plant biomasses, Ivanova et al. (2009) studied biohydrogen production potential from five different plant biomasses without chemical pretreatment by *C. saccharolyticus* at 70 ºC. Among all substrates, the highest hydrogen yield was obtained from wheat straw as 44.7 mL H_2/g dry biomass (Ivanova et al., 2009). In addition, it was reported that the hydrogen yield from unpretreated plant biomass in thermophilic conditions were significantly higher than mesophilic temperatures (Guo et al., 2010; Karlsson et al., 2008). Thus, thermophilic temperatures may have an advantage over mesophilic operations because of higher hydrolysis rate of unpretreated plant biomass at elevated temperatures (Guo et al., 2010).

2.4.2 Animal manure

Animal manure can be an important environmental concern due to release of greenhouses gases to atmosphere. Since it has a high carbohydrate content and buffer capacity, it is a promising feedstock alternative for DF. In the literature, manure or compost have been used in the studies on DF. Xing et al. (2010) investigated the potential of hydrogen production from acid-pretreated dairy manure via DF. The highest H_2 yield was 31.5 mL H_2/g VS with a hydrogen content of 38.6% (Xing et al., 2010). Another study for fermentative hydrogen production using pig slurry was conducted by Kotsopoulos et al. (2009) in a continuous operation at thermophilic (70 ºC) condition. The study revealed that short hydraulic retention time with thermophilic operation prevented the methane production and led to hydrogen generation (Kotsopoulos et al., 2009). In aforementioned study, although high temperature operation, low hydrogen yield as 3.65 mL H_2/g VS was reported from unpretreated pig slurry. Even though animal manure is a promising feedstock for DF, there is a need for optimization of hydrogen production including operation strategies or specific inoculum choice which will provide high yield without the need for feed pretreatment.

CHAPTER 3

MATERIALS AND METHODS

3.1   Dark fermentative hydrogen production

3.1.1   Inoculum, growth medium and cell growth

Active culture of *Caldicellulosiruptor bescii* (DSM 6725) was purchased from
DSMZ - Germany Collection of Microorganisms and Cell Cultures (Braunschweig,
Germany). *C. bescii* was initially grown in a slightly modified DSM 516 medium
and the composition of medium is given in Table 3.1.

Table 3.1 Modified DSM 516 growth medium

Constituent	Amount per L
NH_4Cl	0.33 g
KH_2PO_4	0.33 g
$MgCl_2.6H_2O$	0.33 g
$CaCl_2$	0.25 g
$NaHCO_3$	1.5 g
L-cystine	0.5 g
Crystalline cellulose	5.0 g
Yeast extract	0.5 g
Vitamin solution	10 mL
Trace element solution	1 mL

The vitamin solution contained the following (in mg/L): biotin, 4; folic acid, 4;
pyridoxine-HCl, 20; thiamine-HCl, 10; riboflavin, 10; nicotinic acid, 10; calcium
pantothenate, 10; vitamin B12, 0.2; p-aminobenzoic acid, 10; lipoic acid, 10. The
compounds of vitamin solution were dissolved in deionized water, after, the vitamin
solution was sparged and purged with high purity N_2 gas, which was sterilized via
filter sterilization using 0.22 μm polyethersulfone (PES) syringe filters. The trace
element solution contained the following (in g/L): $FeCl_2.4H_2O$, 2; $ZnCl_2$, 0.05;

$MnCl_2.4H_2O$, 0.05; H_3BO_3 , 0.05; $CoCl_2.6H_2O$, 0.05; $CuCl_2.2H_2O$, 0.03; $NiCl_2.6H_2O$, 0.05; EDTA (tetrasodium salt), 0.5; $(NH_4)_2MoO_4$, 0.05; $AlK(SO_4)_2 12H_2O$, 0.05. To prepare trace element solution, $FeCl_2.4H_2O$ was dissolved in 30 mL of 25% HCl (7.7 M) and total volume was adjusted to 1 L with deionized water. All the glassware were autoclaved at 121 °C for 15 min for sterilization prior to use. Then, remaining salts were added into the solution. All the components, except $NaHCO_3$, crystalline cellulose (Avicel® PH-101), L-cysteine and vitamin solution, were added and mixed thoroughly; then, the solution was sparged and purged with $N_2:CO_2$ (80%:20%) gas mixture for 20 min. The prepared medium was sterilized via autoclave at 121 °C for 15 min. Because of the heat-labile nature, $NaHCO_3$ and L-cystine solutions were prepared separately and filter-sterilized. A special protocol to prepare the crystalline cellulose solution was followed since crystalline cellulose granules have air inside due to the production procedure. For 10X stock solution, 25 g of crystalline cellulose was added into 500 mL deionized water in large thick-wall glass flask that had a connection to a vacuum line inside an anaerobic chamber. The solution was degassed via vacuum for 3 hours. After, 30 min cycle, including 25 min of vacuuming and 5 min of gassing with $N_2:CO_2$ (80%:20%), was repeated for 3 times (Figure 3.1). The solution was autoclaved for sterilization. Then, crystalline cellulose, $NaHCO_3$, L-cystine and vitamin solution were added into growth medium, and the final pH was adjusted to 7.00 ± 0.05 using either NaOH (10% w/v) or HCl (1 N). All liquid transfers to prepare growth medium and inoculations were achieved in anaerobic chamber (818-GB, Plas Labs, MI, USA) which contained high purity N_2 (100%) or $N_2:CO_2$ (80%:20%) gas as an inner atmosphere (Figure 3.2). All solutions were stored at 4 °C in the dark until they were used.

Actively growing *C. bescii* supplied by DSMZ was grown by ensuring anaerobic and aseptic conditions. First, the ratios of 1:10, 1:50 and 1:100 for inoculation were achieved based on the information provided by DSMZ. After serial inoculations, 10% inoculation was used, and all inoculations were incubated in a water bath (SBD-309 Şimşek Laborteknik, Ankara, Turkey) at 75 °C. The growth of *C. bescii* was

monitored via quantification of the cell density with a Thoma counting chamber (Assistent®, Sondheim vor der Rhön, Germany) using a phase-contrast microscope (Zeiss Axio Scope A1 Microscope, Oberkochen, Germany).

Figure 3.1 Preparation setup of crystalline cellulose solution
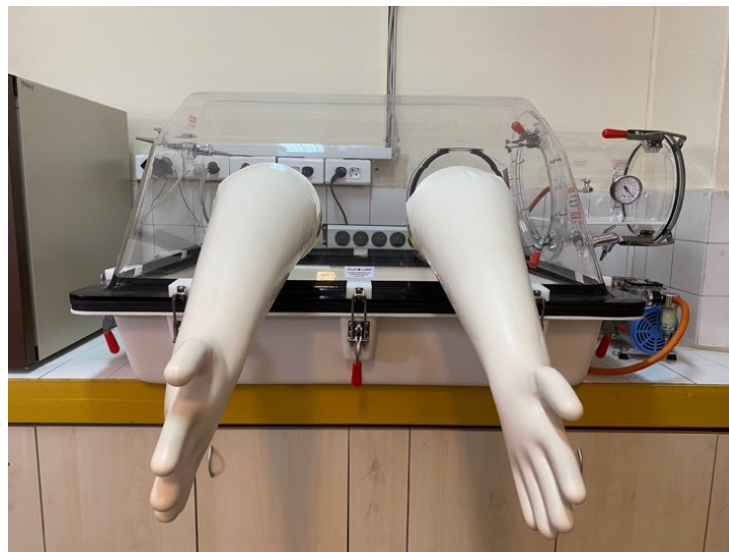
Figure 3.2. Anaerobic chamber used in the experiments

3.1.2   Experimental design and sets

In total, five experimental sets were conducted. Set 1 was operated as an initial biodegradability assessment of unpretreated cattle manure (UCM) by *C. bescii* for 10 days and to determine whether there is any significant inhibition caused by UCM. In Set 1, including controls, five types of reactors were operated. The types of reactors were (i) seed control (SC), (ii) pure substrate control (PC), (iii) UCM added test reactors (UCM), (iv) co-substrate reactors (CO-S) that received both crystalline cellulose (5 g/L) and UCM in corresponding concentrations (2.5, 5 and 10 g VS/L), and (v) negative control (NC) reactors where *C. bescii* inoculum was not added Figure 3.3. The purpose of the reactors can be described as follows: (i) SC reactors were operated to observe background gas and metabolite production, (ii) PC reactors were run to determine the activity of the culture, (iii) UCM reactors were the test reactors including three different concentrations of UCM (2.5, 5 and 10 g VS/L) and used to assess the degradability of UCM by *C. bescii*, (iv) CO-S reactors were run in order to examine any inhibitory effect of UCM on *C. bescii*, and (v) NC reactors were set to determine the impact of the native microorganisms present in UCM. Such a complex waste has never been used as a carbon source without sterilization in *C. bescii* reactors; therefore, in Set 1, UCM concentrations were kept below 10 g VS/L (Yilmazel & Duran, 2021). The inoculum used in this set was grown in the medium described in Section 3.1.1 with 5 g/L of crystalline cellulose (CC) as a carbon source.
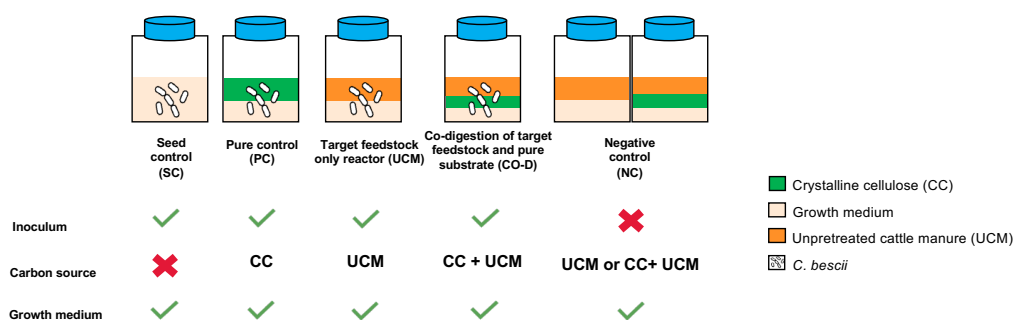
Figure 3.3 Experimental design of Set 1

In Set 2 (Control), Set 3 (Sparging), and Set 4 (Adaptation), biohydrogen production from UCM at higher concentrations (15, 25, and 50 g VS/L) was assessed (Figure 3.4). The experimental design of all sets was identical to Set 1 (initial biodegradability assessment) excluding CO-S reactors. Similar to Set 1, both in Control and Sparging sets, the inoculum (*C. bescii*) was grown with CC and operated for 44 days (Figure 3.4). In the Sparging (Set 3), all conditions were kept the same with the Control set, except gas sparging was applied after each headspace gas sampling for hydrogen measurements. High hydrogen partial pressure in the reactors may become inhibitory for *C. bescii* and decrease the hydrogen production yield (Basen et al., 2014; Kraemer & Bagley, 2007). Therefore, to lower hydrogen solubilization in liquid medium and prevent hydrogen build-up in the reactor headspace, gas sparging was applied with N_2:CO_2 (80%:20%) gas mixture at 5 bar for 3 mins after each gas measurement, and at the end of gas sparging, the total pressure was adjusted to atmospheric pressure.

In the Adaptation set (Set 4), increasing the tolerance of *C. bescii* to UCM was assessed to overcome the substrate inhibition due to high concentrations of UCM. Instead of CC-grown inoculum, UCM-adapted *C. bescii* culture was used as inoculum. In this set, there was no gas sparging applied. Adaptive laboratory evolution (ALE) is a well-known method to develop the capability of cultures under constant selection pressure and it was used for adaptation of *C. bescii* to UCM (Byrne et al., 2021; Dragosits & Mattanovich, 2013). In this study, serial batch cultivation in anaerobic serum bottles was performed. An aliquot of the culture was transferred to a new anaerobic serum bottle with fresh medium and increased concentration of UCM for the development of a specific more favorable phenotype by *C. bescii* to degrade UCM at higher concentrations without any inhibition. In detail, *C. bescii* was incubated in an anaerobic bottle with including 5 g/L of CC as a carbon source. *C. bescii* was incubated until hydrogen production was observed in the headspace. After ~ 18 hrs, hydrogen production was observed in the headspace; then, an aliquot of grown *C. bescii* from this bottle was transferred to another bottle where 5 g/L of CC was replaced with 2.5 g VS/L of UCM as a carbon source. About 20-24 hrs,

hydrogen production from 2.5 g VS/L was observed. Then, an aliquot of culture grown with 2.5 g VS/L of UCM was transferred to an anaerobic bottle which includes 5 g VS/L of UCM as a carbon source. The growth of *C. bescii* at 5 g VS/L of UCM was repeated for three consecutive incubations, finally, *C. bescii* grown in the last incubation (~ 20 hrs) was named as UCM-adapted culture and used as inoculum in the Adaptation set (Set 4). The reactor operation was lasted for 32 days.
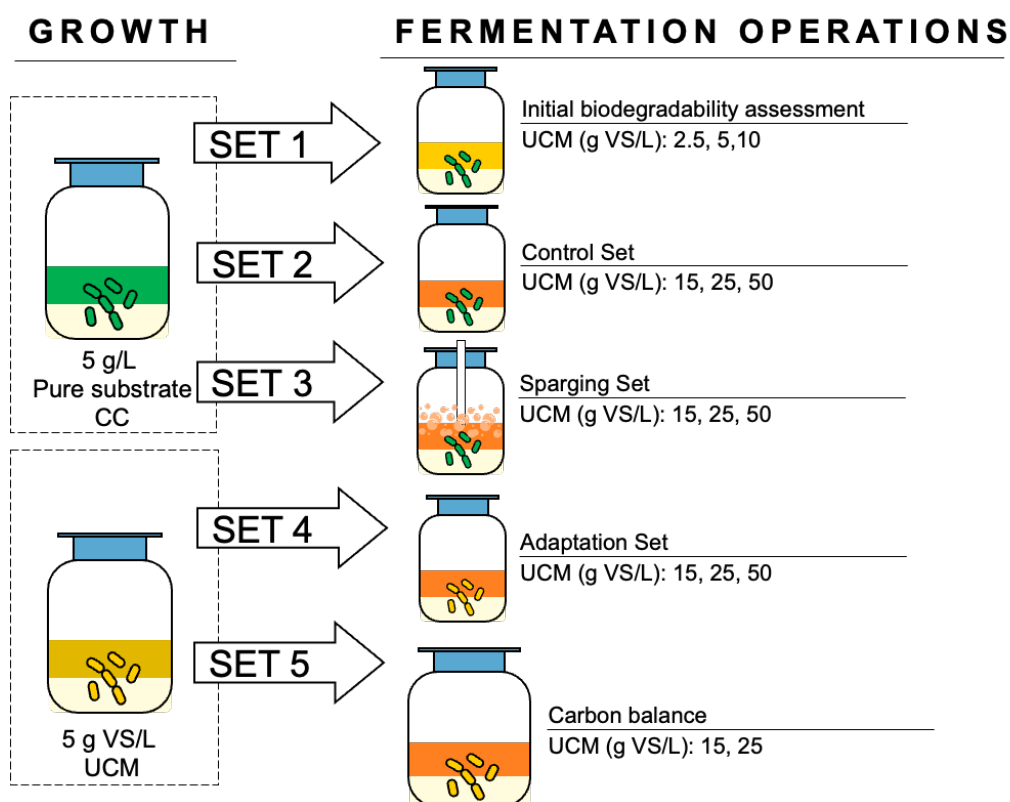
Figure 3.4. The summary of experimental sets operated in the study (CC: crystalline cellulose; UCM: unpretreated cattle manure)

In Set 5, the objective was to perform carbon balance to assess the biodegradation extent of UCM by adapted *C. bescii*. The active reactor volume was doubled (60 mL) and the total volume was 110 mL in this set, and UCM concentrations were set to 15 g VS/L and 25 g VS/L (Figure 3.4). The operation was continued for 50 days. The carbon balance was conducted at the end of batch operation. In Set 5, the inoculum was UCM-adapted *C. bescii*, prepared by following the same adaptation protocol in

52

Set 4. All reactors were run in triplicate on a batch mode and incubated in a water bath at 75 ± 1 °C.

3.1.3   Analytical methods

3.1.3.1   Cattle manure characterization

Cattle manure samples were collected from the feed tank of a biogas plant in Ankara, Turkey. It was blended for 15 mins for homogenization of the sample, and no other pretreatment was applied. The homogenized sample was called as unpretreated cattle manure (UCM) and stored at 4 °C until characterization (Table 3.2). The Standard Methods (APHA et al., 2005) were followed for the total solids (TS) (Section 2540B), volatile solids (VS) (Section 2540E), and chemical oxygen demand (COD) (Section 5220D) analysis. *C. bescii* is a cellulolytic microorganism; thus, the fiber composition of the feed is critical factor. Neutral detergent fiber (NDF), acid detergent fiber (ADF), and acid detergent lignin (ADL) are three major components for fiber content of manure (Wang et al., 1994). UCM samples were sent to NutriLab (Konya, Turkey) for the determination of fiber composition. Elemental analysis of UCM was performed in METU Central Laboratory.

Table 3.2 Characterization of unpretreated cattle manure

Parameters	Unpretreated cattle manure
Total solids (%)	11.2 ± 0.1
Volatile solids (% of TS)	80.9 ± 0.1
Total COD (g/L)	123.9 ± 9.9
Carbon (%)	40.1
Hydrogen (%)	5.06
Nitrogen (%)	0.72
Acid detergent fiber (ADF) (%)	31.58
Neutral detergent fiber (NDF) (%)	50.00
Acid detergent lignin (ADL) (%)	12.47
Hemicellulose (= NDF-ADF) (%)	18.42
Cellulose (= ADF-ADL) (%)	19.11
Lignin (ADL) (%)	12.47

3.1.3.2   Gas measurement

The total gas production was measured using a liquid displacement device. The compositions (H_2, CH_4, CO_2 and N_2) of the headspace gas samples were determined via a gas chromatograph (TRACE GC Ultra, Thermo Scientific, USA) equipped with a thermal conductivity detector (TCD) and two columns connected in series (CP-Moliseve 5A and CP-Porabond Q). The oven, injector and detector temperatures were set to 35 °C, 50 °C and 80 °C, respectively. The carrier gas was selected as helium at a constant pressure of 75 kPa. The injection of gas samples was done using GC syringe (VICI AG, USA) and the injection volume was 150 μL.

The calibration equations for H_2, CH_4, N_2 and CO_2 gases were obtained by 5-point triplicate gas injections of standard gas mixture between 50 μL and 250 μL. The standard gas mixture was consisted of 50% H_2, 30% CO_2, 10% CH_4 and 10% N_2. An example of calibration data and curve for H_2 is given in Table 3.3 and Figure 3.5 respectively.

Table 3.3 H_2 gas calibration for GC-TCD

Injection Volume (μL)	Trial	Peak Area	Mean	Standard Dev.	Coefficient of Variation (%)
50	1	8034	8118.67	264.37	3.26
	2	8415			
	3	7907			
100	1	16813	16671.33	489.14	2.93
	2	16127			
	3	17074			
150	1	24521	24415.67	548.71	2.25
	2	23975			
	3	24751			
200	1	32672	32488.67	14.14	0.04
	2	32142			
	3	32652			
250	1	39923	40416.67	324.56	0.80
	2	40945			
	3	40382			
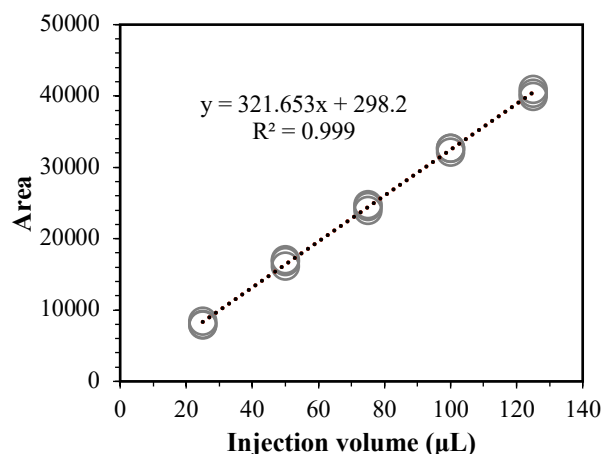
Figure 3.5 H$_2$ gas calibration curve and equation

3.1.3.3   Acetic acid measurement

Acetic acid measurements at the end of each operation for fermentation effluent were done by using a gas chromatograph (TRACE GC Ultra, Thermo Scientific, USA) equipped with a flame ionization detector (FID) connected to a free carboxylic acids analysis column (Nukol, Supelco, Germany). The carrier gas was helium with a flow rate of 6 mL/min dry air and H$_2$ gases were used as detector gases. The temperatures of inlet and detector were set to 250 °C and 280 °C, respectively. The temperature of oven was increased from 100 °C to 200 °C with a rate of 8 °C/min. The fermentation effluent samples were filtered through 0.22 μm pore-size PES syringe filters, diluted with deionized water in the range of the calibration curve, and sample pH was adjusted to below 2 by dilution of the samples with 1 N HCl with a ratio of 5:6 to ensure free forms of the organic acids were present. The injection volume was 2 μL which were done as manual injections using 10 μL liquid GC syringe. To prevent any contamination of the samples, the needle was cleaned with acetone before each injection, and the column was cleaned with methanol after every 3 injections. The calibration curve for acetic acid was achieved using 5-point triplicate calibration for the concentrations between the ranges of 0.7 mM and 10 mM (Table 3.4). Figure 3.6 presents the calibration curve for acetic acid.

Table 3.4 Acetic acid calibration for GC-FID

Concentration (mM)	Trial	Peak Area	Mean	Standard Dev.	Coefficient of Variation (%)
0.7	1	6571176	6538381.3	86008.5	1.3
	2	6440800			
	3	6603168			
1.0	1	8310185	8154696.0	204790.4	2.5
	2	8231245			
	3	7922658			
2.5	1	16834797	15559851.7	1211919.7	7.8
	2	14422744			
	3	15422014			
5.0	1	35102281	36658673.3	1425178.4	3.9
	2	37899866			
	3	36973873			
10.0	1	82385975	80175620.7	2054140.8	2.6
	2	78325296			
	3	79815591			
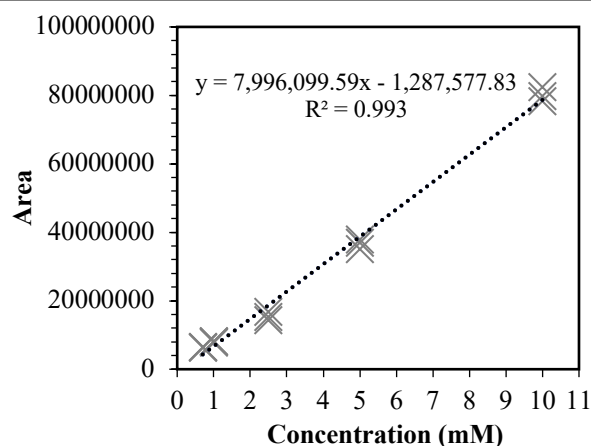
Figure 3.6 Acetic acid calibration curve and equation

3.1.3.4 Total sugar measurement

The total sugar content of the reactor effluents in Set 5 and initial sugar content of cattle manure were determined using the phenol-sulfuric acid method with glucose as a standard. First, 0.05 mL of 80% (w/v) phenol solution and 5 mL of concentrated sulfuric acid (H_2SO_4) solution were sequentially added into 2 mL of liquid sample. After 10 minutes, the samples were vortexed and placed into a water bath at 25 °C for 15 minutes. Then, the absorbance was read via a spectrophotometer (HACH,

USA) at 490 nm (Nielsen, 2013). Figure 3.7 shows the calibration curve and equation.
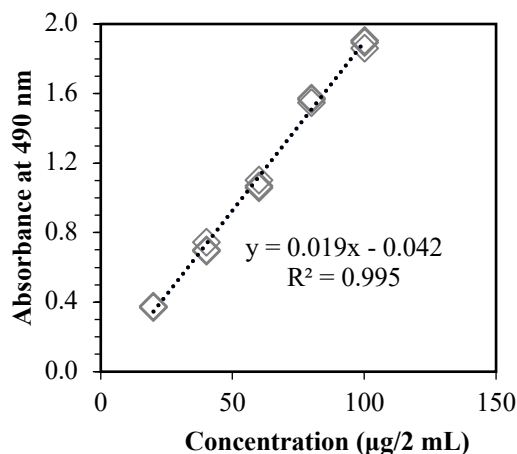
Figure 3.7 The calibration curve and equation for total sugar measurement

3.1.3.5 Protein measurement

In Set 5, prior to the inoculation, the protein content of *C. bescii* culture was determined by Bradford Assay Kit (Bio-Rad, USA) for carbon balance calculations. The 4.5 mL of samples taken from serum bottles were placed into a 5 mL falcon tubes and were centrifuged at 4500 rpm for 15 minutes. The calibration curve (Figure 3.8) for protein measurement was produced using bovine serum albumin (BSA) standards. 980 μL of Bradford Reagent was added to 20 μL BSA standards. Same dilution rate was also applied to the protein extracted samples. Cuvettes were incubated at room temperature for 5 minutes; then, measured with a spectrophotometer (Hach, USA) at 595 nm.
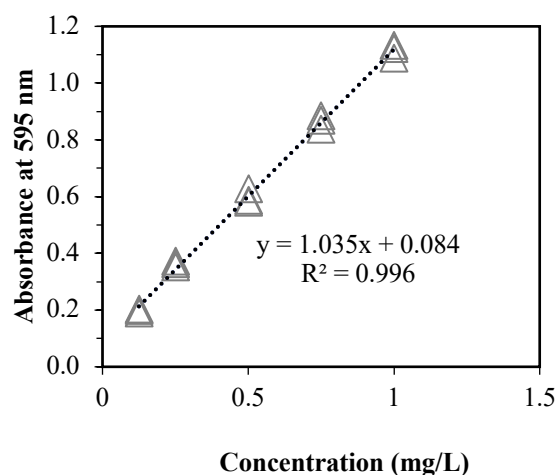
Figure 3.8 Total protein calibration curve and equation

3.1.4   Solubilization assay

Solubilization assays were performed at the end of batch operation for each reactor. It is a similar method to the measurement of total suspended solids except the pore size of the filter and the drying temperature are different. This is a common gravimetric method for plant biomass solubilization; therefore, it was used in this study to analyze the degradability of UCM. The solubilization assay for fermentation of UCM was applied as described in Zurawski et al. (2015) with minor modifications as follows: the reactor content was filtered by vacuum filtration through coarse filter papers (40-60 μm) (Macherey Nagel, Germany). The portion retained on the filter paper was washed two times with deionized water (total volume ~60 mL) at 75 °C and was oven dried at 75 °C until it reached a constant mass. Then, the mass retained on the filter was measured. To determine the initial mass present in a given reactor, an extra reactor of the same conditions (UCM concentration, volume etc.) was prepared (at t=0) and directly subjected to the same solubilization protocol before the reactor operation. The solubilization extent in a reactor was then determined from the mass difference of the recorded initial mass (measured at t=0) and the mass recorded at the end of the batch reactor.

3.1.5 Carbon balance

Carbon balance analysis was conducted for Set 5 reactors by following the protocol described in Kataeva et al. (2013). Larger size reactors (total volume of 110 mL, active volume of 60 mL) were operated to perform the carbon balance. The cell carbon (designated as inoculum), carbon-containing end products (CO_2, lactic acid, acetic acid and total sugar) were determined (explained in Section 3.1.3) for carbon balance. Microbial cell carbon was calculated from the protein amount of inoculum, assuming that the amount of carbon is equal to 50% of inoculum dry weight (Basen et al., 2014). At the end of the reactor operation, about 15% of growth was assumed and included in the carbon balances (Abreu et al., 2012).

3.2 Bioelectrochemical hydrogen production

3.2.1 Inoculum, growth medium and cell growth

Geoglobus acetivorans strain SBH6 (DSM 21716), *Geoglobus ahangari* strain 234 (DSM 27542) and *Ferroglobus placidus* strain AEDII12DO^T (DSM 10642) were purchased from DSMZ - Germany Collection of Microorganisms and Cell Cultures (Braunschweig, Germany). All three cultures were grown using same hyperthermophilic growth medium. The hyperthermophilic growth medium was supplemented with 10 mM acetate as electron donor and 56 mM Fe(III)-citrate (Sigma Aldrich, USA) as electron acceptor. The constituents of growth medium are given in Table 3.5. The steps followed for the preparation of growth medium are as follows: Fe(III)-citrate was dissolved in deionized water at ～95 °C for complete dissolution; then, the solution was cooled to room temperature on the stirrer. The pH of the iron solution was adjusted to 6.0 using 10% (w/v) NaOH. After, other components (salts, 10 mL of vitamin solution and 10 mL of trace element solution), except $NaHCO_3$ and Na-acetate, were added into the solution and the pH of solution was adjusted to 6.8-6.9 using 10% (w/v) NaOH. Finally, $NaHCO_3$ was added into

the solution, which was sparged and purged with gas mixture of N_2:CO_2 (80%:20%) for to make the solution anaerobic.

Table 3.5 Hyperthermophilic growth medium for electro-active archaea

Salts		Buffer	Electron donor	Electron acceptor
NH$_4$Cl	0.24 g/L			
KH$_2$PO$_4$	0.40 g/L			
MgCl$_2$.6H$_2$O	4.30 g/L	NaHCO$_3$ 2.5 g/L	Na-Acetate 8.2 g/L	Fe(III)-citrate 13.7 g/L
CaCl$_2$.2H$_2$O	0.14 g/L			
NaCl	18 g/L			
KCl	0.34 g/L			

Vitamin Solution		Trace element solution	
Pyridoxine-HCl	10 mg/L	Nitriloacetic Acid	1.5 g/L
Thiamin-HCl	5 mg/L	MgSO$_4$. 7H$_2$O	3.0 g/L
Riboflavin	5 mg/L	NaCl	1.0 g/L
Nicotinic Acid	5 mg/L	MnSO$_4$. 7H$_2$O	0.5 g/L
Calcium Pantothenate	5 mg/L	NiCl$_2$. 6H$_2$O	0.2 g/L
Vitamin B12	5 mg/L	FeSO$_4$. 7H$_2$O	0.1 g/L
p-Aminobenzoic Acid	5 mg/L	CoCl$_2$	0.1 g/L
Lipoic (Thioctic) Acid	5 mg/L	CaCl$_2$. 2H$_2$O	0.1 g/L
Biotin	2 mg/L	ZnSO$_4$	0.1 g/L
Folic Acid	2 mg/L	CuSO$_4$. 5H$_2$O	0.1 g/L
		AlK (SO$_4$)$_2$	0.01 g/L
		H$_3$BO$_3$	0.01 g/L
		Na$_2$MoO$_4$. 2H$_2$O	0.01 g/L
		Na$_2$SeO$_3$	0.01 g/L
		Na$_2$WO$_4$	0.01 g/L

Na-acetate was separately prepared and added into the hyperthermophilic growth medium in an anaerobic chamber, and final pH of the growth medium was adjusted to 6.85 ± 0.05. Before use, all glassware was autoclaved at 121 °C for 15 minutes for sterilization. Inoculations and liquid transfers were accomplished inside an anaerobic chamber. Inoculations were made at the ratio of 1:10 and in the serum bottles including N_2:CO_2 (80%:20%) atmosphere at dark. *G. acetivorans* and *G. ahangari* were incubated at 80 °C, *F. placidus* was incubated at 85 °C. To prevent any cross-contamination, the inoculations for each exoelectrogenic archaea were achieved in different time periods, and the anaerobic chamber was sterilized with ethanol before and after each session. The laboratory supplies were replaced with new sterile ones before each inoculation.

3.2.2 Adaptation of *G. acetivorans* to dark fermentation effluent

A serial transfer technique was used to adapt pure culture exoelectrogen *G. acetivorans* to DF effluent, so that it can produce high stable current density, which in turn will increase hydrogen production in MECs. Adaptation experiments were started with a 10% transfer from acetate-grown *G. acetivorans* culture into the sealed tubes containing same hyperthermophilic growth medium except the carbon source was replaced from 10 mM acetate to co-substrate of pure acetate:DF effluent (50%:50% v/v, total of 10 mM acetate). After the growth was observed for three serial inoculation, co-substrate grown pure cultures were transferred to a hyperthermophilic growth medium including only DF effluent (consisting of 10 mM acetate) as an electron donor. With this stepwise serial transfer procedure, the growth of *G. acetivorans* culture was achieved in all serial inoculations that are supplemented with only DF effluent after 18 inoculations.

3.2.3 MEC Construction and Operation

Single chamber Mini-MECs with an active volume of 5 mL were constructed with materials as described previously (Kas & Yilmazel, 2022). Briefly, commercial graphite plate (Grade GM-10, dimensions: 1.5 cm x 1.0 cm x 0.3 cm) was used as an anode material and stainless-steel (SS) mesh (Type 304, mesh size 50, dimensions: 1.5 cm x 1.0 cm) was selected as a cathode material in Mini-MECs (Figure 3.9). Mini-MEC reactors were used in Set 1 including Run 1.1 and Run 1.2. For Set 2 (Run 2.1, Run 2.2 and Run 2.3), single chamber MECs were constructed with borosilicate bottles which have 65 mL of active volume (130 mL of total volume) (Figure 3.9). A graphite plate (Grade GM-10, dimensions: 2.5 cm x 2.5 cm x 0.3 cm) and a carbon fiber brush (2.5 cm long and 2.5 cm in diameter) were used as anode materials, and cathode was stainless-steel (SS) mesh (Type 304, mesh size 50, dimensions: 2.5 cm x 2.5 cm) (Figure 3.9). The electrode preparation protocols for graphite plate and SS mesh were applied as described in Yilmazel et al. (2018):

graphite electrodes were sandpapered using 400, 800 and 1500 grit size sandpapers and left in 1 N HCl for overnight. The same procedure for sandpapering was applied for SS mesh electrodes and the electrodes were sonicated with deionized water. Carbon fiber brush electrodes were pretreated at 450 ºC for 30 min. All single chamber MECs were purged with N_2:CO_2 (80%:20%) gas mixture to remove any oxygen, and autoclaved before any medium addition for sterilization (121 ˚C, 20 minutes). Single chamber MECs were filled with hyperthermophilic growth medium (conductivity ~ 26 mS/cm at room temperature) excluding ferric citrate, inside an anaerobic chamber.

For Set 3, two-chamber MECs were constructed and operated in H-shaped glass bottles which were consisted of an anode compartment (active volume of 90 mL) and a cathode compartment (active volume of 90 mL) separated by an anion exchange membrane (AMI 7001, Membranes International, Glen Rock, NJ) (Figure 3.9). All two-chamber reactors contained carbon fiber brush as anode and SS mesh as cathode. The anode compartment had received the same hyperthermophilic medium with single chamber MECs, and the cathode chamber was filled with 1 M KCl. The cathode chamber pH was adjusted to 10 via addition of NaOH (10% w/v). The two-chamber MECs were autoclaved for sterilization (20 min at 121 ˚C) before any inoculation and medium addition and inoculated with actively growing *G. acetivorans* at a 10% volume in an anaerobic chamber.

Run 2.1, Run 2.3 and Run 3 were operated as duplicate. Run 1.1, Run 1.2 and Run 2.2 were operated as triplicate, which were placed in an incubator (ThermoFisher Scientific, USA) at 80 ˚C. Acetate-grown *G. acetivorans* was used as an inoculum in Run 1.1, Run 2.1, Run 2.2, Run 2.3 and Run 3. In Run 1.2, hyperthermophilic enriched co-cultures were used as an inoculum. The adapted culture was utilized in Run 2.2, Run 2.3 and Run 3 as an inoculum source. The operation mode of all reactors was fed-batch. At the end of each cycle, hydrogen production in the headspace was determined via GC. To start a new cycle in single chamber MECs, the reactor content was replaced with fresh medium inside the

anaerobic chamber, and the headspace was purged with N_2:CO_2 (80%:20%) gas mixture. In the case of two-chamber MECs, the medium in anode part of two-chamber MECs was replaced and the catholyte (1 M KCl solution) in the cathode chamber was also replenished. Anode chamber was then purged with N_2:CO_2 (80%:20%) gas mixture and cathode chamber was purged with N_2 gas to remove any other gases. In the first cycle of all reactors, 10% of the liquid inside the reactor was kept inside, while all reactor content was replaced with fresh medium in the following cycles. During the operation of MECs, applied voltage was selected as 0.7 V which was same as in the previous works related iron reducing hyperthermophilic archaea (Kas & Yilmazel, 2022; Yilmazel et al., 2018). MECs were operated using a power supply (Marxlow, China) with a 10 Ω resistor connected in series for recording voltage using a multimeter (Keysight Technologies, USA) recording the voltage at 10 min intervals.
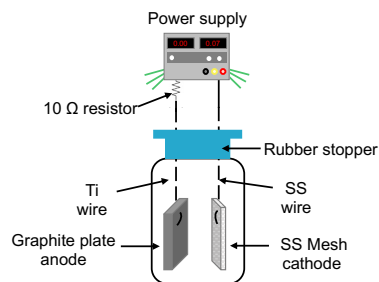
Figure 3.9 Reactor configurations (A) Mini-MEC, (B) Single chamber MEC and
(C) Two-chamber MEC

3.2.4   Experimental design and sets

The experimental design consisted of 3 main sets: (1) culture selection, (2) DF effluent utilization, and (3) two-chamber operation (Figure 3.10). The reactors for Set 1 were operated in Mini-MECs. Set 2 was referred here as ''DF effluent utilization'' which includes 3 different experimental runs and operated in single-chamber MECs with an active volume of 65 mL. Set 3 (two-chamber operation) was conducted using double-chamber (H-shaped cell) reactors.
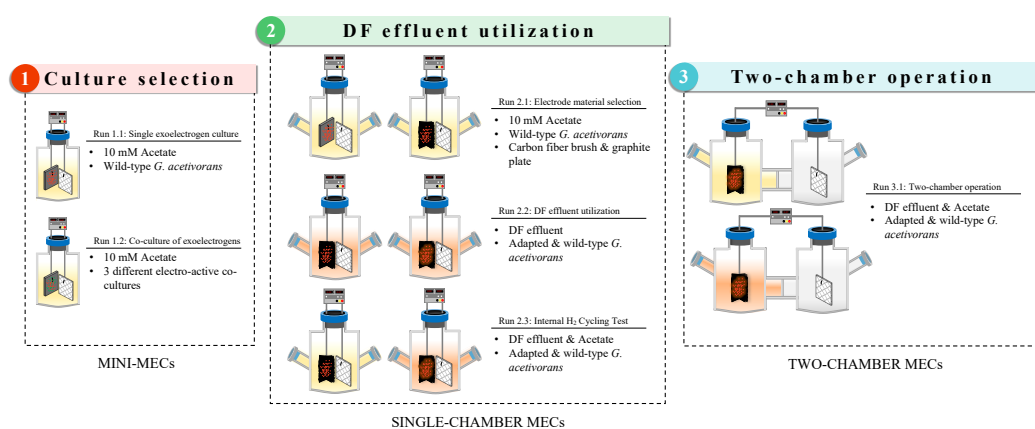
Figure 3.10 Experimental design of bioelectrochemical hydrogen production sets

3.2.4.1   Experimental runs of Set 1: Culture selection

In Set 1, the reactors were fed with 10 mM pure acetate as substrate. In Run 1.1, Mini-MECs were operated for 55 days as triplicate including 4 different groups as: (1) seed control, (2) abiotic control, (3) open-circuit control and (4) test reactors (Table 3.6). The purpose of Run 1.1 operation was to observe the current production by *G. acetivorans* in Mini-MECs and to compare the results to previous studies with *G. acetivorans* (Kas & Yilmazel, 2022) and with closely related species (Yilmazel et al., 2018). The operation was completed after 5 cycles and the current production became stable for 4 cycles (excluding the first cycle). During the operation, a new cycle was started by replacing the total reactor content with new media when the

current production dropped below 0.3 mA. The reactor headspace was also replenished with $N_2:CO_2$ (80%:20%) gas mixture after each medium replacement.

Table 3.6 Summary of the reactors operated in Run 1.1

Reactor group	Inoculum	External Voltage	Electron donor
Seed control (SC)	*G. acetivorans*	0.7 V	-
Abiotic control (AC)	-	0.7 V	Acetate
Open-circuit control (OC)	*G. acetivorans*	-	Acetate
Test reactor	*G. acetivorans*	0.7 V	Acetate

The aim of the Run 1.2 was to construct enriched hyperthermophilic exoelectrogenic cultures for enhanced hydrogen production in MECs. The three hyperthermophilic cultures have been isolated from different places in the world yet they can be found similar places because of their growth requirements, therefore, possible synergistic effects between them could be beneficial for hydrogen production. Run 1.2 was operated similar to Run 1.1 experiments, except the inoculum source was a co-culture. In Run 1.2, three different co-cultures of the exoelectrogens were used (Table 3.7) and the operation time was 12-14 days. These co-cultures were grown in serum bottles in the same hyperthermophilic growth medium (Table 3.5) inoculating each exoelectrogenic culture as the ratio of 1:20 to the serum bottles. Then, these co-cultures were used to inoculate Mini-MECs. The co-cultures were mixtures of (i) *G. ahangari* and *G. acetivorans* (AH-AT), (ii) *G. acetivorans* and *F. placidus* (AT-FP), and (iii) of *G. ahangari* and *F. placidus* (AH-FP).

Table 3.7 Summary of the reactors operated in Run 1.2

Reactor group	Co-culture inoculum	External Voltage	Electron donor
Seed control (SC)	AH-AT AT-FP AH-FP	0.7 V	-
Abiotic control (AC)	-	0.7 V	Acetate
Open-circuit control (OC)	AH-AT AT-FP AH-FP	-	Acetate
Test reactor	AH-AT AT-FP AH-FP	0.7 V	Acetate

3.2.4.2   Experimental runs of Set 2: DF effluent utilization

After Mini-MEC operations were completed, *G. acetivorans* was selected as the culture to further investigate hydrogen production in MEC system. To investigate the potential of hyperthermophilic archaeon *G. acetivorans* in MEC, three different experimental runs in Set 2 were operated as: Run 2.1: electrode material selection, Run 2.2: DF effluent utilization, and Run 2.3: internal hydrogen cycling (Figure 3.10).

The anode material is an important component of the process since the biofilm formation and electron transfer in MECs is affected by the features of the anode. Increasing the available surface area of anode enhances the current density as it enables higher amount of microbial attachment (Park et al., 2022). In most of the previous hyperthermophilic BES studies carbon block type electrodes were used as an anode material, yet there is no comparison of different anode materials (Kas & Yilmazel, 2022; Yilmazel et al., 2018). In Run 2.1, two different electrodes (as graphite plate and carbon fiber brush) were tested as an anode material using 10 mM pure acetate as a sole carbon source in single chamber MECs. Hyperthermophilic pure culture of *G. acetivorans* is grown in hyperthermophilic medium (explained in Section 2.1) including 10 mM acetate as an electron donor and used as an inoculum in Run 2.1. The experimental design of MECs included four types of reactors: (1) seed control, (2) abiotic control, (3) open-circuit control, and (4) test reactors (Table 3.8).

Table 3.8 Summary of the reactors operated in Run 2.1

Reactor group	Inoculum	External Voltage	Anode electrode	Electron donor
Seed control (SC)	*G. acetivorans*	0.7 V	CFB GP	-
Abiotic control (AC)	-	0.7 V	CFB GP	Acetate
Open-circuit control (OC)	*G. acetivorans*	-	CFB GP	Acetate
Test reactor	*G. acetivorans*	0.7 V	CFB GP	Acetate

CFB: Carbon fiber brush; GP: Graphite plate

DF effluent is a promising substrate for MEC process since it is significantly rich in acetate. Yet, the use of such a complex effluent as a feedstock may affect the performance of MEC operation. In Run 2.2, the potential of DF effluent utilization by pure culture *G. acetivorans* was tested in single chamber MECs with carbon fiber brush as an anode. DF effluent was obtained from Part 1-Dark fermentative hydrogen production experiments which were hyperthermophilic reactors fed with unpretreated cattle manure. DF effluent was filtered using a coarse filter paper (40-60 µm) to separate the solid and liquid portions, and the liquid portion was used as a substrate in MECs. Hyperthermophilic medium including same minerals and vitamins was amended with DF effluent (consisting of 10 mM acetate) instead of pure acetate as an electron donor (conductivity ~ 28 mS/cm). Acetate-grown *G. acetivorans* culture (wild-type) and DF-adapted cultures were used as an inoculum in this run. In order to enhance the capability of hyperthermophilic *G. acetivorans* to utilize DF effluent, stepwise adaptation strategy was followed for the growth of adapted inoculum (described in Section 2.2), which is named as DF-adapted culture. The same experimental design used in Run 2.1 was followed (Table 3.9).

Table 3.9 Summary of the reactors operated in Run 2.2

Reactor group	Inoculum	External Voltage	Electron donor
Seed control (SC)	Adapted *G. acetivorans* Wild-type *G. acetivorans*	0.7 V	-
Negative control (NC)	-	0.7 V	DF effluent
Open-circuit control (OC)	Adapted *G. acetivorans* Wild-type *G. acetivorans*	-	DF effluent
Test reactor	Adapted *G. acetivorans* Wild-type *G. acetivorans*	0.7 V	DF effluent

The ability of internal hydrogen cycling phenomenon of hyperthermophilic *G. acetivorans* was previously shown using Midi-MECs with the wild type and proven that there is internal hydrogen cycling (Kas & Yilmazel, 2022). In this context, to compare the internal hydrogen cycling of the adapted culture and the wild type *G. acetivorans* internal hydrogen cycling test was conducted using single chamber MECs consisting of carbon fiber brush as anode (Run 2.3). For the first two cycles,

carbon source was present: the reactors were fed with hyperthermophilic MEC medium DF effluent (10 mM acetate; DF-adapted culture as an inoculum) and for ACE-fed WT reactors, 10 mM pure acetate was used as a carbon source in hyperthermophilic MEC medium. After two cycles, the reactor medium was replaced with a medium lacking any carbon source and headspace was purged with a gas mixture of N_2:CO_2 (80%:20%). In the fourth cycle, reactor headspaces were pressurized with a gas mixture of H_2:CO_2 (80%:20%) at 200 kPa in which the aim of the operation was to supplement hydrogen gas as a sole electron donor as described earlier (Yilmazel et al., 2018). The three cycles of (1) sole electron donor as acetate or DF effluent, (2) no electron donor, and (3) H_2 as the sole electron donor was repeated one more time. Finally, to observe whether there is any recovery of current generation, reactors were operated by changing the electron donor from H_2 to a carbon source.

3.2.4.3   Experimental run of Set 3: Two-chamber operation

Two-chamber MECs were operated as duplicates in Set 3 to test the current generation from a carbon source as a sole electron donor by acetate grown and DF-adapted cultures preventing any H_2 presence in the anode chamber. The advantage of using two-chamber is that there is no H_2 in the anode chamber. Each MECs consisted of two 150 mL compartments separated by an anion exchange membrane (AMI 7001, Membranes International, Glen Rock, NJ). Anode compartments of acetate-fed reactors (ACE-fed WT) received hyperthermophilic medium supplemented with 10 mM acetate as an electron donor inoculated with acetate grown *G. acetivorans*, and other two MECs were fed with same minerals and vitamins but supplemented with DF effluent (consisting of 10 mM acetate) as a sole electron donor inoculated with DF-adapted culture (Table 3.10). The cathode compartment of all two-chamber MECs received 1 M KCl (pH of 10). The carbon fiber brush was used as an anode electrode and SS mesh was used as a cathode electrode.

Table 3.10 Summary of the reactors operated in Run 3.1

Reactor group	Inoculum	External Voltage	Electron donor
Test reactor	Adapted *G. acetivorans* Wild-type *G. acetivorans*	0.7 V	DF effluent Acetate

3.2.4.4 Operational parameters of experimental sets

All reactors except open-circuit controls were operated with an applied voltage of 0.7 V and the operation temperature was set to 80 °C. Current generation was monitored throughout the reactor operations. Hydrogen production was analyzed at the end of each cycle before replacing the spent medium with fresh hyperthermophilic MEC medium and the consumption of acetate was determined by measuring acetate concentration of the reactor effluents. Cycling voltammetry (CV) analysis was done for Run 2.1, Run 2.2 and Set 3. The image analyses using scanning electron microscopy (SEM) and confocal laser scanning microscopy (CLSM) were conducted for Run 2.1 and Run 2.2 after the test period was completed.

3.2.5 Analytical methods

3.2.5.1 Dark fermentation effluent characterization

DF effluent was collected at the end of DF operation conducted with 15, 25 and 50 g VS/L of unpretreated cattle manure. DF effluents were pooled together, and the characterization analyses were achieved as described in Chapter 3.1.3. The characterization of DF effluent is given in Table 3.11.

Table 3.11 Characterization of DF effluent

Parameters	Unpretreated cattle manure
Total solids (%)	1.91 ± 0.01
Volatile solids (% of TS)	0.92 ± 0.03
Total COD (mg/L)	23108 ± 102
pH	5.91 ± 0.17
Acetic acid (mM)	85.19 ± 0.24

3.2.5.2   Hydrogen gas measurement

The total gas production of Mini-MEC reactors (Set 1) was measured by glass syringe (20 mL), and due to larger volume of total gas production a liquid displacement device was used to find the total gas production of MEC reactors (Set 2 and Set 3). The headspace gas compositions of the reactors were determined as described in Chapter 3.1.3.2, except, the injection volume was 250 μL. An example of calibration data and curve for H_2 is given in Table 3.12 and Figure 3.11.

Table 3.12 H_2 gas calibration for GC-TCD

Injection Volume (μL)	Trial	Peak Area	Mean	Standard Dev.	Coefficient of Variation (%)
100	1	16730	16939.7	361.3	2.13
	2	17448			
	3	16641			
200	1	31416	30566.3	757.7	2.48
	2	30707			
	3	29576			
300	1	44487	45262.0	832.5	1.84
	2	46417			
	3	44882			
400	1	57921	57184.0	1882.5	3.29
	2	59031			
	3	54600			
500	1	72859	70814.5	149.5	0.21
	2	70964			
	3	70665			
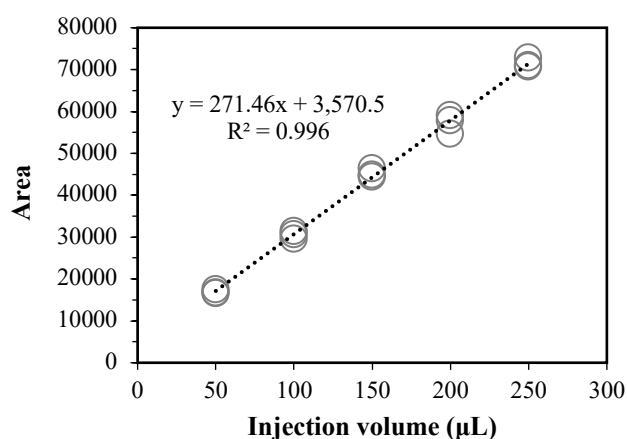
Figure 3.11 H_2 gas calibration curve and equation

3.2.5.3 Acetic acid measurement

Acetic acid measurements at the end of each cycle for reactor supernatant were done as described in Chapter 3.1.3.3. The acetic acid calibration was done for lower acetic acid concentrations (0.1 mM – 1.0 mM). Table 3.13 presents the calibration data and Figure 3.12 shows the calibration curve and equation.

Table 3.13 Acetic acid calibration data (0.1-1 mM)

Concentration (mM)	Trial	Peak Area	Mean	Standard Dev.	Coefficient of Variation (%)
0.1	1	335710	353164.7	12654.4	3.6
	2	365313			
	3	358471			
0.3	1	805632	762063.7	42094.7	5.5
	2	775412			
	3	705147			
0.5	1	1636435	1766192.0	91825.8	5.2
	2	1826563			
	3	1835578			
0.7	1	2139964	2254467.3	81920.2	3.6
	2	2296451			
	3	2326987			
1.0	1	3286489	3282491.3	68510.6	2.1
	2	3196656			
	3	3364329			

$y = 3,340,354.4x - 53,308.5$
$R^2 = 0.985$
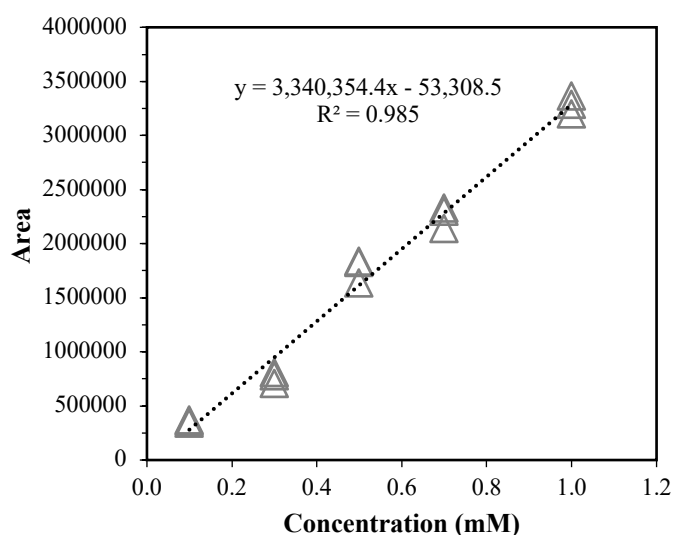
Figure 3.12 Acetic acid calibration curve and equation (0.1-1 mM)

3.2.5.4   Ferrous iron measurement

Ferrous iron (Fe(II)) concentration was measured to assess the growth of *G. acetivorans* since it is dependent on ferric iron (Fe(III)) reduction (as an electron acceptor) to ferrous iron for microbial growth (Slobodkina et al., 2009). The phenanthroline method (APHA et al., 2005) was used to measure ferrous iron concentration of the samples taken from growth bottles during incubation. The calibration curve was constructed using hyperthermophilic growth medium as a standard iron solution which included 56 mM ferric iron; then, it was diluted to 1 mM, 5mM, 10 mM, 15 mM and 20 mM to use as standard solutions. Since the 1,10-phenanthroline is a specific reagent to measure ferrous iron, all ferric iron should be reduced to ferrous iron; therefore, hydroxylamine hydrochloride was used as the reducing agent. 1 mL of hydroxylamine hydrochloride solution was added into volumetric flasks containing standard solutions. Then, 20 mL 1,10-phenanthroline solution was added and the solutions were mixed well. After waiting 2-3 minutes for color development, the absorbance of each solution was measured at 510 nm. After calibration curve was obtained (Figure 3.13), the accuracy check was achieved using ferrous ammonium sulfate solution (1 g/L (17.9 mM) of ferrous iron).
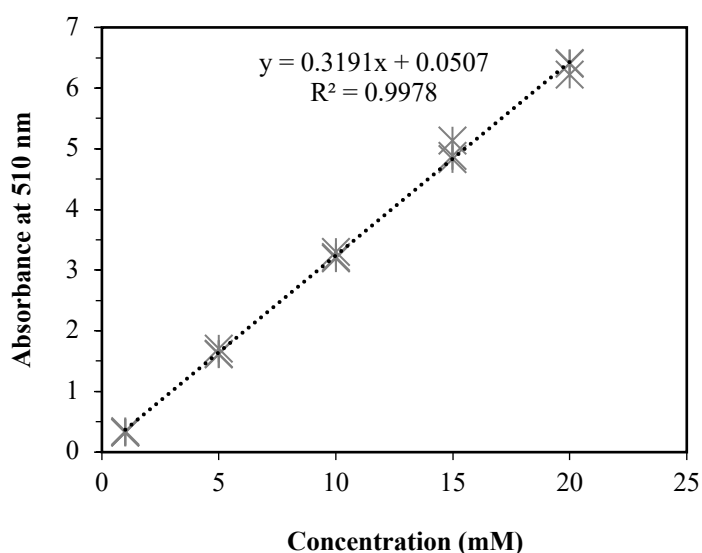
Figure 3.13 Ferrous iron calibration curve

3.2.6   Calculations

3.2.6.1   Current density

The current production of reactors was continuously monitored as the voltage across the external resistor (10 Ω) connected to the anode electrode. Current density (j) was determined according to Ohm's law, which is normalized to the total anode surface area (A) and to the active volume of the reactor (V) which is shown as J_v (Equation 3-1).

$$j\left(\frac{A}{m^2}\right) = \frac{I}{A} = \frac{V}{R.A} \qquad\qquad j_v\left(\frac{A}{m^3}\right) = \frac{I}{v} \qquad\qquad\qquad \text{(Equation 3-1)}$$

3.2.6.2   Coulombic efficiency

Coulombic efficiency (C_E) is the ratio of charge passed through the electrode theoretically to actual transferred amount. In other words, it can be defined as the ratio of measured electrons from current generation to electrons that are available from substrate removal. C_E was calculated dividing total coulombs by converting the acetate consumption to the total coulombs consumed (Equation 3-2). Acetate consumption was calculated as the difference between the acetate concentration at initial for each cycle (10 mM) and measured acetate concentration at the end of each cycle. Total coulombs were calculated by the integration of current over time. I is the current, F is the Faraday's constant (96,485C/mol.e$^-$) and n_{th} is acetate consumption converted to Coulombs (eight electrons per acetate, using g COD/g acetate conversion rate of 1.07) (D. Call & Logan, 2008).

$$C_E \, (\%) = \frac{\int_{t=0}^{t} I dt}{n_{th}} \, x \, 100 \qquad\qquad\qquad \text{(Equation 3-2)}$$

3.2.6.3   Cathodic hydrogen recovery

Cathodic hydrogen recovery, r_{cat}, was calculated (Equation 3-3) from the amount of H_2 (mole H_2) measured (n_R) dividing by the H_2 (mole H_2) that could be produced based on the current measurement (n_E) which was estimated by the integration of the area under the current density curve and dividing into the Faraday's constant (D. Call & Logan, 2008).

$$r_{cat} (\%) = \frac{n_R}{n_E} \text{ x } 100 = \frac{n_R}{\frac{\int_{t=0}^{t} I dt}{2F}}$$ (Equation 3-3)

3.2.6.4   Hydrogen production rate

The volumetric maximum hydrogen production rate (Q_{H_2}) was determined according to Equation 3-4 (Logan et al., 2008):

$$Q_{H_2} \left(\frac{m^3 \ H_2}{m^3 \ \text{active volume . day}}\right) = \frac{J_v \left(\frac{A}{m^3}\right).r_{cat}(\frac{C}{s}A^{-1}).(0.5 \frac{mol \ H_2}{mol \ e^-})(86400 \frac{s}{d})}{F.(\frac{C}{mol \ e^-})c_g(T)(\frac{mol \ H_2}{L})(\frac{10^3 L}{m^3})}$$ (Equation 3-4)

Where $J_v \left(\frac{A}{m^3}\right)$ is the current averaged over six hours of peak production and normalized to active volume, $c_g \left(\frac{mol}{L}\right)$ is the molar density of hydrogen gas at reactor temperature (K) and 1 bar, r_{CAT} is the cathodic hydrogen recovery, F is the Faraday' constant (96,485 C/mol.e⁻).

3.2.7   Biofilm analyses

3.2.7.1   Electrochemical analysis

CV is a powerful electrochemical method usually used to examine the reduction and oxidation processes of molecular species (Elgrishi et al., 2018). CV analysis was performed to examine the extracellular electron transfer by *G. acetivorans* biofilm to anode, using a potentiostat (Gamry Instruments, USA) with an Ag/AgCl (3.5 M

KCl) reference electrode (CORRTEST, China) and scan rate of 1 mV/s at 80 °C. Potential values reported are versus Ag/AgCl equivalent to + 165 mV vs. SHE at the reactor operation temperature of 80 ºC. CV analysis of anode was achieved in the range of -0.7 V to 0.2 V vs. Ag/AgCl for all reactors. CV analysis was performed under different conditions as turnover (with an electron donor) and non-turnover (without electron donor), which were analyzed at the peak current of the last cycle of respective reactor operation. CV analysis of negative and open-circuit controls were also performed for only Run 2.1, Run 2.2. and Set 3 following same procedure with turnover and non-turnover conditions.

3.2.7.2   Scanning electron microscopy (SEM)

The anodes of MEC reactors (Run 2.1 and Run 2.2) were sacrificed for SEM analysis of biofilms after the reactor operation was completed. The graphite plate anodes were cut into small pieces with a sterile lancet in the sterile laminar hood. The carbon fiber brush samples were collected from the electrodes at the end of cycles with a sterile scissor. For SEM imaging, the samples were placed into separate petri dishes filled with 4% paraformaldehyde (PFA) solution in 0.1 M PBS (pH 7.4) and waited at 4 ºC for 8 hours. The samples were washed three times with 0.1 M PBS solution and five minutes intervals. Series of dehydration was done with 25%, 50%, 75%, 95% and 100% ethanol each for 3 times for a duration of five minutes as described elsewhere (Kas & Yilmazel, 2022). Fixed anode samples were kept in a 100% fresh ethanol solution until air drying, that is performed in the sterile fume hood at room temperature. After fixation, samples were sent for Au/Pd coating and SEM imaging to METU-Central Laboratory.

3.2.7.3   Confocal laser scanning microscopy (CLSM)

For CLSM analysis, the anode samples for Run 2.1 and Run 2.2. reactors were collected immediately after the reactor operation inside of the anaerobic chamber

with a sterile scissor, during this time the anaerobic chamber was made dark by covering its top. The collected samples were washed with 1X wash buffer to remove the residues on the anode surfaces. With Bacterial Viability Assay Kit (ab189818, ABCAM, UK), according to instructions, the samples were stained for live/dead observation in dark anaerobic chamber filled with N_2:CO_2 (80%:20%) mixture gas and, the observation was achieved using confocal laser scanning microscopy (LSM 510, Zeiss, Germany) in the METU Central Laboratory.

CHAPTER 4

RESULTS AND DISCUSSION

4.1   Dark fermentative hydrogen production

4.1.1   Growth of *Caldicellulosiruptor bescii*

C. bescii was grown in growth medium (Table 3.1) including 5 g/L of crystalline cellulose as a carbon source which is insoluble in water. Due to its complex structure compared to cellobiose, crystalline cellulose may induce the production of different enzymes that can be useful for the degradation of target feedstock, unpretreated cattle manure. Crystalline cellulose is insoluble in water; therefore, it causes the high turbidity of the media. As a result, the cell density was measured by phase-contrast microscope with Thoma counting chamber. The cell densities of inoculum were ranged from 2.5 x 10^7 cells/mL to 5.5 x 10^8 cells/mL. The doubling time of *C. bescii* with crystalline cellulose was calculated as 3.9 hours (Figure 4.1).
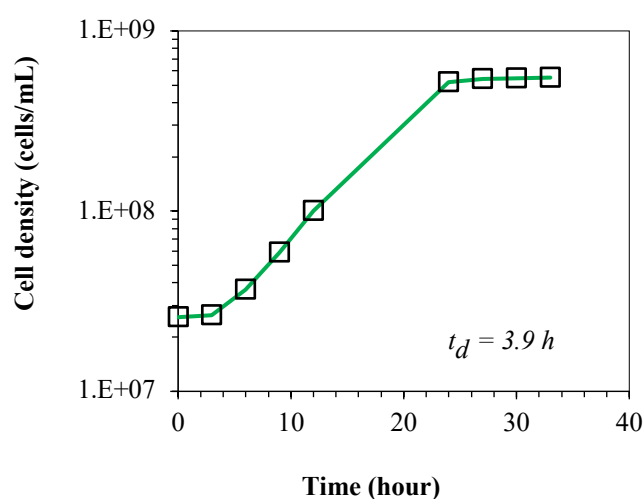
Figure 4.1 Growth curve of *C. bescii* on 5 g/L of crystalline cellulose

4.1.2 Initial degradability assessment of UCM

In Set 1, the net hydrogen production of PC was 3.7 ± 0.1 mL (Figure 4.2) and except for 2.5 g VS/L UCM concentration, all UCM reactors produced more hydrogen than PC, where 5 g/L CC was used as a carbon source. In UCM reactors, average net hydrogen productions were 1.4 ± 0.3 mL at 2.5 g VS/L, 5.2 ± 0.8 mL at 5 g VS/L and 8.9 ± 0.8 mL at 10 g VS/L and the hydrogen percentage was around 30% in all test reactors. Further, UCM reactor containing 10 g VS/L of UCM produced 45% higher hydrogen (as mL H_2) than CO-S (10) reactors. This indicated that UCM was being utilized as a sole carbon source effectively and may be used at even higher concentrations for further hydrogen production. In the follow-up sets, higher UCM concentrations were tested for hydrogen production. In Set 1, there was no hydrogen production in negative controls, indicating that the hydrogen production was relying on *C. bescii* culture activity. Also, methane was not detected in any reactor headspace.
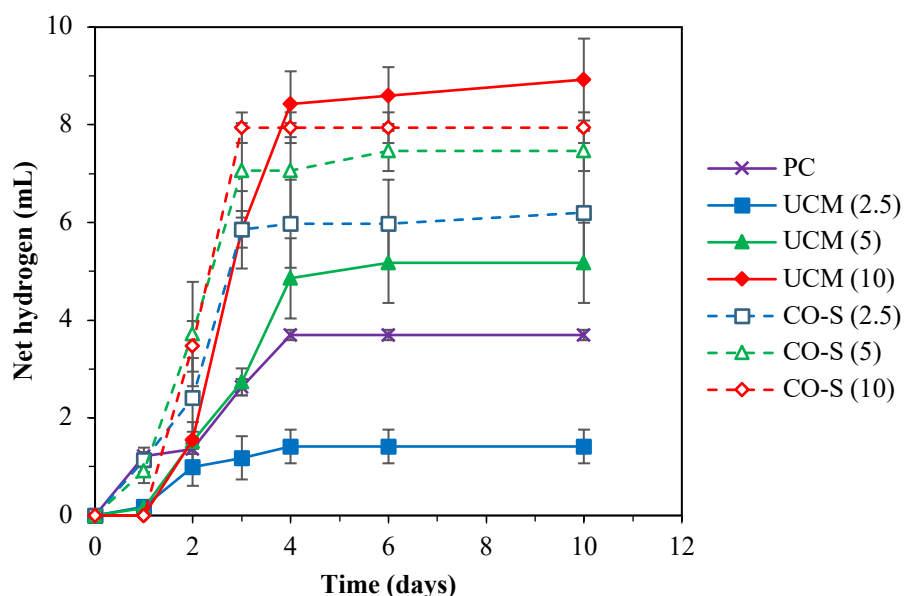
Figure 4.2 Average net hydrogen production as mL at STP for degradability assessment (PC: Pure substrate control, UCM: Unpretreated cattle manure reactors at 2.5, 5 or 10 g VS/L concentrations, CO-S: Co-substrate of UCM and crystalline cellulose at 5 g/L were added)

4.1.3   Biohydrogen production potential at higher concentrations of UCM

In Set 2 (Control), the average net hydrogen production at 15 g VS/L added reactor was 32.5 ± 0.6 mL (Figure 4.3A, blue line), dropping slightly to 27.6 ± 2.9 mL at 25 g VS/L UCM concentration (Figure 4.3B, blue line). There was no net hydrogen production in the case of 50 g VS/L UCM (Figure 4.3C, blue line). This is clear evidence of the feedstock inhibition impact of UCM at 50 g VS/L, which may be caused by either high hydrogen partial pressure in the headspace or the high concentration of nitrogenous compounds of the feed (Łukajtis et al., 2018). High NH_4^+-N concentrations generated via fermentation of animal manure may inhibit the enzymatic activity due to proton depletion or charge imbalances (H. Chen et al., 2021). H_2 production from organic substrates is governed by the thermodynamics of the hydrogenase reactions (Angenent et al., 2004). Obligate anaerobes, such as *C. bescii*, use ferredoxin to transfer electrons and it is estimated that hydrogen production via fermentation can continue as long as the H_2 partial pressure is below about 30 kPa (Angenent et al., 2004). In the Control set, hydrogen partial pressure (Appendix A) reached to $\sim$35 kPa at 15 g VS/L and 33 kPa at 25 g VS/L UCM concentrations.

There was no methane production in the reactors, which indicates that no methanogenic microorganisms were active in cattle manure at high reactor operation temperature. Additionally, there was no hydrogen production in negative control reactors. This clearly proves that the hydrogen production was related to *C. bescii* activity and native microorganisms present in manure were not responsible for hydrogen production.

In the Control set, the highest hydrogen production yield of 72.2 ± 1.3 mL H_2/g VS_{added} was obtained from 15 g VS/L of UCM (Table 4.1). The hydrogen yield at 25 g VS/L was averaged at 36.8 ± 3.9 mL H_2/g VS_{added}, almost half of 15 g VS/L. In addition to the yield, the hydrogen production rate also decreased with the increase in manure concentration (Table 4.1). Similar to these results, a decrease in hydrogen

yield with increasing substrate concentration was reported for different substrates, such as garden waste when degradation by *C. saccharolyticus*, a closely related specie to *C. bescii*, was studied (Angela. Abreu et al., 2019). Additionally, Talluri et al. (2013) also observed a significant inhibition on biohydrogen production by *C. saccharolyticus* when the concentration of unpretreated switchgrass was increased.

4.1.4 Impact of sparging

In the Control set, there was a significant amount of hydrogen production from UCM, yet hydrogen partial pressures were higher than 30 kPa. Therefore, to alleviate the potential inhibitory impact of hydrogen build-up in the headspace and increase the yield from UCM, intermittent gas sparging was applied in Set 3 (Sparging). The results were promising, and there was a considerable increase in the net hydrogen production yields; 40% in 15 g VS/L and 47% in 25 g VS/L compared to the Control set. Further, with the aid of intermittent gas sparging, 12.5 ± 0.6 mL of net H_2 production was recorded at 50 g VS/L (Figure 4.3C, green line). Also, the hydrogen production rates were significantly increased upon sparging. These results prove that the inhibition during UCM fermentation was partly due to hydrogen solubilization in the liquid medium and high hydrogen partial pressure in the reactor headspace.

It is well-known that the high hydrogen partial pressure negatively impacts hyperthermophilic biohydrogen production due to the product inhibition on the hydrogen-producing microorganisms (Kraemer & Bagley, 2007). Sparging the headspace with a gas other than hydrogen may have lowered hydrogen solubilization in medium and its accumulation in the headspace. Previously, it was illustrated that sparging with $N_2:CO_2$ (80%:20%) gas mixture significantly increased the growth rate of *C. bescii* when fed with 5 g/L and 10 g/L of crystalline cellulose, compared to simple headspace gas flushing (Basen et al., 2014).

4.1.5 Impact of culture adaptation

In Set 4 (Adaptation), UCM-adapted *C. bescii* culture was inoculated into the reactors, and the highest hydrogen production yields among the three sets (Control, Sparging, and Adaptation) were recorded in this set. Hydrogen production yield at 15 g VS/L was 161.3 ± 1.6 mL H_2/g VS_{added}, which is around 123% higher than the yield recorded in the Control set. The hydrogen yield achieved in the Adaptation set is also nearly 60% higher than the yield (101.1 ± 6.1 mL H_2/g VS_{added}) recorded in the Sparging set at the same concentration (Table 4.1); clearly, only partial performance enhancement is possible via sparging. These results indicate that the inhibition due to substrate has a higher impact on hydrogen production yield compared to product inhibition caused by hydrogen accumulation in the headspace.

Similarly, at UCM concentration of 25 g VS/L, the yield was 142% higher than the yield attained in the Control set at the same concentration. The lowest hydrogen yield in the Adaptation set was again recorded at 50 g VS/L, slightly higher than the yield recorded in Set 2. However, the use of adapted culture showed a significant increase in the hydrogen production rate at each UCM concentration. Around 16% higher hydrogen production yield was recorded compared to the Sparging set. Similar to the yield, the use of adapted culture showed a significant increase in the hydrogen production rate; the highest recorded rate was attained as 7.77 ± 0.08 mL H_2/L/h under UCM concentration of 25 g VS/L (Table 4.1). The increase in the hydrogen production rate was around 180% compared to the Control set. The hydrogen production rate is an important parameter that will determine the processing time of feedstock and in turn, may impact the volume of the reactor. The reason for higher yield and rate is caused by the adaptation of the culture to feedstock which possibly led to an advantageous phenotype and expression of specific enzymes, resulting in enhanced hydrogen production from UCM (Dragosits & Mattanovich, 2013).
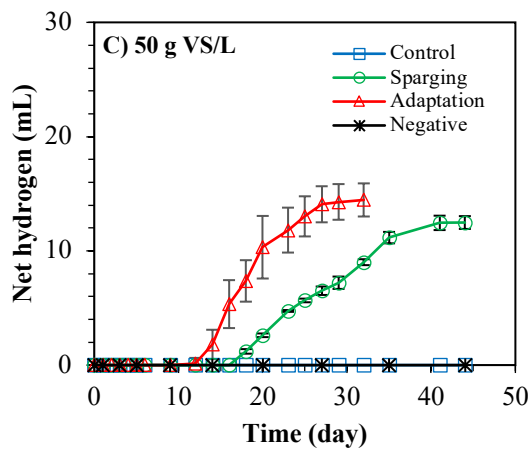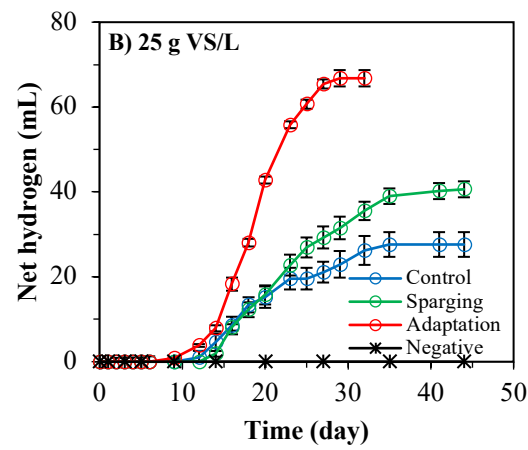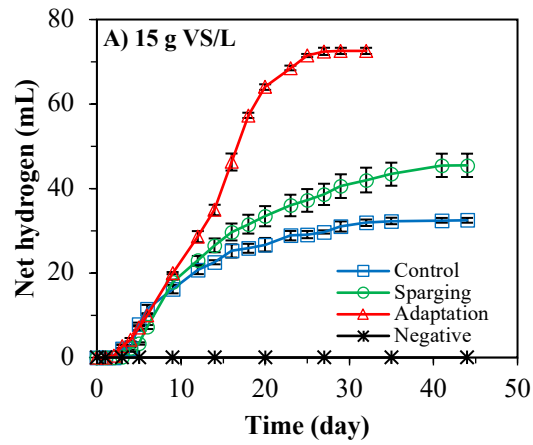
Figure 4.3 Average net hydrogen production from UCM at concentrations of A) 15 g VS/L, B) 25 g VS/L and C) 50 g VS/L in Control (Set 2), Sparging (Set 3) and Adaptation (Set 4)

84

Table 4.1 Biohydrogen production yield and rate in each set

Experimental Set	UCM (g VS/L)	Hydrogen production yield[a] (mL/ g VS)	Hydrogen production rate[a] (mL H_2/L/h)
Control (Set 2)	15	72.2 ± 1.3	3.52 ± 0.32
	25	36.8 ± 3.9	2.77 ± 0.17
	50	-	-
Sparging (Set 3)	15	101.1 ± 6.1 (40.0)	4.13 ± 0.31 (17.3)
	25	54.2 ± 2.5 (47.3)	3.41 ± 0.33 (23.1)
	50	8.3 ± 0.4	1.06 ± 0.04
Adaptation (Set 4)	15	161.3 ± 1.6 (123.4)	6.65 ± 0.04 (88.9)
	25	89.1 ± 2.6 (142.1)	7.77 ± 0.08 (180.5)
	50	9.6 ± 1.0	1.74 ± 0.25
Carbon balance (Set 5)	15	143.5 ± 4.2	7.02 ± 0.19
	25	73.0 ± 4.2	7.03 ± 0.49

[a]: In parenthesis percent increase with respect to Control set are given.

The maximum yield was reported with 15 g VS/L of UCM by the adapted *C. bescii* culture (161.3 ± 1.6 mL H_2/ g VS_{added}). Although there is still inhibition at 50 g VS/L dosage on *C. bescii*, the significant increase in hydrogen production yield with the use of UCM-adapted *C. bescii* inoculum shows the great potential to use *C. bescii* based systems at high organic loadings. In another work, Pawar (2014) used ALE techniques for the adaptation of *C. saccharolyticus* to higher glucose concentrations which enabled higher hydrogen production and decreased the impact of substrate inhibition. Furthermore, ALE was used for adaptation of different *Caldicellulosiruptor* species to high sugar concentrations, and a comparison among different species was presented (Byrne et al., 2021). In this recent study, *C. bescii* was ranked the third highest adaptable member of the genus among the five that were tested, showing significant enhancement in growth kinetics when fed with relatively high concentrations of pure glucose up to 40 g/L (Byrne et al., 2021).

4.1.6 Solubilization of UCM and liquid fermentation end products

Total net mass solubilization at each concentration (15, 25 and 50 g VS/L) was obtained by subtracting the solubilization in the SC from the corresponding UCM reactors. Bar plots in Figure 4.4A show the extent of solubilization attained in respective negative controls (inner bars) along with total mass solubilization at each UCM concentration. As expected from the high hydrogen production yields, the highest total UCM solubilization of 73.1 ± 1.5% was achieved with the adapted culture in Set 4 (Adaptation) at 15 g VS/L of UCM. Whereas the minimum total solubilization of 25.8 ± 1.0% was observed in the Control set in the 50 g VS/L UCM-added reactors, in which there was no hydrogen production. As expected, the solubilization in 50 g VS/L of UCM in Control (Set 2) and its negative control were similar, and this proves that the solubilization in this reactor was due to processes that are unrelated to *C. bescii* activity.

The solubilization attained in the respective negative controls at each UCM concentration shows the extent of solubilization due to other processes unrelated to *C. bescii* activity. For example, thermal degradation may cause solubilization in negative controls as no *C. bescii* inoculum was added to these reactors. This point is proven by the extent of solubilization in different negative controls operated in the Control, Sparging, and Adaptation sets. For instance, solubilization extents of negative controls among different sets were all around 27% for 15 g VS/L of UCM. Independent of the UCM concentration, the extent of solubilization in negative controls was less than 29%. This result is another proof supporting that biodegradation in the UCM reactors has been performed by *C. bescii* rather than native microorganisms present in the manure.

The extent of solubilization directly linked to *C. bescii* activity in UCM reactors which can be estimated by subtracting the solubilization level in the corresponding negative controls from the total solubilization. At 15 g VS/L UCM, the average solubilization resulted from the activity of *C. bescii* was 46.6 ± 1.1% in the Adaptation set. In other words, *C. bescii* was responsible for 65% of total

solubilization (73.1 ± 1.5%). This rate of solubilization is considerably higher than any other reported solubilization level with *C. bescii*. For example, Zurawski et al. (2015) reported 40.3 ± 1.0% of total solubilization of unpretreated switchgrass (5 g/L) by *C. bescii* during a 7-day batch reactor operation. In another study, 38.4% of total solubilization was reported during 7 days of operation by *C. bescii* from 5 g/L of switchgrass and different poplar types in batch reactors (Conway et al., 2017). Straub et al. (2019) recently reported total solubilization of unpretreated switchgrass (50 g/L) as 46.3%, when *C. bescii* was used as an inoculum for continuous reactor operation. Compared to the earlier studies, substantially higher solubilization of unpretreated feedstock was achieved in this study; however, the incubation times of other studies were significantly shorter than the reactor operation time of this study which may impact the results.

The initial pH of all reactors was 7.0, and the final pH values of 15 g VS/L UCM concentrations were 6.15 ± 0.03 in the Control (Set 2), 6.11 ± 0.04 in the Sparging (Set 3) and 5.86 ± 0.02 in the Adaptation (Set 4). The final pH values of 25 g VS/L UCM were 6.08 ± 0.03 in the Control set, 6.04 ± 0.03 in the Sparging set and 5.91 ± 0.04 in the Adaptation set. The final pH values of 50 g VS/L UCM were 5.82 ± 0.05 in the Control set, 5.63 ± 0.03 in the Sparging set and 5.81 ± 0.06 in the Adaptation set. Except 50 g VS/L of UCM, the pH values in the Adaptation set were lower than the Control and Sparging sets. The drop in the pH is related to acids produced during the fermentation. Previously, the major acidic fermentation products generated by *C. bescii* were listed as acetic acid and lactic acid; hence, we quantified acetic acid and lactic acid concentrations at the end of batch operation (Yang et al., 2010; Yilmazel & Duran, 2021). Also, VFAs, namely, butyric, propionic, isobutyric, butyric, isovaleric, n-valeric, isocaproic, n-caproic, and heptanoic acids were measured, but none were detected. The net acid productions (outer bars) and respective negative controls (inner bars) are shown in Figure 4.4B and Figure 4.4C. The measured acetic acid concentration in the Adaptation set was around 65.3 ± 2.1 mM at 15 g VS/L UCM, which is almost three times higher than the accumulated amount in the negative control. For 15 g VS/L UCM, the acetic acid concentration measured from

the negative controls did not change significantly among different sets, ranging from 16.6 ± 1.3 mM to 21.1 ± 0.7 mM (Figure 4.4B). The release of acetic acid may be a result of thermal degradation since the reactors were operated at 75 °C. Similar to these results, Kataeva et al. (2013) observed the release of unchanged monolignols at lower concentrations in abiotic control compared to the treatment with *C. bescii*. In general, the amount of acetic acid accumulation in the Adaptation (Set 4) was twice as high as the Control (Set 2), consistent with the higher hydrogen production via adaptation. At 25 g VS/L, around two times higher *C. bescii* acetic acid production (58.8 ± 2.2 mM) was recorded in the Adaptation set compared to the Control set (31.2 ± 3.2 mM). Average acetic acid concentrations measured in negative controls of the Control set (42.6 ± 2.7 mM) and the Sparging set (35.8 ± 0.2 mM) were similar, and greater than the Adaptation set (22.5 ± 1.0 mM). This may be related to the 12 days of shorter incubation time of reactors in the Adaptation set. Compared to 15 g VS/L and 25 g VS/L reactors, in all sets, the highest amount of acetic acid concentrations in negative controls were measured at 50 g VS/L of UCM; 90.9 ± 3.2 mM in the Control set, 88.0 ± 6.6 mM in the Sparging set, and 75.4 ± 3.4 mM in the adaptation set. The higher acetic acid concentration via abiotic thermal degradation at 50 g VS/L reactors is related to the high initial UCM concentration. There was no accumulation of lactic acid in negative controls (Fig. 3C, no inner bars), which indicates the lactic acid production is a result of *C. bescii* activity. The lactic acid productions did not change significantly and were around 5-6 mM among different sets at 15 g VS/L and 25 g VS/L. The highest concentration of 11 mM was recorded in the Adaptation set at 50 g VS/L, which may indicate a change in the metabolic pathway of UCM-adapted *C. bescii* under high load stress.
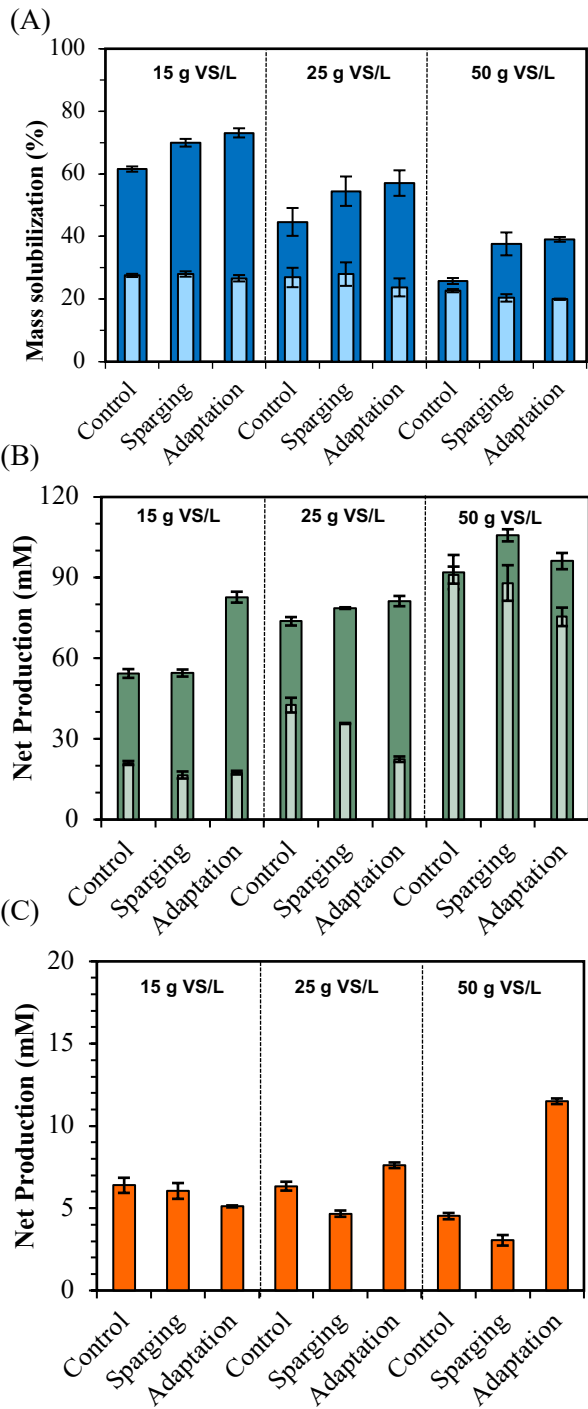
Figure 4.4 (A) Extent of solubilization of UCM at 15 g VS/L, 25 g VS/L and 50 g VS/L of UCM in each experimental set. (Inner light blue bars indicate the extent of solubilization recorded for respective negative controls.) Average net production of liquid fermentation products in each set (B) Acetic acid and (C) Lactic acid at UCM concentration of 15 g VS/L, 25 g VS/L and 50 g VS/L. (Inner bars indicate the production in negative controls. Outer bars indicate net acid production in UCM added test reactors.)

4.1.7 Carbon balance

In Set 5, carbon balance was conducted in larger-size reactors fed with 15 g VS/L (R15) and 25 g VS/L (R25) of UCM and inoculated with UCM-adapted *C. bescii*. The net hydrogen production in each reactor is shown in Figure 4.5, corresponding to the following yields of 143.5 ± 4.2 mL H_2/g VS_{added} (in R15) and 73.0 ± 4.2 mL H_2/g VS_{added} (in R25). These reactors were operated for 50 days, and several outages during the first week of incubation may have slightly impacted the start-up time and extended lag phase. Even with doubling the active volume, the maximum hydrogen production yields attained in our study (Table 4.1) were significantly higher than other studies in the literature.
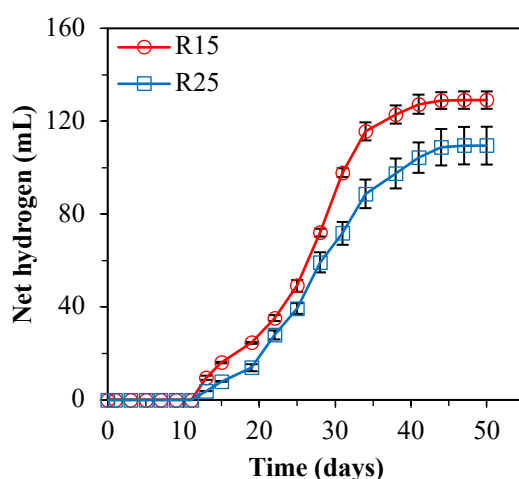
Figure 4.5 Average net hydrogen production from UCM at concentrations of 15 g VS/L (R15) and 25 g VS/L (R25) at carbon balance reactors (Data shown is normalized to standard temperature and pressure (STP, 0ºC and 1 atm).

The total mass solubilization in R15 was $80.8 \pm 2.8\%$, and R25 was $62.5 \pm 2.0\%$. When negative controls were subtracted, *C. bescii*-related solubilizations were calculated as 48% in R15 and 36% in R25. These solubilization rates are only slightly higher than Set 4 (Adaptation). Upon carbon balance, it was shown that most of the carbon in the product was in sugar form, which proves that *C. bescii* solubilized UCM to simple sugars and could not convert all of them to hydrogen. This can be a result of either product, *i.e.,* acetic acid, hydrogen, or substrate inhibition which

90

causes to decrease in microbial activity of *C. bescii*. The other main carbon end-products generated by *C. bescii* during UCM fermentation were acetic acid, lactic acid, and CO_2. About 6%-7% of acetic acid production was resulted due to thermal abiotic degradation of UCM (Figure 4.6, red dotted column). Therefore, the acetic acid production because of *C. bescii* activity were counted as 19.7% and 17.6% in 15 g VS/L and 25 g VS/L, respectively. Other than those products, cell carbon content was also calculated and referred to as inoculum in Figure 4.6. Although UCM has very complex structure, the carbon balances between the feedstock and fermentation products for both reactors were approximately 100%. Independent of initial UCM concentration, the distribution of carbon was similar in both reactors, with only slight differences.
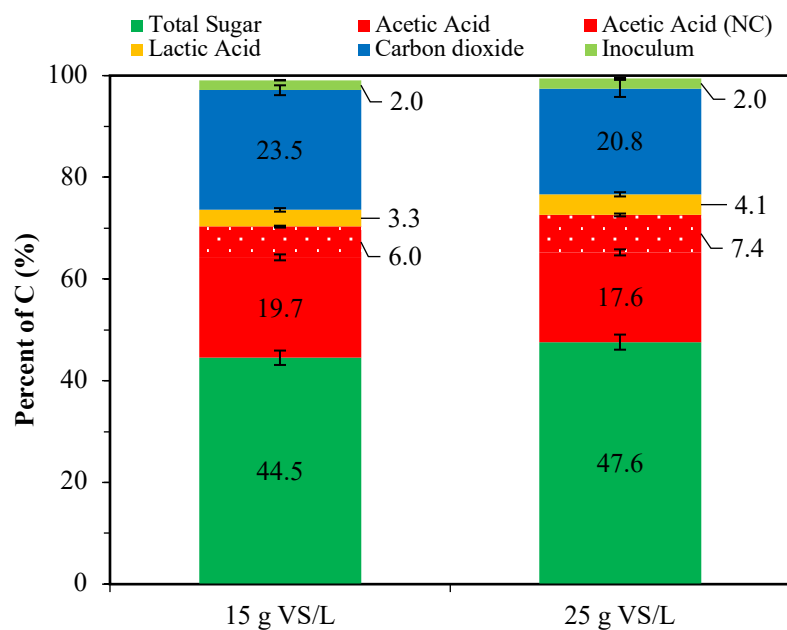
Figure 4.6 Carbon balance in larger volume reactors in Set 5 for 15 g VS/L and 25 g VS/L of UCM (Dotted column shows acetic acid production of negative controls produced from abiotic thermal degradation)

Interestingly, it was shown that *C. bescii* degraded a constant fraction of UCM to produce total sugars independent of initial UCM concentration. Basen et al. (2014) reported similar results with unpretreated switchgrass; regardless of the initial concentration in the range of 1-50 g/L, *C. bescii* degraded a constant fraction of the

feed. This implies that the characteristics of the feed in fact is a critical factor in its degradation. Overall, our study showed that most of the carbon in UCM was converted to solubilized liquid products.

4.2 Bioelectrochemical hydrogen production

4.2.1 Growth of *G. acetivorans* on acetate and DF effluent

Initially, *G. acetivorans* was grown in hyperthermophilic growth medium consisting of 10.8 mM acetate as electron donor and ferric citrate as electron acceptor (Table 3.5). *G. acetivorans* has the ability to oxidize acetate into CO_2 with ferric forms of iron (Fe^{3+}) present as electron acceptor. The stoichiometric reaction for the iron reduction and acetate oxidation is given in the Equation 4-1.

$$CH_3COO^- + 8Fe(III) + 4H_2O \rightarrow 2HCO^- + 9H^+ + 8Fe\,(II) \qquad \text{(Equation 4-1)}$$

The growth of *G. acetivorans* was visible in the growth tubes since the color change due to iron reduction and precipitate production after incubation. Because of color change, OD measurement could not be used for growth observation. Thus, the growth study was conducted by measuring acetate consumption and ferrous iron formation (Figure 4.7).
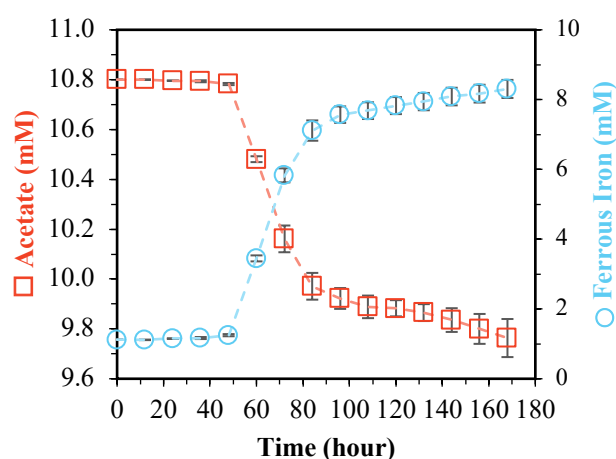
Figure 4.7 Growth study of *G. acetivorans* with 10.8 mM acetate and ferric citrate

At the end of 7 days incubation, the acetate consumption was 1.04 ± 0.08 mM which the final concentration of acetate dropped by 9.6% from the initial concentration of 10.8 mM. Initial Fe (II) concentration was 1.12 mM which was present in the inoculum. At final, the net Fe (II) production was reached to 7.19 ± 0.26 mM.

In a previous study, it was reported that the highest level of Fe (II) formation by *G. acetivorans* was around 5-6 mM when ferric iron was supplemented in soluble form of ferric citrate (Slobodkina et al., 2009). The ratio of Fe (II) production to acetate consumption was recorded as 7.5 (Slobodkina et al., 2009). Kas (2021) also performed the similar growth experiment with *G. acetivorans* and the ratio of Fe (II) production to acetate consumption was around 6.8-6.9. In this study, the ratio of Fe (II) generation to acetate consumption was found as 6.93 ± 0.07 which is very close to the result of Kas (2021), indicating a slight deviation from the stoichiometric ratio of 8.

4.2.2   Set 1: Culture selection

4.2.2.1   Reactor performance of Run 1.1

Run 1.1 is the first reactor set for bioelectrochemical hydrogen production with *G. acetivorans* in Mini-MECs fed with 10 mM acetate. Total of 5 cycles ($\sim$ 55 days) were performed during which the current production was observed continuously. Mini-MECs were operated as triplicates, and the current densities replicated to high extent for four repetitive cycles (Figure 4.8). First two cycles were counted as biofilm formation stage; therefore, these were not included for current density generation. The peak current densities were averaged as for quadruplicate reactors 1.09 ± 0.02 A/m^2 over last 3 cycles of operation at 80 °C. Hydrogen production throughout the last four cycles was also stable. The average hydrogen production rate (Q_{H_2}) was calculated as 0.52 ± 0.03 m^3 H$_2$/m^{3}d over last 3 cycles. Seed control reactors showed an insignificant current production at the beginning of the reactor operation which

may be a result of residual acetate coming from the inoculum. When the MEC media was replaced after current production, there was no hydrogen or current generation in acetate control reactors. In addition, abiotic controls did not produce any current or hydrogen during the operation which indicates that current was produced by *G. acetivorans*.
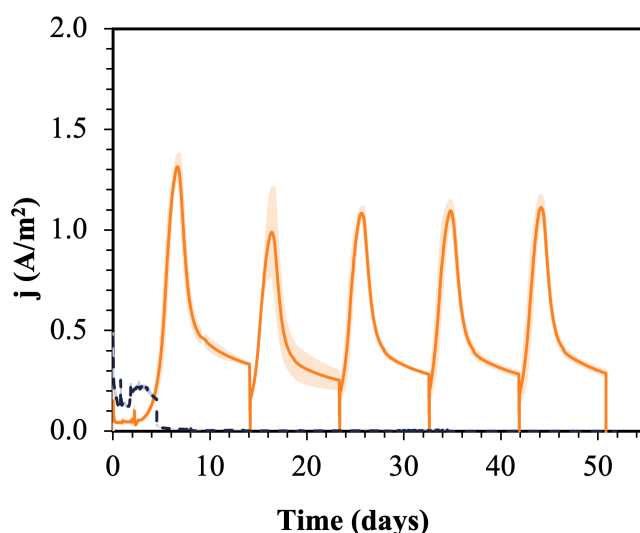
Figure 4.8 Normalized current generation for Run 1.1 (orange line: test average, black dashed line: seed control)

Kas and Yilmazel (2022) reported higher peak current production (1.53 ± 0.24 A/m²) for *G. acetivorans* in Mini-MEC operation. The difference in the current production may be caused by the activity of inoculum since the lag phase in this run lasted about 4 days which is higher than the previously reported operation (Kas and Yilmazel, 2022). In addition, biofilm formation was continued for 30 days ($\sim$10 cycles) in the mentioned study (Kas & Yilmazel, 2022) which might be reason for higher current production. Yet, the hydrogen production rate was reported as 0.57 ± 0.06 m³ H_2/m³d (Kas & Yilmazel, 2022) which was very close to the hydrogen production rate of Run 1.1 (0.52 ± 0.03 m³/m³d). As a result, even with the lower current generation, hydrogen production rate was considerably high in Mini-MEC reactors operated in this study. Yilmazel et al. (2018) reported current production by two different hyperthermophilic exoelectrogenic archaea (*G. ahangari* and *F. placidus*) in Mini-

94

MEC reactors. All three cultures of *G. ahangari, G. acetivorans* and *F. placidus* belong to the same family *Archaeoglobales*; thus, *G. ahangari* and *F. placidus* exhibit significant similarities to *G. acetivorans* in terms of their genomic structure (Mardanov et al., 2015). The reported peak current productions were 0.57 ± 0.10 A/m^2 for *G. ahangari* and 0.68 ± 0.11 A/m^2 for *F. placidus* using the same reactor configuration (Yilmazel et al., 2018). When compared to other hyperthermophilic exoelectrogens, *G. acetivorans* showed a significantly higher current production in Mini-MEC reactors.

4.2.2.2 Reactor performance of Run 1.2

In the last run of Mini-MECs, Run 1.2 was operated using three different hyperthermophilic exoelectrogenic pure cultures as *G. ahangari* (AH), *G. acetivorans* (AT) and *F. placidus* (FP). Since these pure cultures have similar abilities and living conditions, they might be present in the same environment and their co-culture may present a synergistic effect. To examine their effect as a co-culture, Run 1.2 was operated by three different co-cultures called as AH-FP (co culture of *G. ahangari* and *F. placidus*), AT-FP (co culture of *G. acetivorans* and *F. placidus*) and AH-AT (co culture of *G. ahangari* and *G. acetivorans*). Total of 4 cycles were operated for each reactor and current production was recorded continuously (Figure 4.9). During the operation, the first cycle was counted for biofilm formation and the last three cycles were run as test cycles; thus, data of the last three cycles were taken into consideration in yield and rate calculations.

During the test period, the peak current production was averaged as 0.33 ± 0.07 A/m^2 for AH-AT, 0.66 ± 0.14 A/m^2 for AH-FP, and 0.61 ± 0.15 A/m^2 for AT-FP. The highest performance in terms of current production was obtained in AH-FP reactors; however, AT-FP also showed a similar current production with AH-FP reactors. On the other hand, AH-ATs showed a significantly lower current production during the test period which might be caused due to the competition between the same genus species in the MECs. About 85% and 90% of acetate was consumed in AH-FP and

95

AT-FP reactors, respectively. However, only 45% of acetate consumption was recorded in AH-AT reactors which indicates a negative effect on these pure culture to each other. Christiansen & Loeschcke (1990) explained that the competition between the co-existing species from the same genus is higher than co-existing species of the same family. Therefore, individuals of the same species have a higher competitive behavior to each other compared to the other species in the same family. The result of Run 1.2 also supports that although all three cultures belong to same family, co-cultures including *F. placidus* showed a similar performance in Mini-MECs; yet, AH-AT culture expressed significant decrease in the performance which may be resulted due to their higher competitiveness and possible negative effects on each other and considerably lower competition between *F. placidus*.

Similar to the acetate consumption, the hydrogen production rates for AH-FP (0.43 $\pm$ 0.05 m^3 H$_2$/m^{3}d) and AT-FP (0.47 $\pm$ 0.01 m^3 H$_2$/m^{3}d) reactors showed significantly higher rates compared to AH-AT reactors (0.18 $\pm$ 0.09 m^3 H$_2$/m^{3}d). Thus, the co-culture of *G. acetivorans* and *G. ahangari* showed an important decrease in performance compared to their pure culture studies (Kas & Yilmazel, 2022; Yilmazel et al., 2018). Although the outcomes of AH-FP and AT-FP were better than AH-AT reactors, the current production and hydrogen production rate recorded in these reactors were still lower than the pure culture of *G. acetivorans* in Mini-MECs (Run 1.1). As the microorganisms have similar mechanisms, they did not show any synergistic effect but rather they presented a decrease in the performance of Mini-MECs compared to their pure culture studies. Based on the results of Run 1.1 and Run 1.2, single pure culture of *G. acetivorans* as a superior performant in Mini-MEC system was selected as an inoculum for further reactor operations in MECs.
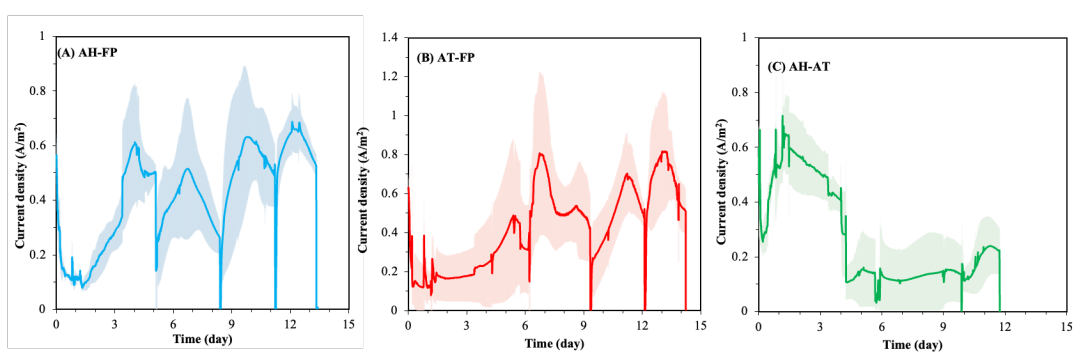
Figure 4.9 Normalized current production for Run 1.2 as (A) AH-FP, (B) AT-FP and (C) AH-AT (AH: *G. ahangari;* AT: *G. acetivorans;* FP: *F. placidus*)

4.2.3   Set 2: DF effluent utilization

4.2.3.1   Run 2.1: Electrode material selection

Current generation

MEC operation was continued for 4 cycles corresponding to 17 days and 27 days for carbon fiber brush (CFB) and graphite plate reactors (GP), respectively (Figure 4.10). At the biofilm formation stage (cycle 1), the current production started to increase immediately in CFB reactors and the peak current production of 1.85 ± 0.08 A/m^2 (84.8 ± 3.7 A/m^3) in 3 days. Yet, GP reactors reached to a peak current of 0.86 ± 0.59 A/m^2 (27.9 ± 10.3 A/m^3) in 8 days and showed a significant lag phase ($\sim$6 days) during biofilm formation. CFB reactors presented steady current generation from day 4 to day 17 and the average peak current generation was recorded as 1.38 ± 0.11 A/m^2 (63.27 ± 3.46 A/m^3) over 3 cycles. On the other hand, GP reactors also showed a considerably high current production after biofilm formation as 1.25 ± 0.09 A/m^2 (39.03 ± 2.98 A/m^3). Although the current productions were similar between CFBs and GPs, the duration of operation was 37% longer in GP reactors compared to CFB reactors. In addition, CFB reactors also presented significant enhancement in volumetric current density (J_v) by about 62%.

97
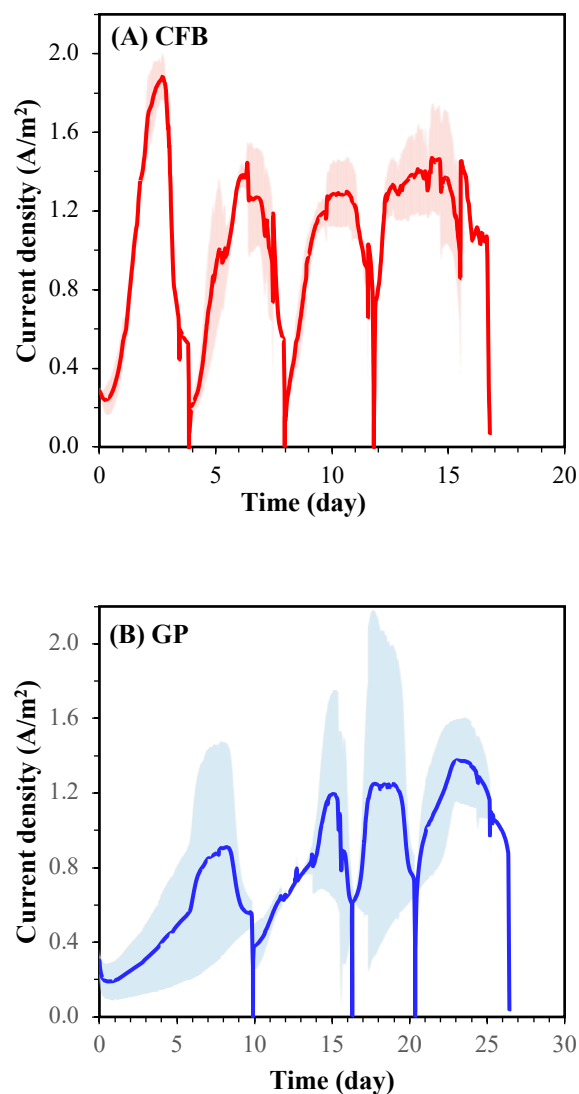
Figure 4.10 Normalized current production by *G. acetivorans* in Run 2.1 (A) CFB reactors (B) GP reactors

Hydrogen production

During the Run 2.1, stable hydrogen production was observed in both CFB and GP reactors inoculated with *G. acetivorans* in single chamber MECs. The maximum hydrogen gas percent in the headspace was 55.4 ± 5.2 % for CFB reactors and 45.4 ± 1.3 % for GP reactors (Figure 4.11). Hydrogen generation was measured at the end of each cycle for each reactor and normalized to the active volume of the reactors. Similar to the current generation, CFB reactors showed a significant enhancement in

hydrogen production rate (Figure 4.11). Over the last three cycles, the averaged hydrogen production rate for CFB reactors was 0.44 ± 0.06 m^3 H$_2$/m^{3}d, which was 2.3 times higher than GP reactors (0.19 ± 0.01 m^3 H$_2$/m^{3}d).
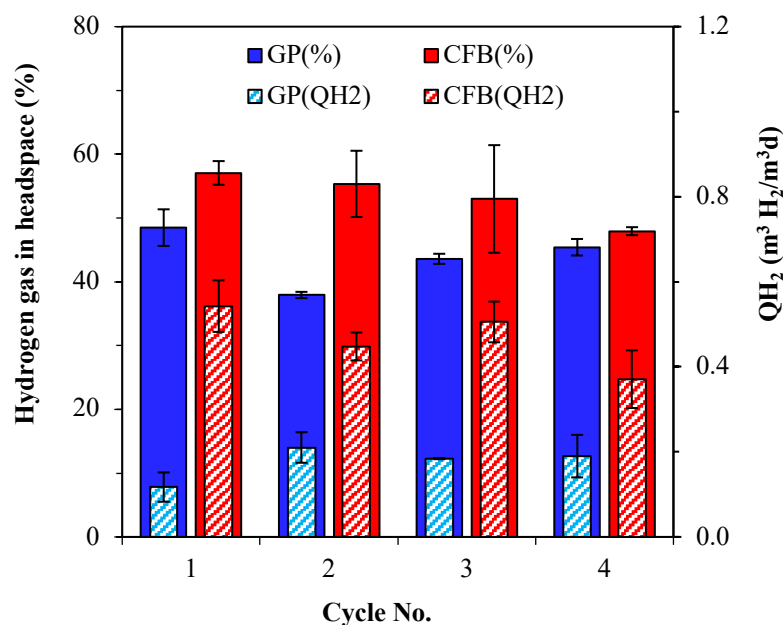
Figure 4.11 Hydrogen gas percentages and hydrogen production rates for Run 2.1 (outer bars shows hydrogen gas percentage and inner bars indicate the hydrogen production rate; red/dashed red bars: CFB reactors; blue/dashed blue bars: GP reactors)

The peak current densities in the CFB reactors were 1.2 times higher than GP reactors, yet the hydrogen production rates showed 2.3 times enhancement in CFB reactors compared to GP reactors. This difference between the current and hydrogen generation might be the result of different contributions of internal hydrogen recycling to the current production. Internal H$_2$ cycling refers to the use of H$_2$, where produced at the cathode in single chamber MECs, by exoelectrogenic microorganisms as an electron donor to produce current in MECs. In CFB reactors, cycle time was very short; thus, the contribution of hydrogen as an electron donor might be smaller than GP reactors. To investigate this hypothesis, efficiency parameters of C_E and r_{CAT} are calculated.

Efficiency calculations

The efficiency assessment of Run 2.1 was achieved as described in Chapter 3.2.6 using the parameters as C_E and r_{CAT}. To determine these parameters, substrate utilization was quantified at the end of each cycle by determining acetate concentration. A significant portion of acetate was utilized by *G. acetivorans* in CFB reactors and acetate consumption was found as (n_{AC}) 83.5 ± 2.6 % for 3 cycles of the test period. The acetate consumption of GP reactors was 73.6 ± 2.5 %; as a result, CFB reactors showed 13.4% higher acetate consumption compared to GP reactors during the run period. Coulombic efficiencies (C_E) for CFBs were averaged at 233.9 ± 49.5 % and for GPs were averaged at 306.5 ± 33.5 % for 3 cycles of the test period (Figure 4.12). During the operation, all C_E values were above 100% for all cycles which demonstrates that charge passed through the cycle time was not particularly a result of acetate consumption during the operation of both CFBs and GPs. This is an indication of that *G. acetivorans* could use another electron donor for current generation in single chamber MECs. It was reported that hyperthermophilic iron reducing archaea species including *G. acetivorans*, *G. ahangari* and *F. placidus* can use hydrogen gas as a sole electron donor during the growth with the presence of various electron acceptors (Manzella et al., 2015; Mardanov et al., 2015; Smith et al., 2015). The utilization of the cathode produced hydrogen by the culture for further current production is called internal hydrogen cycling; and this may explain higher than 100% CE (H. S. Lee & Rittmann, 2010). Previously, it has been shown that *G. ahangari* and *F. placidus* may use hydrogen gas as an electron donor in Mini-MECs to a lower extent (Yilmazel et al., 2018). Kas & Yilmazel (2022) also proved that with *G. acetivorans* hydrogen cycling is happening.
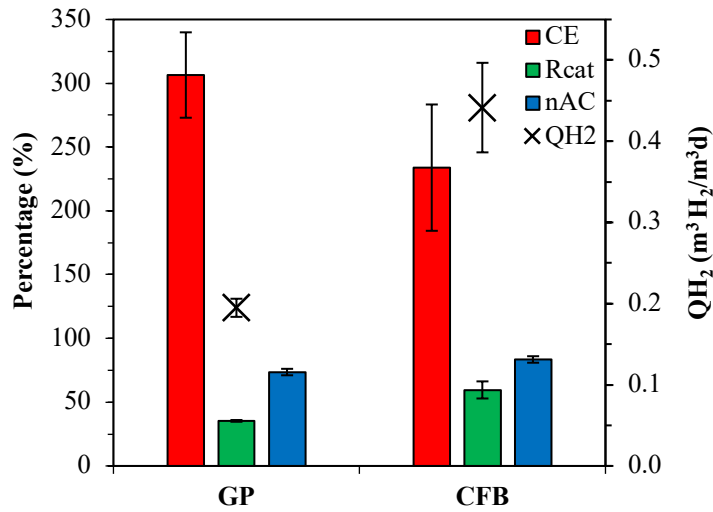
Figure 4.12 Coulombic efficiency (C_E), cathodic hydrogen recovery (r_{CAT}) and acetate consumption (n_{AC}) efficiencies in Run 2.1

The average cathodic hydrogen recoveries (r_{CAT}) were 59.6 ± 6.7 % for CFBs and 35.3 ± 0.7 % for GPs. For CFB reactors, about two-thirds of the hydrogen was recovered than estimated values based on the current generation. In case of GP reactors, the hydrogen recovery was counted only one third of the hydrogen expected from current production. Lower r_{CAT} values are also consistent with internal hydrogen cycling. Based on r_{CAT} and C_E values (Table 4.2), it may be concluded that *G. acetivorans* use hydrogen generated in the system as an electron donor, which was investigated in other experimental sets and further discussed in Chapter 4.2.3.3. It was reported that long hydraulic retention times (HRT) in a continuous single chamber MEC lead to more severe hydrogen cycling (H. S. Lee & Rittmann, 2010). Due to the lower surface area of GP, biofilm formation might be prolonged which may result in higher contribution of hydrogen cycling to current production.

Table 4.2 The overall performance results for Run 2.1

Reactor	j (A/m²)	C_E (%)	r_{CAT} (%)	Q_{H2} (m³ H₂/m³d)
CFB	1.38 ± 0.11	233.9 ± 49.5	59.6 ± 6.7	0.44 ± 0.06
GP	1.25 ± 0.09	306.5 ± 33.5	35.3 ± 0.7	0.19 ± 0.01

Biofilm analysis

101

The biofilm on anode electrodes were analyzed by (1) CV, (2) SEM and (3) CLSM methods.

At the last cycle of reactor operation, CV analyses were conducted in the range of -0.7 V and 0.2 V vs Ag/AgCl reference electrode at the point where near to the peak current production for both GPs and CFBs. CV curves of both CFB and GP anodes (Figure 4.13) showed S-shaped sigmoidal curves and there were no significant redox peaks in the CV analysis of abiotic reactors or spent medium of the test reactors. These indicate that biofilm on anode is involved in the extracellular electron transfer via DET.
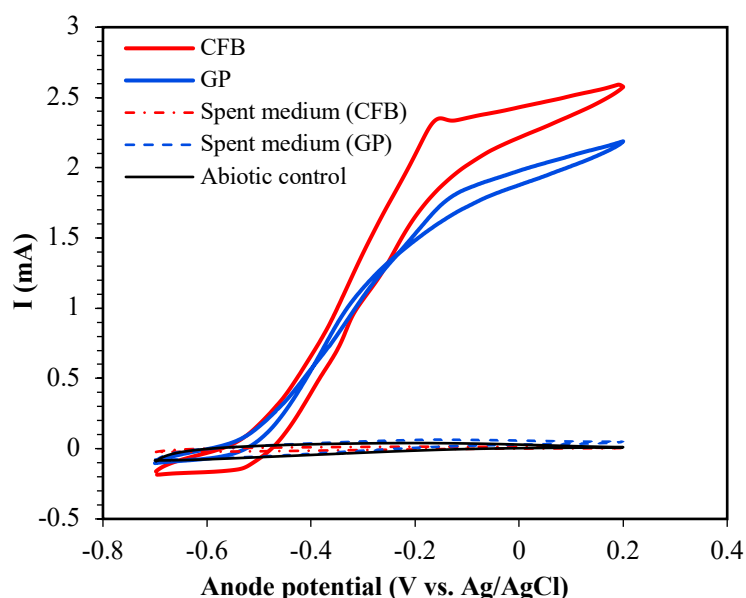
Figure 4.13 Cyclic voltammograms of *G. acetivorans* in Run 2.1 (red line: turnover of CFB; blue line: turnover of GP; dashed red line: spent medium of CFB; dashed blue line: spent medium of GP; black line: abiotic)

Since SEM and CLSM analyses are destructive analysis and dependent on the biofilm viability SEM and CLSM imaging were both conducted after the reactor operation was completed. After the last cycle of the operation was finalized, the anodes of one CFB and one GP reactors were prepared for SEM analysis. In addition, a bare abiotic CFB and GP were prepared with the same protocol as control samples. SEM images of bioanodes for GP and CFB are given in Figure 4.14. The electrode

surfaces showed a complex structure formation on anode electrode. The circular shapes present in the SEM images are consistent with the irregular cocci shape of *G. acetivorans*, and its size as in the range of dia. 0.3 – 0.5 μm.
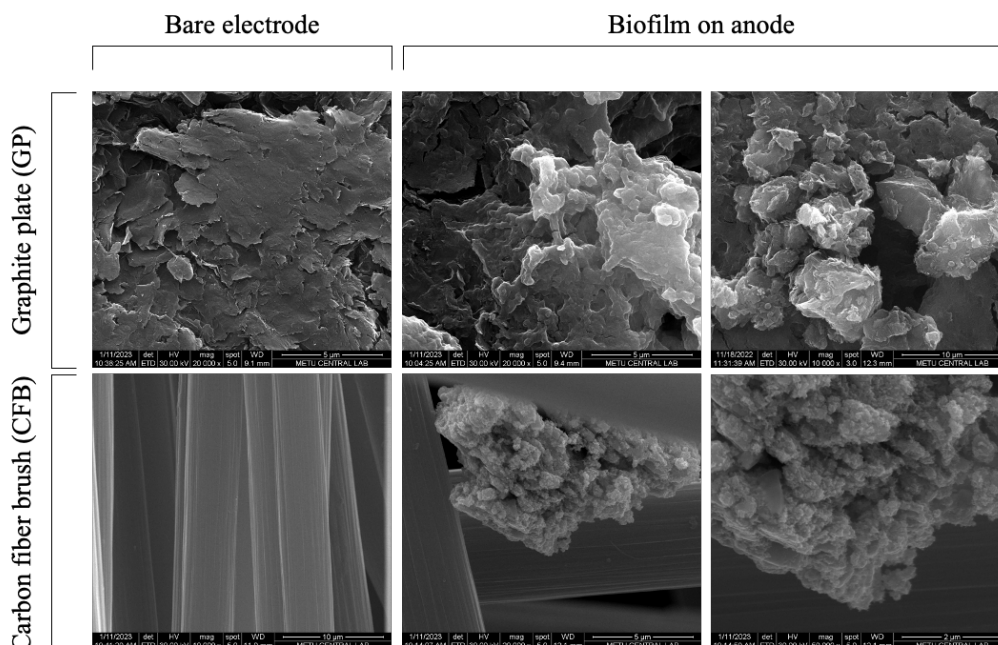
Figure 4.14 SEM images for Run 2.1

CLSM is a beneficial tool to visualize the spatial structure of biofilm on anode and differentiate live and dead cells attached to the anodes (S. Chen et al., 2017). As illustrated in Figure 4.15, the apparent biofilm viability was observed in CFB biofilm compared to GP biofilm. The thickness of GP biofilm was measured as 60 μm and the thickness of CFB biofilm was 40 μm. In the literature, the thickness of biofilm has a high variety even the same specie was used (Klein et al., 2023). In general, biofilm thickness more than 50 μm is referred as highly thick biofilm formed on electrode surface (R. Kumar et al., 2015). However, the thickness of biofilm is not directly correlated with the performance of BES; thus, the abundance of active cells on anode biofilm has a great influence on the reactor performance.

The biofilm formation on GP anodes showed a two-layer structured biofilm as live inner layer and dead outer layer. This orientation might be the reason for longer operation time due to higher biofilm resistance and acetate depletion (Schrott et al.,

2014). Similarly, Renslow et al. (2013) reported that the majority of cells in thicker biofilm of *G. sulfurreducens* on anode are metabolically inactive due to acetate depletion and act as electrical conduit for the active top layer. The thickness of CFB biofilm was considerably lower compared to GP biofilm; yet there was a higher abundance of live cells compared to dead cells. This may explain the higher current production in a shorter time in CFB. In their study, Sreelekshmy et al. (2020) investigated different electrode materials as anode in MFCs based on their three-dimensional (3D) microporous structure in which concluded that flat/plain electrodes showed a higher density of dead cells on the electrode surface compared to the electrodes with higher porosity (Sreelekshmy et al., 2020). Besides that, the authors expressed that dead cells accumulated on the electrode surface increase the charge transfer resistance; therefore, the efficiency of electron transfer between live cells and electrode decreases (Sreelekshmy et al., 2020).
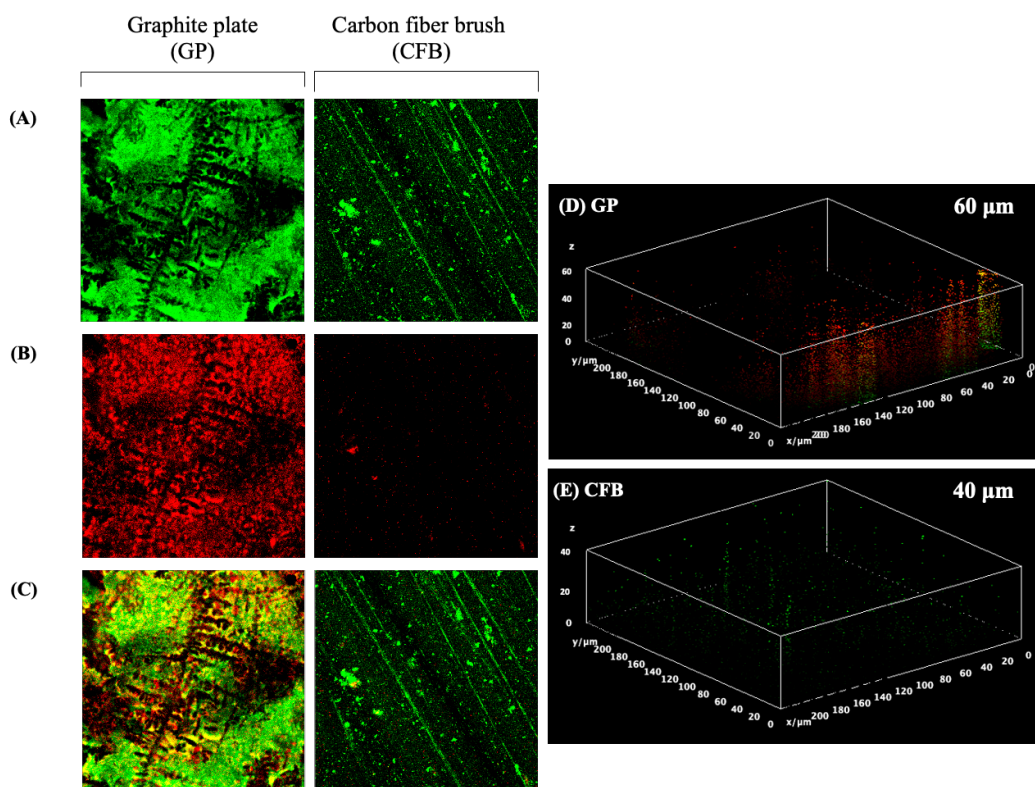
Figure 4.15 Confocal laser scanning microscope (CLSM) images from a LIVE/DEAD assay of *G. acetivorans* biofilm anode in Run 2.1 (A) Live cells (green), (B) Dead cells (red), (C) Live and dead cells, (D) 3D images of GP anode

biofilm with a biofilm thickness of 60 μm and (E) 3D images of CFB anode
biofilm with a biofilm thickness of 40 μm

4.2.3.2   Run 2.2: Utilization of dark fermentation effluent in single chamber MEC

Current generation

As reported previously (Kas & Yilmazel, 2022), *G. acetivorans* could utilize dark fermentation effluent to produce current with a GP anode in Mini-MECs, however, biofilm formation was previously completed using acetate (old biofilm); therefore, the current production was detrimentally affected compared to acetate-fed reactors. The stepwise adaptation process was carried on establishing if adapted *G. acetivorans* could produce high current density while fed with DF effluent. To understand the impact of culture adaptation, single chamber MECs were run as triplicates and inoculated with acetate grown wild type and adapted *G. acetivorans* cultures. The substrate was DF effluent for all reactors. The difference between the reactors was the inoculum source, where ADP reactors received adapted culture as an inoculum and acetate grown wild type cultures were inoculated into WT reactors. The anode material was selected as CFB for all the reactors as a result of its superior performance in Run 2.1.

The duration of Run 2.2 operation was about 15 days for ADP and 42 days for WT reactors. Current densities during biofilm formation stage (the first cycle) were averaged at 1.48 ± 0.51 A/m^2 (70.2 ± 20.0 A/m^3) for ADP and 1.20 ± 0.23 A/m^2 (61.5 ± 3.7 A/m^3) for WT reactors (Figure 4.16). The duration of biofilm formation was significantly longer (~ 4.7 times) in WT reactors than ADP reactors. This can be explained with the impact of adaptation since the inoculum in ADPs was familiar with DF effluent during the growth, additionally, acetate-grown *G. acetivorans* in WT reactors might be partially inhibited due to the content of the DF effluent. MECs were operated for a total of four cycles. The current generation in WTs showed a significant decrease, and the peak current production was averaged at 0.34 ± 0.04

A/m^2 (15.4 ± 3.2 A/m^3) over the last three cycles. On the other hand, ADP reactors generated a stable current density over the last three cycles as 1.58 ± 0.07 A/m^2 (73.0 ± 3.3 A/m^3) (Figure 4.16). About 4.6 times enhancement in current generation was recorded in ADP reactors compared to WTs. This is a clear proof of the adaptation on inoculum which enhances the ability of *G. acetivorans* to utilize DF effluent with a high stable current production.
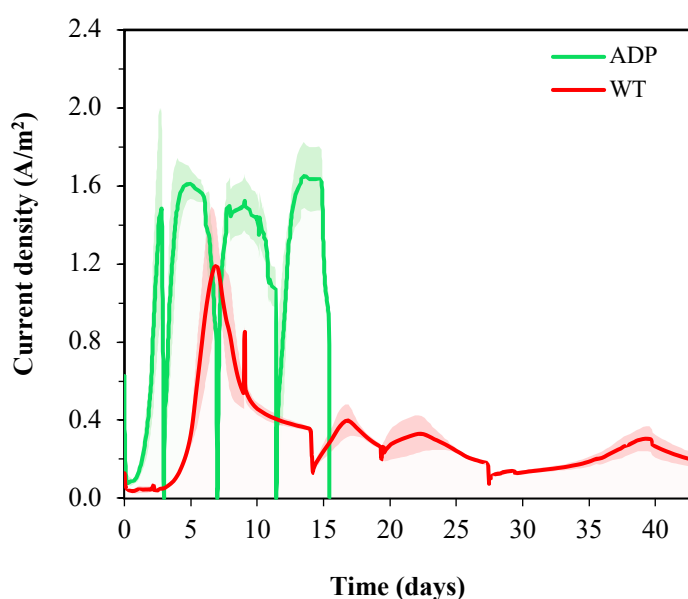
Figure 4.16 Normalized current production by *G. acetivorans* in Run 2.2 (green line: average current production in ADP reactors; red line: average current production in WT reactors; colored area: variance from average current generation)

Hydrogen production

In terms of hydrogen production, ADP reactors showed a significant enhancement compared to WT reactors. During the test period, the highest hydrogen gas percent in the headspace was 59.6 ± 3.4 % for ADP and 20.8 ± 2.1 % for WT reactors (Figure 4.17). The hydrogen production was analyzed at the end of each cycle for each reactor and normalized to the active volume of the reactors. The hydrogen production rates were averaged as 0.52 ± 0.07 m^3 H$_2$/m^{3}d for ADP, and 0.05 ± 0.02 m^3 H$_2$/m^{3}d for WT. Q$_{H_2}$ of ADP was 11.5 times higher than Q$_{H_2}$ of WTs, which were highly similar to the current generation, and it can be seen that DF effluent negatively

affected the performance of wild-type (non-adapted, acetate grown) *G. acetivorans* in single chamber MECs. Previously, Kas & Yilmazel (2022) reported about 80% of acetate consumption by wild-type *G. acetivorans* when Midi-MECs fed with DF effluent; however, the biofilm was formed using acetate for a long time. Although the hydrogen production rates were similar between DF effluent fed reactors and acetate fed reactors, the current generation was negatively affected by the addition of DF effluent (Kas & Yilmazel, 2022). Compared with the results of Kas & Yilmazel (2022), the acetate consumption was lower in this study; yet, the current production was similar around 0.32 A/m^2. In addition, Kas (2021) conducted Mini-MECs fed with DF effluent and inoculated with wild-type *G. acetivorans* without any previous biofilm formation and adaptation which resulted a hydrogen production rate as ~ 0.08 m^3 H$_2$/m^{3}d. This is very close to the result achieved in WT reactors; however, the reactor volume and electrode material are different in these studies.
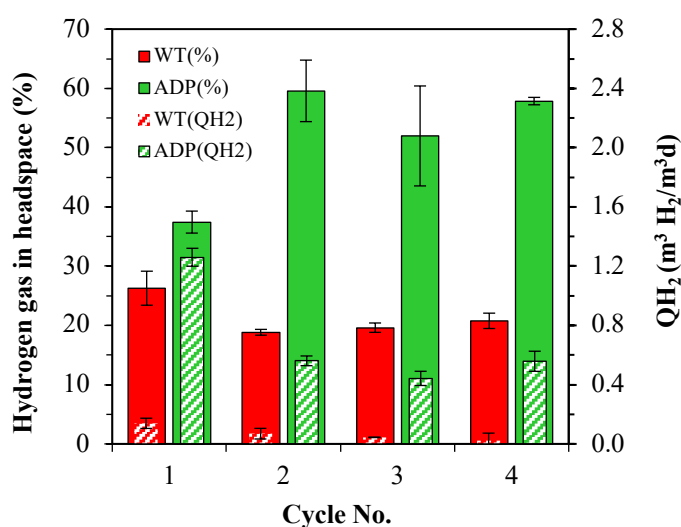
Figure 4.17 Hydrogen gas percentages and hydrogen production rates for Run 2.2 (outer bars shows hydrogen gas percentage and inner bars indicate the hydrogen production rate; green/dashed green bars: ADP reactors; red/dashed red bars: WT reactors)

Although the increase in current production of ADP was 4.6 times compared to WTs, the increase in Q$_{H_2}$ was much more. This 2.5 times difference between current generation and hydrogen production rate between ADP and WT reactors might be

the result of different levels of internal hydrogen cycling in the respective MECs. As mentioned in Chapter 4.2.3.1, *G. acetivorans* can use hydrogen gas produced in the system as a sole electron donor to produce current. The acetate-grown *G. acetivorans* showed an important inhibition when fed with DF effluent; thus, all acetate consumed may not be used for current production by *G. acetivorans*; yet, hydrogen might be utilized for that purpose.

Also, Q_{H_2} of ADP reactors was 1.2 times higher than CFB reactors fed with 10 mM acetate in Run 2.1. Although the reactors were fed with pure substrate in Run 2.1, adapted culture showed a considerable increase in both current and Q_{H_2} in Run 2.2. It may be also resulted due to the inability of adapted culture to use hydrogen as an electron donor as effective as acetate-grown *G. acetivorans.* Sapireddy et al. (2021) expressed that inability of hydrogen recycling is a unique feature which enables the maximum energy recovery in the form of H_2 in a single chamber MEC. Yet, to elucidate this characteristics of adapted culture, genomic analysis is required, and this is out of the scope of this thesis.

The hydrogen yield of two-stage DF-MEC system

The main objective of this study is to enhance hydrogen production from UCM via two-stage DF-MEC system at hyperthermophilic temperatures. To investigate the hydrogen production performance, the hydrogen yield of ADP was calculated. ADP was selected because of its superior performance on DF effluent utilization. The assumptions to calculate the H_2 yield were given as: (i) the highest hydrogen yield was achieved in the first part (DF operation) from 15 g VS/L of UCM via adapted culture; therefore, the feed rate (in terms of VS) was calculated based on this reactor, (ii) the feed rate of MECs was equivalent to 1:10 of DF influent, (iii) the hydrogen production was calculated by taking the average of three cycles for ADP, and (iv) the hydrogen yield for one cycle operation was taken into consideration. Based on these assumptions, the hydrogen yield of ADP was resulted as 345.5 ± 13.5 mL H_2/g VS_{added}. The highest hydrogen yield achieved in DF operation from adapted culture was 161.3 mL H_2/g VS_{added} at UCM concentration of 15 g VS/L. Overall hydrogen

yield achieved via two-stage hyperthermophilic DF-MEC system was 506.8 ± 13.6 mL H_2/g VS_{added}.

Efficiency calculations

Over the 3 cycles, acetate consumption was averaged at 98.0 ± 1.0 % for ADP and 54.7 ± 2.3 % for WT. Almost all acetate was consumed by the adapted culture, yet acetate-grown *G. acetivorans* only consumed the half of the acetate in the reactor. Also, C_E (%) values for WT reactors showed a significant difference compared to ADP as averaged at 225.4 ± 64.2 % for WT and 109.2 ± 6.7 % for ADP (Figure 4.18). The higher than 100% C_E indicates internal hydrogen cycling. Yet, with adapted culture even though the C_E values were still higher than 100%, thus if hydrogen gas has contributed to current production, it may be limited by 9 % in the ADP reactors. In terms of cathodic hydrogen recovery, ADP showed a superior performance ($\sim$2.4 times) in comparison to WT (Table 4.3). Since it was suspected that the hydrogen production was low, and may be used for current production by WT, overall hydrogen recovery (R_{H_2}) was also lower than ADPs even though the C_E values were significantly higher. Over the 3 cycles of test period, the overall hydrogen recoveries were 60.3 ± 7 % for ADP and 49.0 ± 2.7 % for WT.
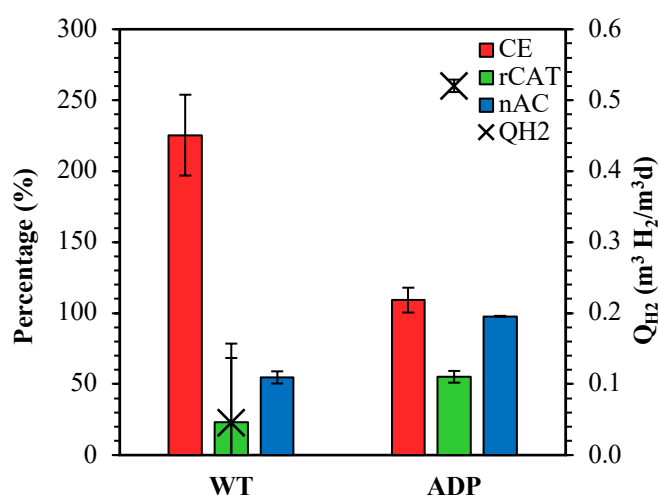
Figure 4.18 Coulombic efficiency (C_E), cathodic hydrogen recovery (r_{CAT}), acetate consumption (n_{AC}) and hydrogen production rate (Q_{H_2}) for DF effluent test in Run 2.2

Table 4.3 The overall performance results for Run 2.2

Reactor	j (A/m^2)	C_E (%)	r_{CAT} (%)	Q_{H2} (m^3 H$_2$/m^{3}d)
ADP	1.58 ± 0.07	109.2 ± 6.7	55.2 ± 5.7	0.52 ± 0.07
WT	0.34 ± 0.04	225.4 ± 64.2	23.0 ± 6.8	0.05 ± 0.02

Biofilm analysis

Figure 4.19 presents the CVs of Run 2.2 under DF effluent supply. The CV analysis of both ADP and WT showed a S-shaped sigmoidal curve. The absence of significant redox peaks in the spent medium and the S-shaped curves during turn-over CV suggest the presence of extracellular electron transfer via DET as discussed in Chapter 3.2.7.1. CV analysis was done in the last cycle of the operation at the time that peak current density was reached. The peak in CV of ADP was higher than WT reactors, which is consistent with the cycle current production.
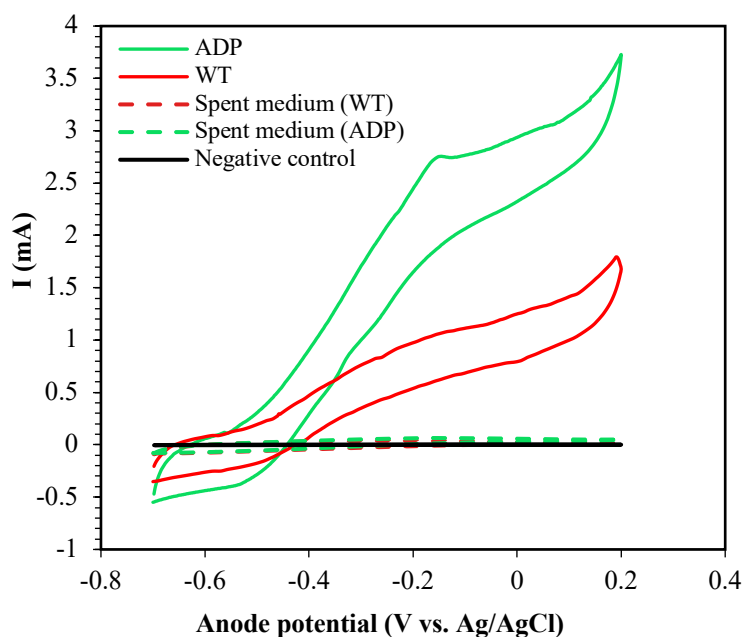
Figure 4.19 Cyclic voltammograms for Run 2.2 (red line: turnover of WT; green line: turnover of ADP; dashed red line: spent medium of WT; dashed green line: spent medium of ADP; black line: abiotic)

SEM images of bioanodes shown in Figure 4.20 demonstrates a stack of irregular cocci similar to the Run 2.1. The cells on WT bioanodes were considerably smaller

110

than ADP biofilm. In addition, ADP bioanodes showed a relatively denser network of biofilm. The lower density and smaller size of biomass on WT bioanodes may be a result of severe biofilm inhibition due DF effluent feed.
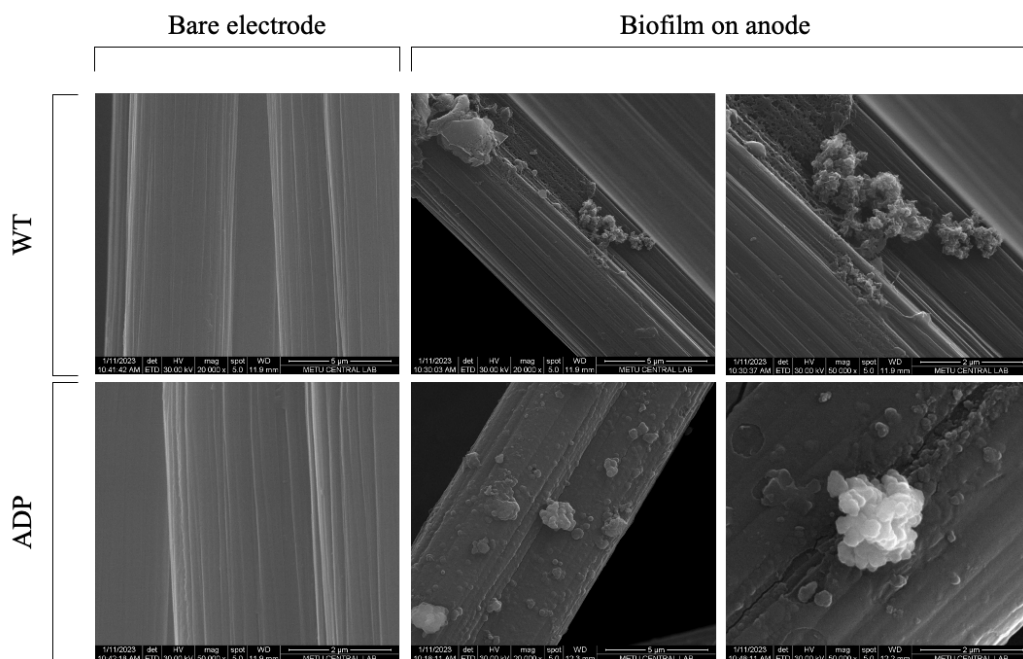
Figure 4.20 SEM images of bioanodes in Run 2.2

The viability and activity of anode biofilm was investigated using CLSM imaging to test whether the significant difference in current production would be linked with the anode biofilm structure. CLSM imaging results for Run 2.2 were illustrated in Figure 4.21. As shown, WT anodes were covered with highly dense dead biofilm which caused to lower current production and longer operation time. As reported by Chen et al. (2017), the abundance of dead cells causes to decrease in current production due to their inactiveness and less conductivity. The anode biofilm of ADP showed a high viability and high coverage of electrode surface. High current production in ADP reactors can be attributed to the significant coverage of live biofilm with a considerable thickness of 118 μm. Sun et al. (2017) reported that complete living biofilm on anode leads to high performance compared to two-layer biofilm structure on anode. Further, Hussain et al. (2021) suggests that increase in thickness of anodic biofilm can enhance the biofilm conductivity if biofilm is metabolically active;

therefore, biofilm thickness combined with the abundance of living cells is one of the important factors affecting substrate-utilization rate in biofilm anodes. In line with the results, adaptation strategy can be beneficial to enhance the biofilm viability on MEC systems which enables the higher performance on current and hydrogen production.
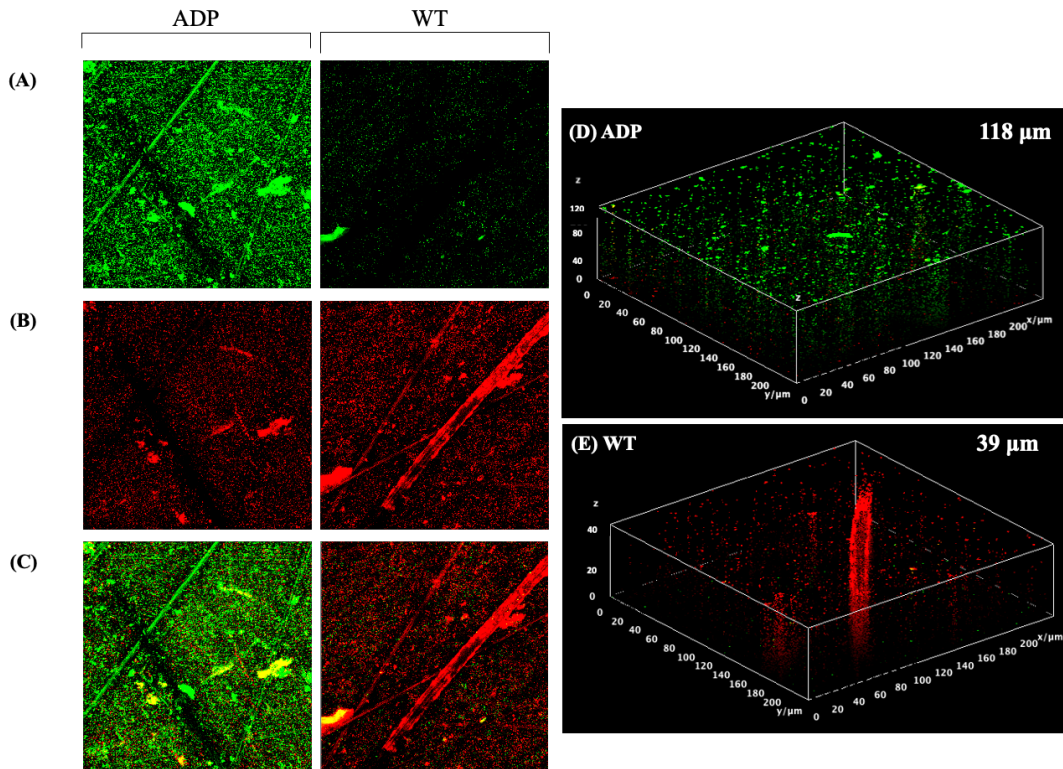
Figure 4.21 Confocal laser scanning microscope (CLSM) images from a LIVE/DEAD assay of *G. acetivorans* biofilm anode in Run 2.2 (A) Live cells (green), (B) Dead cells (red), (C) Live and dead cells, (D) 3D images of ADP anode biofilm with a biofilm thickness of 118 μm and (E) 3D images of WT anode biofilm with a biofilm thickness of 39 μm

4.2.3.3   Run 2.3: Internal hydrogen cycling test

In Run 2.1, the reactors fed with 10 mM acetate and the acetate consumption considerably high in CFB reactors during the test period (83.5 ± 2.6 %), yet, the C_E values for all cycles were significantly above 100% indicating the possible internal hydrogen cycling phenomenon which was reported in previous studies using single

chamber MECs. It was presented that *G. acetivorans* has ability to use H_2 as a sole electron donor while Fe(III) is present as an electron acceptor in the growth medium (Slobodkina et al., 2009). Further results about internal hydrogen cycling by *G. acetivorans* in Mini-MECs were reported by Kas & Yılmazel (2022), which showed that *G. acetivorans* can use the hydrogen gas generated in the system as an electron donor and the solid-state electrode as an electron acceptor. In Run 2.2, the acetate consumption was very close to the 100% and the C_E values were slightly higher than 100% for ADP reactors. It was assumed that the use of H_2 to produce current by adapted culture was much lower than acetate-grown and acetate-fed *G. acetivorans*. It was suggested that the fermentation effluent might cause an inhibition on H_2 consumption mechanism of *G. acetivorans*. To investigate, internal hydrogen cycling test was operated using single chamber MECs inoculated with adapted culture and control MECs (fed with acetate) inoculated with acetate-grown *G. acetivorans*.

The results of internal hydrogen cycling test showed that adapted culture could not use hydrogen as an electron donor as much as acetate grown culture. In the fourth cycle of the experiment, hydrogen was provided as a sole electron donor to the reactors. In reactors inoculated with adapted culture, only a slight increase was observed in the current generation compared to the cycle that no electron donor was present in the medium (Cycle 3). The average current production when H_2 was only electron donor (Cycle 4) for adapted culture was recorded as 0.31 ± 0.08 A/m^2 (Figure 4.22). The current generation when H_2 was provided as a sole electron donor is similar to the current production in Cycle 3. On the other hand, acetate-grown culture showed a significant current production as 0.84 ± 0.12 A/m^2 when the reactor was only supplemented with H_2 as an electron donor. The extent of current production from H_2 was about 60% of current production from acetate for ACE-fed WTs. To ensure this feature of adapted culture, 3 cycles of media replacement of: (i) no electron donor, (ii) H_2 as the sole electron donor, (iii) acetate as the sole electron donor have been repeated twice. Thus, the results of the internal hydrogen cycling

test presented that adapted culture could not use hydrogen gas as an electron donor like wild type to produce considerable current in single chamber MECs.
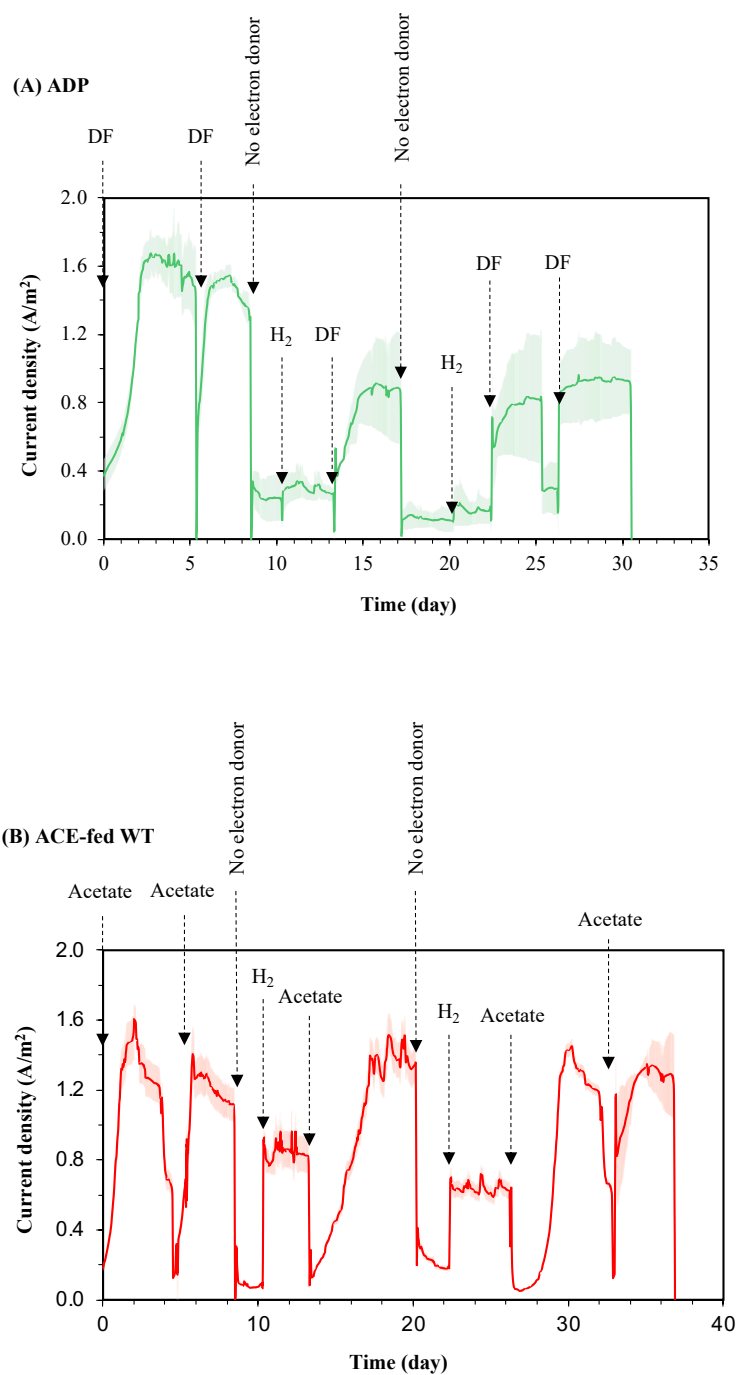
Figure 4.22 Normalized current production of internal hydrogen cycling test (A) ADP and (B) ACE-fed WT

4.2.4 Set 3: Two-chamber MEC operation

A two-chamber reactor (H-cell MECs) operation is necessary to be sure that H_2 is not contributing highly to the current generation and the substrate is being consumed for current production in the MEC. The anode and cathode chambers were separated using an anion exchange membrane to prevent the any hydrogen leakage to the anodic chamber. Current production in two-chamber MECs is given in Figure 4.23.
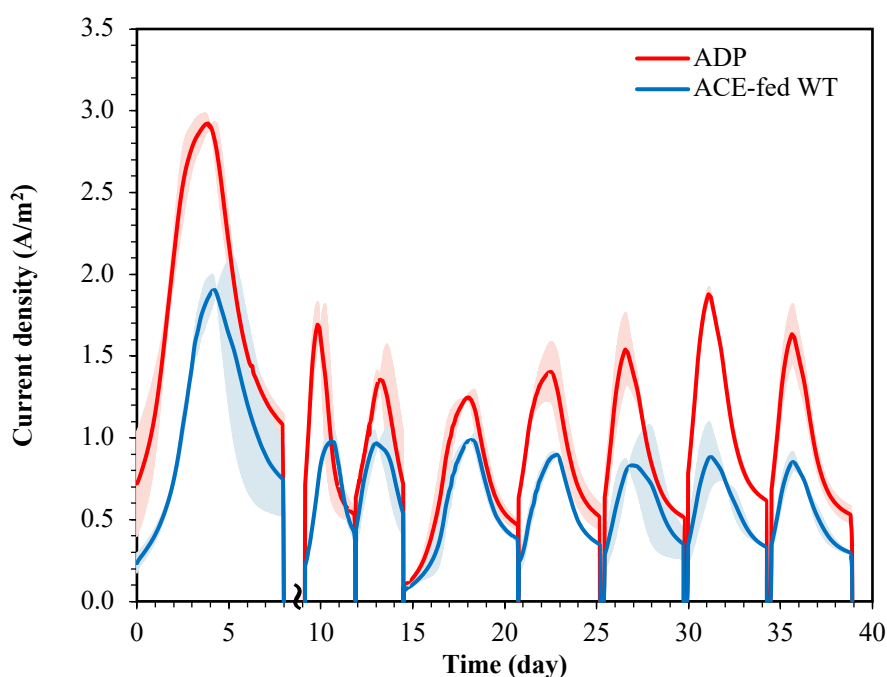
Figure 4.23 Normalized current production for two-chamber reactor operation

At the end of the first cycle, the reactors failed as a result of a high gas production, but the electrodes were kept in anaerobic conditions and the operation continued using the same electrodes. Due to the failure, the average of the last 5 cycles have been taken into consideration. The current production was averaged at 1.69 ± 0.17 A/m^2 for adapted culture fed with DF effluent and 0.86 ± 0.03 A/m^2 for control reactors fed with acetate. Compared to the single chamber MEC operations, adapted culture showed even higher current generation over the test period which was about 7%. The increase in current production might be resulted because of hydrogen generation in separated chamber which prevents the H_2 accumulation in the

headspace. In contrast, ACE-fed WTs could produce only 45%-60% of current produced in single chamber MECs (Run 2.1, CFB) which also shows that acetate-grown *G. acetivorans* uses H_2 as an electron donor to produce current in single chamber MEC.

Hydrogen production rates for both reactors was stable during the last 5 cycles. The averaged hydrogen production rates were resulted as 0.57 ± 0.04 m^3 H_2/m^{3}d for ADPs and 0.30 ± 0.03 m^3 H_2/m^{3}d for ACE-fed WTs (Figure 4.24). About 2 times increase in Q_{H2} was observed in ADP compared to ACE-fed WT. Adapted culture showed both enhancement in hydrogen generation and performance efficiency compared to ACE-fed WT.
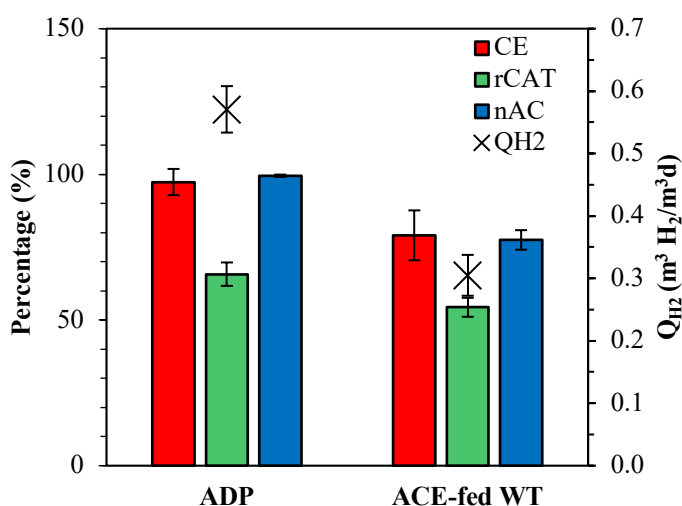
Figure 4.24 Coulombic efficiency (CE), cathodic recovery (rCAT), acetate consumption (nAC) and hydrogen production rate (Q_{H2}) of G. acetivorans two-chamber MECs (A) ADP reactors (B) ACE-fed WT reactors

Over the last 5 cycles, acetate consumption was measured as $99.5 \pm 0.04\%$ for ADP and $77.5 \pm 3.4\%$ for ACE-fed WTs (Figure 4.24). It can be clearly seen that adapted culture have an ability to consume almost all acetate presented in DF effluent. On the other hand, acetate-grown *G. acetivorans* only consumed three fourths of pure acetate. Over the last 5 cycles, the average coulombic efficiencies were $97.3 \pm 4.5\%$ for ADP and $79.1 \pm 8.6\%$ for ACE-fed WT. Based on the C_E values, adapted culture can use almost all electrons to produce current in MEC reactor. In line with these

results, cathodic hydrogen recoveries were higher in ADPs ($65.7 \pm 4.0\%$) about 21% compared to ACE-fed WTs ($54.3 \pm 3.2\%$). Therefore, based on the results achieved in internal hydrogen cycling test and two-chamber operation, there is a significant possibility that adapted culture may not utilize hydrogen as an electron donor in contrast to the acetate-grown culture.

CHAPTER 5

CONCLUSION

In this thesis, the enhancement of H_2 production from UCM via two-stage hyperthermophilic DF and MEC system was studied. In the first part, two different strategies, as intermittent gas sparging and culture adaptation, were examined for DF operation. In the second part, bioelectrochemical H_2 production from DF effluent via MEC was investigated including culture and electrode material selection, the utilization of DF effluent via culture adaptation.

The results of the first part of the experiments showed that cellulolytic bacterium *C. bescii* can degrade UCM at industrially relevant concentrations up to 50 g VS/L to produce hydrogen. During DF of such as complex waste, the inhibition of pure culture is inevitable at the first time test, especially at high concentrations. However, the inhibition due to product or feedstock can be prevented via different applications. As a result of this study, both strategies (sparging and adaptation) enhanced hydrogen production from UCM by *C. bescii*. Further, the adaptation of the culture to such a complex waste is proven to be a powerful strategy. Adapted *C. bescii* showed a remarkable potential for biohydrogen production from high concentrations of UCM, with the highest dark fermentative hydrogen yield of 161.3 ± 1.6 mL H_2/g VS_{added} achieved with animal manure feed so far. Dark fermentative hydrogen production from high substrate loads necessary to develop industrial scale processes is possible using the adapted *C. bescii*. Carbon balance showed that the effluent had considerably high amounts of organic acids, which presents an opportunity for a sequential operation of DF with another compatible reactor system as MEC.

In the second part of the experiments, bioelectrochemical hydrogen production from DF effluent was studied in MEC at 80 °C. In this experimental work, important results have been obtained regarding high temperature applications from renewable

feedstocks as DF effluent, which are very limited in number in the BES literature. Comparing the results of single chamber MEC operations, adapted culture can enhance the reactor performance and hydrogen production rate (0.52 ± 0.07 m^3 H$_2$/m^{3}d) from DF effluent about 11.5 times compared to acetate-grown culture (0.05 ± 0.02 m^3 H$_2$/m^{3}d) without showing any alteration. Further research on the adapted culture including hydrogen internal cycling phenomenon and two-chamber operations also revealed that adaptation procedure may cause to ineffectiveness of hydrogen consumption mechanism in adapted culture of *G. acetivorans*. This change in mechanism is a beneficial trait since hydrogen production rate was significantly enhanced due to inability of adapted culture to consume hydrogen to generate current.

As a result, hyperthermophilic hydrogen production from UCM has been enhanced using two-stage operation of DF and MEC, achieving total hydrogen yield of 506.8 ± 13.6 mL H$_2$/g VS. The adaptation of pure cultures showed a superior performance in both hydrogen production systems. Hence, these results will be useful for future research on improving the effectiveness of biohydrogen production from DF and MEC systems.

CHAPTER 6

RECOMMENDATION

Hyperthermophilic biohydrogen production via two-stage DF and MEC system is an emerging technology. Despite the recent research in fundamental mechanisms and bench-scale investigations, there are several recommendations for future research as summarized follows:

- The results of this study showed that pure cultures can be operated in lab-scale reactors with non-sterile feedstocks at hyperthermophilic temperatures. The further research is necessary to optimize the system for larger scale operations. For this purpose, it is suggested to implement continuous two-stage operation of DF and MEC system to develop an efficient hydrogen production from unpretreated renewable feedstocks.

- During this study, different biofilm imaging techniques have been used to observe the electro-activity of biofilm in MECs. Yet, all imaging analyses were done at the end of reactor operations. It could be useful to investigate the viability of biofilm depending on time which gives a significant understanding about the biofilm formation process and the viability of biofilm depending on time.

- In this work, hyperthermophilic biohydrogen production was achieved via two-stage operation. For future, these systems can be integrated and operated as a single bioreactor using suitable pure cultures in compliance with the requirements of two systems.

REFERENCES

Abreu, A. A., Karakashev, D., Angelidaki, I., Sousa, D. Z., & Alves, M. M. (2012). Biohydrogen production from arabinose and glucose using extreme thermophilic anaerobic mixed cultures. *Biotechnology for Biofuels*, *5*, 1–12. https://doi.org/10.1186/1754-6834-5-6

Abreu, A., Tavares, F., Alves, M. M., & Pereira, M. A. (2016). Boosting dark fermentation with co-cultures of extreme thermophiles for biohythane production from garden waste. *Bioresource Technology*, *219*, 132–138. https://doi.org/10.1016/j.biortech.2016.07.096

Abreu, Angela., Tavares, F., Alves, M. M., Cavaleiro, A. J., & Pereira, M. A. (2019). Garden and food waste co-fermentation for biohydrogen and biomethane production in a two-step hyperthermophilic-mesophilic process. *Bioresource Technology*, *278*(January), 180–186. https://doi.org/10.1016/j.biortech.2019.01.085

Almatouq, A., & Babatunde, A. O. (2017). Concurrent hydrogen production and phosphorus recovery in dual chamber microbial electrolysis cell. *Bioresource Technology*, *237*, 193–203. https://doi.org/10.1016/j.biortech.2017.02.043

Amin, M., Shah, H. H., Bashir, B., Iqbal, M. A., Shah, U. H., & Ali, M. U. (2023). Environmental Assessment of Hydrogen Utilization in Various Applications and Alternative Renewable Sources for Hydrogen Production: A Review. In *Energies* (Vol. 16, Issue 11). MDPI. https://doi.org/10.3390/en16114348

Angenent, L. T., Karim, K., Al-Dahhan, M. H., Wrenn, B. A., & Domíguez-Espinosa, R. (2004). Production of bioenergy and biochemicals from industrial and agricultural wastewater. In *Trends in Biotechnology* (Vol. 22, Issue 9, pp. 477–485). https://doi.org/10.1016/j.tibtech.2004.07.001

APHA, AWWA, & WPCF. (2005). Standard Methods for the Examination of Water and Wastewater. *American Public Health Association, Washington.*

Badalamenti, J. P., Krajmalnik-Brown, R., & Torres, C. I. (2013). Generation of high current densities by pure cultures of anode-respiring Geoalkalibacter spp. Under alkaline and saline conditions in microbial electrochemical cells. *MBio*, *4*(3). https://doi.org/10.1128/mBio.00144-13

Bakonyi, P., Kumar, G., Koók, L., Tóth, G., Rózsenberszki, T., Bélafi-Bakó, K., & Nemestóthy, N. (2018). Microbial electrohydrogenesis linked to dark fermentation as integrated application for enhanced biohydrogen production: A review on process characteristics, experiences and lessons. In *Bioresource Technology* (Vol. 251, pp. 381–389). Elsevier Ltd. https://doi.org/10.1016/j.biortech.2017.12.064

Basen, M., Rhaesa, A. M., Kataeva, I., Prybol, C. J., Scott, I. M., Poole, F. L., & Adams, M. W. W. (2014). Degradation of high loads of crystalline cellulose and of unpretreated plant biomass by the thermophilic bacterium Caldicellulosiruptor bescii. *Bioresource Technology*, *152*, 384–392. https://doi.org/10.1016/j.biortech.2013.11.024

Bing, W., Wang, H., Zheng, B., Zhang, F., Zhu, G., Feng, Y., & Zhang, Z. (2015). Caldicellulosiruptor changbaiensis sp. nov., a cellulolytic and hydrogen-producing bacterium from a hot spring. *International Journal of Systematic and Evolutionary Microbiology*, *65*(1), 293–297. https://doi.org/10.1099/ijs.0.065441-0

Blumer-Schuette, S. E., Lewis, D. L., & Kelly, R. M. (2010). Phylogenetic, microbiological, and glycoside hydrolase diversities within the extremely thermophilic, plant biomass-degrading genus caldicellulosiruptor. *Applied and Environmental Microbiology*, *76*(24), 8084–8092. https://doi.org/10.1128/AEM.01400-10

Boodhun, B. S. F., Mudhoo, A., Kumar, G., Kim, S. H., & Lin, C. Y. (2017). Research perspectives on constraints, prospects and opportunities in biohydrogen production. *International Journal of Hydrogen Energy*, *42*(45), 27471–27481. https://doi.org/10.1016/j.ijhydene.2017.04.077

Bora, A., Mohanrasu, K., Angelin Swetha, T., Ananthi, V., Sindhu, R., Chi, N. T. L., Pugazhendhi, A., Arun, A., & Mathimani, T. (2022). Microbial electrolysis cell (MEC): Reactor configurations, recent advances and strategies in biohydrogen production. *Fuel*, *328*. https://doi.org/10.1016/j.fuel.2022.125269

Bredholt, S., Sonne-Hansen, J., Nie, P., Mathrani', M., & Ahring', B. K. (1999). Caldicellulosiruptor kristjanssonii sp. nov., a cel lulolytic, extremely thermophi l ic, anaerobic bacterium. In *international Journal of Systematic Bacteriology* (Vol. 49).

Byrne, E., Björkmalm, J., Bostick, J. P., Sreenivas, K., Willquist, K., & Niel, E. W. J. Van. (2021). Characterization and adaptation of Caldicellulosiruptor strains to higher sugar concentrations , targeting enhanced hydrogen production from lignocellulosic hydrolysates. *Biotechnology for Biofuels*, 1–14. https://doi.org/10.1186/s13068-021-02058-x

Cabrol, L., Marone, A., Tapia-Venegas, E., Steyer, J. P., Ruiz-Filippi, G., & Trably, E. (2017). Microbial ecology of fermentative hydrogen producing bioprocesses: Useful insights for driving the ecosystem function. *FEMS Microbiology Reviews*, *41*(2), 158–181. https://doi.org/10.1093/femsre/fuw043

Cakr, A., Ozmihci, S., & Kargi, F. (2010). Comparison of bio-hydrogen production from hydrolyzed wheat starch by mesophilic and thermophilic dark fermentation. *International Journal of Hydrogen Energy*, *35*(24), 13214–13218. https://doi.org/10.1016/j.ijhydene.2010.09.029

Call, D. F., Merrill, M. D., & Logan, B. E. (2009). High surface area stainless steel brushes as cathodes in microbial electrolysis cells. *Environmental Science and Technology*, *43*(6), 2179–2183. https://doi.org/10.1021/es803074x

Call, D., & Logan, B. E. (2008). Hydrogen production in a single chamber microbial electrolysis cell lacking a membrane. *Environmental Science and Technology*, *42*(9), 3401–3406. https://doi.org/10.1021/es8001822

Carmona-Martínez, A. A., Pierra, M., Trably, E., & Bernet, N. (2013). High current density via direct electron transfer by the halophilic anode respiring bacterium Geoalkalibacter subterraneus. *Physical Chemistry Chemical Physics*, *15*(45), 19699–19707. https://doi.org/10.1039/c3cp54045f

Chen, H., Wu, J., Wang, H., Zhou, Y., Xiao, B., Zhou, L., Yang, M., Xiong, Y., & Wu, S. (2021). Dark co-fermentation of rice straw and pig manure for biohydrogen production : effects of different inoculum pretreatments and substrate mixing ratio. *Environmental Technology*. https://doi.org/10.1080/09593330.2020.1770340

Chen, S., Fang, Y., Jing, X., Luo, H., Chen, J., & Zhou, S. (2018). Enhanced electrosynthesis performance of Moorella thermoautotrophica by improving cell permeability. *Bioelectrochemistry*, *121*, 151–159. https://doi.org/10.1016/j.bioelechem.2018.02.003

Chen, S., Jing, X., Tang, J., Fang, Y., & Zhou, S. (2017). Quorum sensing signals enhance the electrochemical activity and energy recovery of mixed-culture electroactive biofilms. *Biosensors and Bioelectronics*, *97*, 369–376. https://doi.org/10.1016/j.bios.2017.06.024

Chen, W., Feng, H., Shen, D., Jia, Y., Li, N., Ying, X., Chen, T., Zhou, Y., Guo, J., & Zhou, M. (2018). Carbon materials derived from waste tires as high-performance anodes in microbial fuel cells. *Science of the Total Environment*, *618*, 804–809. https://doi.org/10.1016/j.scitotenv.2017.08.201

Cheng, S., & Logan, B. E. (2007). Sustainable and efficient biohydrogen production via electrohydrogenesis. *Proceedings of the National Academy of Sciences of the United States of America*, *104*(47), 18871–18873. https://doi.org/10.1073/pnas.0706379104

Cheonh, P. Y. Y., Kansedo, J., Lau, J. S. Y., & Tan, Y. H. (2022). 5.13 - Renewable Biomass Wastes for Biohydrogen Production. In *Comprehensive Renewable Energy, Second Edition: Volume 1-9* (Vols. 1–9, pp. 273–298). Elsevier. https://doi.org/10.1016/B978-0-12-819727-1.00091-1

Christiansen, F. B., & Loeschcke, V. (n.d.). *2 Evolution and Competition*.

Conway, J. M., McKinley, B. S., Seals, N. L., Hernandez, D., Khatibi, P. A., Poudel, S., Giannone, R. J., Hettich, R. L., Williams-Rhaesa, A. M., Lipscomb, G. L., Adams, M. W. W., & Kelly, R. M. (2017). Functional analysis of the glucan degradation locus in Caldicellulosiruptor bescii reveals essential roles of component glycoside hydrolases in plant biomass deconstruction. *Applied and Environmental Microbiology*, *83*(24), 1–22. https://doi.org/10.1128/AEM.01828-17

Cui, M., & Shen, J. (2012). Effects of acid and alkaline pretreatments on the biohydrogen production from grass by anaerobic dark fermentation. *International Journal of Hydrogen Energy*, *37*(1), 1120–1124. https://doi.org/10.1016/j.ijhydene.2011.02.078

De Vrije, T., Mars, A. E., Budde, M. A. W., Lai, M. H., Dijkema, C., De Waard, P., & Claassen, P. A. M. (2007). Glycolytic pathway and hydrogen yield studies of the extreme thermophile Caldicellulosiruptor saccharolyticus. *Applied Microbiology and Biotechnology*, *74*(6), 1358–1367. https://doi.org/10.1007/s00253-006-0783-x

Dessì, P., Porca, E., Waters, N. R., Lakaniemi, A. M., Collins, G., & Lens, P. N. L. (2018). Thermophilic versus mesophilic dark fermentation in xylose-fed fluidised bed reactors: Biohydrogen production and active microbial community. *International Journal of Hydrogen Energy*, *43*(11), 5473–5485. https://doi.org/10.1016/j.ijhydene.2018.01.158

Dragosits, M., & Mattanovich, D. (2013). Adaptive laboratory evolution - principles and applications for biotechnology. In *Microbial Cell Factories* (Vol. 12, Issue 1). https://doi.org/10.1186/1475-2859-12-64

Egorova, K., & Antranikian, G. (2005). Industrial relevance of thermophilic Archaea. *Current Opinion in Microbiology*, *8*(6), 649–655. https://doi.org/10.1016/j.mib.2005.10.015

Ehrlich, H. L. (2008). Are gram-positive bacteria capable of electron transfer across their cell wall without an externally available electron shuttle? *Geobiology*, *6*(3), 220–224. https://doi.org/10.1111/j.1472-4669.2007.00135.x

Elgrishi, N., Rountree, K. J., McCarthy, B. D., Rountree, E. S., Eisenhart, T. T., & Dempsey, J. L. (2018). A Practical Beginner's Guide to Cyclic Voltammetry. *Journal of Chemical Education*, *95*(2), 197–206. https://doi.org/10.1021/acs.jchemed.7b00361

El-Naggar, M. Y., Gorby, Y. A., Xia, W., & Nealson, K. H. (2008). The molecular density of states in bacterial nanowires. *Biophysical Journal*, *95*(1). https://doi.org/10.1529/biophysj.108.134411

Elsharnouby, O., Hafez, H., Nakhla, G., & El Naggar, M. H. (2013). A critical literature review on biohydrogen production by pure cultures. *International Journal of Hydrogen Energy*, *38*(12), 4945–4966. https://doi.org/10.1016/j.ijhydene.2013.02.032

Feng, Y., Yang, Q., Wang, X., & Logan, B. E. (2010). Treatment of carbon fiber brush anodes for improving power generation in air-cathode microbial fuel cells. *Journal of Power Sources*, *195*(7), 1841–1844. https://doi.org/10.1016/j.jpowsour.2009.10.030

Ferraren-De Cagalitan, D. D. T., & Abundo, M. L. S. (2021). A review of biohydrogen production technology for application towards hydrogen fuel cells. In *Renewable and Sustainable Energy Reviews* (Vol. 151). Elsevier Ltd. https://doi.org/10.1016/j.rser.2021.111413

Fu, Q., Fukushima, N., Maeda, H., Sato, K., & Kobayashi, H. (2015). Bioelectrochemical analysis of a hyperthermophilic microbial fuel cell generating electricity at temperatures above 80 °C. *Bioscience, Biotechnology and Biochemistry*, *79*(7), 1200–1206. https://doi.org/10.1080/09168451.2015.1015952

Fu, Q., Kobayashi, H., Kawaguchi, H., Wakayama, T., Maeda, H., & Sato, K. (2013). A thermophilic gram-negative nitrate-reducing bacterium, calditerrivibrio nitroreducens, exhibiting electricity generation capability. *Environmental Science and Technology*, *47*(21), 12583–12590. https://doi.org/10.1021/es402749f

Gautam, R., Nayak, J. K., Ress, N. V., Steinberger-Wilckens, R., & Ghosh, U. K. (2023). Bio-hydrogen production through microbial electrolysis cell: Structural components and influencing factors. In *Chemical Engineering Journal* (Vol. 455). Elsevier B.V. https://doi.org/10.1016/j.cej.2022.140535

Gilroyed, B. H., Chang, C., Chu, A., & Hao, X. (2008). Effect of temperature on anaerobic fermentative hydrogen gas production from feedlot cattle manure using mixed microflora. *International Journal of Hydrogen Energy*, *33*(16), 4301–4308. https://doi.org/10.1016/j.ijhydene.2008.06.016

Gopalakrishnan, B., Khanna, N., & Das, D. (2019). Dark-Fermentative Biohydrogen Production. In *Biomass, Biofuels, Biochemicals: Biohydrogen, Second Edition* (pp. 79–122). Elsevier. https://doi.org/10.1016/B978-0-444-64203-5.00004-6

Guo, X. M., Trably, E., Latrille, E., Carrre, H., & Steyer, J. P. (2010). Hydrogen production from agricultural waste by dark fermentation: A review. *International Journal of Hydrogen Energy*, *35*(19), 10660–10673. https://doi.org/10.1016/j.ijhydene.2010.03.008

Gupta, N., Pal, M., Sachdeva, M., Yadav, M., & Tiwari, A. (2016). Thermophilic biohydrogen production for commercial application: the whole picture.

International Journal of Energy Research, *40*, 127–145. https://doi.org/0.1002/er.3438

Hafenbradl, D., Keller, M., Dirmeier, R., Rachel, R., Roßnagel, P., Burggraf, S., Huber, H., & Stetter, K. O. (1996). Ferroglobus placidus gen. nov., sp. nov., a novel hyperthermophilic archaeum that oxidizes Fe2+ at neutral pH under anoxic conditions. *Archives of Microbiology*, *166*(5), 308–314. https://doi.org/10.1007/s002030050388

Hallenbeck, P. C. (2012). Microbial technologies in advanced biofuels production. In *Microbial Technologies in Advanced Biofuels Production* (Vol. 9781461412083). Springer US. https://doi.org/10.1007/978-1-4614-1208-3

Hamilton-Brehm, S. D., Mosher, J. J., Vishnivetskaya, T., Podar, M., Carroll, S., Allman, S., Phelps, T. J., Keller, M., & Elkins, J. G. (2010). Caldicellulosiruptor obsidiansis sp. nov., an anaerobic, extremely thermophilic, cellulolytic bacterium isolated from obsidian pool, yellowstone National Park. *Applied and Environmental Microbiology*, *76*(4), 1014–1020. https://doi.org/10.1128/AEM.01903-09

Hu, H., Fan, Y., & Liu, H. (2008). Hydrogen production using single-chamber membrane-free microbial electrolysis cells. *Water Research*, *42*(15), 4172–4178. https://doi.org/10.1016/j.watres.2008.06.015

Huang, C.-Y., Patel, B. K., Mah', R. A., & Baresi3, L. (1998). Caldicellulosiruptor o wensensis sp. nov., an anaerobic, extremely thermophilic, xylanolytic bacterium. In *International Journal of Systematic Bacteriology* (Vol. 48).

Hussain, A., Lee, J., Ren, H., & Lee, H. S. (2021). Spatial distribution of biofilm conductivity in a Geobacter enriched anodic biofilm. *Chemical Engineering Journal*, *404*. https://doi.org/10.1016/j.cej.2020.126544

Hussy, I., Hawkes, F. R., Dinsdale, R., & Hawkes, D. L. (2005). Continuous fermentative hydrogen production from sucrose and sugarbeet. *International*

Journal of Hydrogen Energy, *30*(5), 471–483. https://doi.org/10.1016/j.ijhydene.2004.04.003

IEA. (2022). *World Energy Outlook 2022*. www.iea.org/t&c/

Ivanova, G., Rákhely, G., & Kovács, K. L. (2009). Thermophilic biohydrogen production from energy plants by Caldicellulosiruptor saccharolyticus and comparison with related studies. *International Journal of Hydrogen Energy*, *34*(9), 3659–3670. https://doi.org/10.1016/j.ijhydene.2009.02.082

Jeremiasse, A. W., Bergsma, J., Kleijn, J. M., Saakes, M., Buisman, C. J. N., Cohen Stuart, M., & Hamelers, H. V. M. (2011). Performance of metal alloys as hydrogen evolution reaction catalysts in a microbial electrolysis cell. *International Journal of Hydrogen Energy*, *36*(17), 10482–10489. https://doi.org/10.1016/j.ijhydene.2011.06.013

Kadier, A., Jiang, Y., Lai, B., Rai, P. K., Chandrasekhar, K., Mohamed, A., & Kalil, M. S. (2019). Biohydrogen production in microbial electrolysis cells from renewable resources. In *Bioenergy and Biofuels* (Issue January). https://doi.org/10.1201/9781351228138-12

Kadier, A., Kalil, M. S., Abdeshahian, P., Chandrasekhar, K., Mohamed, A., Azman, N. F., Logroño, W., Simayi, Y., & Hamid, A. A. (2016). Recent advances and emerging challenges in microbial electrolysis cells (MECs) for microbial production of hydrogen and value-added chemicals. In *Renewable and Sustainable Energy Reviews* (Vol. 61, pp. 501–525). Elsevier Ltd. https://doi.org/10.1016/j.rser.2016.04.017

Kadier, A., Simayi, Y., Kalil, M. S., Abdeshahian, P., & Hamid, A. A. (2014). A review of the substrates used in microbial electrolysis cells (MECs) for producing sustainable and clean hydrogen gas. In *Renewable Energy* (Vol. 71, pp. 466–472). Elsevier Ltd. https://doi.org/10.1016/j.renene.2014.05.052

Karlsson, A., Vallin, L., & Ejlertsson, J. (2008). Effects of temperature, hydraulic retention time and hydrogen extraction rate on hydrogen production from the

fermentation of food industry residues and manure. *International Journal of Hydrogen Energy*, *33*(3), 953–962. https://doi.org/10.1016/j.ijhydene.2007.10.055

Kaş, A. (2021). *HYPERTHERMOPHILIC HYDROGEN PRODUCTION BY GEOGLOBUS ACETIVORANS IN MICROBIAL ELECTROLYSIS CELLS A THESIS SUBMITTED TO THE GRADUATE SCHOOL OF NATURAL AND APPLIED SCIENCES OF MIDDLE EAST TECHNICAL UNIVERSITY.*

Kas, A., & Yilmazel, Y. D. (2022). High current density via direct electron transfer by hyperthermophilic archaeon, Geoglobus acetivorans, in microbial electrolysis cells operated at 80 °C. *Bioelectrochemistry*, *145*. https://doi.org/10.1016/j.bioelechem.2022.108072

Kashefi, K., Tor, J. M., Holmes, D. E., Gaw Van Praagh, C. V., Reysenbach, A. L., & Lovley, D. R. (2002). Geoglobus ahangari gen. nov., sp. nov., a novel hyperthermophilic archaeon capable of oxidizing organic acids and growing autotrophically on hydrogen with Fe(III) serving as the sole electron acceptor. *International Journal of Systematic and Evolutionary Microbiology*, *52*(3), 719–728. https://doi.org/10.1099/ijs.0.01953-0

Kataeva, I., Foston, M. B., Yang, S. J., Pattathil, S., Biswal, A. K., Poole, F. L., Basen, M., Rhaesa, A. M., Thomas, T. P., Azadi, P., Olman, V., Saffold, T. D., Mohler, K. E., Lewis, D. L., Doeppke, C., Zeng, Y., Tschaplinski, T. J., York, W. S., Davis, M., … Adams, M. W. W. (2013). Carbohydrate and lignin are simultaneously solubilized from unpretreated switchgrass by microbial action at high temperature. *Energy and Environmental Science*, *6*(7), 2186–2195. https://doi.org/10.1039/c3ee40932e

Kataoka, N., Miya, A., & Kiriyama, K. (1997). Studies on hydrogen production by continuous culture system of hydrogen-producing anaerobic bacteria. *Water Science and Technology*, *36*(6–7), 41–47. https://doi.org/10.1016/S0273-1223(97)00505-2

Khongkliang, P., Jehlee, A., Kongjan, P., Reungsang, A., & O-Thong, S. (2019). High efficient biohydrogen production from palm oil mill effluent by two-stage dark fermentation and microbial electrolysis under thermophilic condition. *International Journal of Hydrogen Energy*, *44*(60), 31841–31852. https://doi.org/10.1016/j.ijhydene.2019.10.022

Khongkliang, P., Kongjan, P., Utarapichat, B., Reungsang, A., & O-Thong, S. (2017). Continuous hydrogen production from cassava starch processing wastewater by two-stage thermophilic dark fermentation and microbial electrolysis. *International Journal of Hydrogen Energy*, *42*(45), 27584–27592. https://doi.org/10.1016/j.ijhydene.2017.06.145

Kim, B. H., Ikeda, T., Park, H. S., Kim, H. J., Hyun, M. S., Kano, K., Takagi, K., & Tatsumi, H. (1999). Electrochemical activity of an Fe(III)-reducing bacterium, Shewanella putrefaciens IR-1, in the presence of alternative electron acceptors. *Biotechnology Techniques*, *13*(7), 475–478. https://doi.org/10.1023/A:1008993029309

Kim, D. H., & Kim, M. S. (2012). Thermophilic fermentative hydrogen production from various carbon sources by anaerobic mixed cultures. *International Journal of Hydrogen Energy*, *37*(2), 2021–2027. https://doi.org/10.1016/j.ijhydene.2011.07.043

Klein, E. M., Knoll, M. T., & Gescher, J. (2023). Microbe–Anode Interactions: Comparing the impact of genetic and material engineering approaches to improve the performance of microbial electrochemical systems (MES). In *Microbial Biotechnology* (Vol. 16, Issue 6, pp. 1179–1202). John Wiley and Sons Ltd. https://doi.org/10.1111/1751-7915.14236

Kobayashi, H., Nagashima, A., Kouyama, M., Fu, Q., Ikarashi, M., Maeda, H., & Sato, K. (2017). High-pressure thermophilic electromethanogenic system producing methane at 5 MPa, 55°C. *Journal of Bioscience and Bioengineering*, *124*(3), 327–332. https://doi.org/10.1016/j.jbiosc.2017.04.001

Kotsopoulos, T. A., Fotidis, I. A., Tsolakis, N., & Martzopoulos, G. G. (2009). Biohydrogen production from pig slurry in a CSTR reactor system with mixed cultures under hyper-thermophilic temperature (70 °C). *Biomass and Bioenergy*, *33*(9), 1168–1174. https://doi.org/10.1016/j.biombioe.2009.05.001

Kraemer, J. T., & Bagley, Æ. D. M. (2007). *Improving the yield from fermentative hydrogen production*. 685–695. https://doi.org/10.1007/s10529-006-9299-9

Krieg, T., Sydow, A., Schröder, U., Schrader, J., & Holtmann, D. (2014). Reactor concepts for bioelectrochemical syntheses and energy conversion. In *Trends in Biotechnology* (Vol. 32, Issue 12, pp. 645–655). Elsevier Ltd. https://doi.org/10.1016/j.tibtech.2014.10.004

Kumar, G., Bakonyi, P., Zhen, G., Sivagurunathan, P., Koók, L., Kim, S. H., Tóth, G., Nemestóthy, N., & Bélafi-Bakó, K. (2017). Microbial electrochemical systems for sustainable biohydrogen production: Surveying the experiences from a start-up viewpoint. In *Renewable and Sustainable Energy Reviews* (Vol. 70, pp. 589–597). Elsevier Ltd. https://doi.org/10.1016/j.rser.2016.11.107

Kumar, N., & Das, D. (2001). *Continuous hydrogen production by immobilized Enterobacter cloacae IIT-BT 08 using lignocellulosic materials as solid matrices*. www.elsevier.com/locate/enzmictec

Kumar, R., Singh, L., Wahid, Z. A., & Din, M. F. M. (2015). Exoelectrogens in microbial fuel cells toward bioelectricity generation: A review. In *International Journal of Energy Research* (Vol. 39, Issue 8, pp. 1048–1067). John Wiley and Sons Ltd. https://doi.org/10.1002/er.3305

Lalaurette, E., Thammannagowda, S., Mohagheghi, A., Maness, P. C., & Logan, B. E. (2009). Hydrogen production from cellulose in a two-stage process combining fermentation and electrohydrogenesis. *International Journal of Hydrogen Energy*, *34*(15), 6201–6210. https://doi.org/10.1016/j.ijhydene.2009.05.112

Lee, H. S., & Rittmann, B. E. (2010). Significance of biological hydrogen oxidation in a continuous single-chamber microbial electrolysis cell. *Environmental Science and Technology*, *44*(3), 948–954. https://doi.org/10.1021/es9025358

Lee, H. S., Vermaas, W. F. J., & Rittmann, B. E. (2010). Biological hydrogen production: Prospects and challenges. In *Trends in Biotechnology* (Vol. 28, Issue 5, pp. 262–271). https://doi.org/10.1016/j.tibtech.2010.01.007

Lee, L. L., Crosby, J. R., Rubinstein, G. M., Laemthong, T., Bing, R. G., Straub, C. T., Adams, M. W. W., & Kelly, R. M. (2020). The biology and biotechnology of the genus Caldicellulosiruptor: recent developments in 'Caldi World.' *Extremophiles*, *24*(1), 1–15. https://doi.org/10.1007/s00792-019-01116-5

Lee, L. L., Izquierdo, J. A., Blumer-Schuette, S. E., Zurawski, J. V., Conway, J. M., Cottingham, R. W., Huntemann, M., Copeland, A., Chen, I. M. A., Kyrpides, N., Markowitz, V., Palaniappan, K., Ivanova, N., Mikhailova, N., Ovchinnikova, G., Andersen, E., Pati, A., Stamatis, D., Reddy, T. B. K., … Kelly, R. M. (2015). Complete genome sequences of Caldicellulosiruptor sp. strain Rt8.B8, Caldicellulosiruptor sp. strain Wai35.B1, and "Thermoanaerobacter cellulolyticus." *Genome Announcements*, *3*(3). https://doi.org/10.1128/genomeA.00440-15

Lee, S. H., Lee, S., Lee, S. M., Cha, J., Lee, H. S., & Kang, S. G. (2023). Biohydrogen Production from Food Waste Using Glucose-Adapted Hyperthermophilic Archaeon. *Waste and Biomass Valorization*. https://doi.org/10.1007/s12649-023-02049-z

Li, X., Zhang, R., Qian, Y., Angelidaki, I., & Zhang, Y. (2017). The impact of anode acclimation strategy on microbial electrolysis cell treating hydrogen fermentation effluent. *Bioresource Technology*, *236*, 37–43. https://doi.org/10.1016/j.biortech.2017.03.160

Lin, R., Cheng, J., & Murphy, J. D. (2017). Unexpectedly low biohydrogen yields in co-fermentation of acid pretreated cassava residue and swine manure. *Energy*

Conversion and Management, *151*(July), 553–561. https://doi.org/10.1016/j.enconman.2017.09.006

Liu, H., Grot, S., & Logan, B. E. (2005). Electrochemically assisted microbial production of hydrogen from acetate. *Environmental Science and Technology*, *39*(11), 4317–4320. https://doi.org/10.1021/es050244p

Liu, H., Hu, H., Chignell, J., & Fan, Y. (2010). Microbial electrolysis: Novel technology for hydrogen production from biomass. *Biofuels*, *1*(1), 129–142. https://doi.org/10.4155/bfs.09.9

Ljunggren, M., Willquist, K., Zacchi, G., & Van Niel, E. W. J. (2011). A kinetic model for quantitative evaluation of the effect of hydrogen and osmolarity on hydrogen production by Caldicellulosiruptor saccharolyticus. *Biotechnology for Biofuels*, *4*, 1–15. https://doi.org/10.1186/1754-6834-4-31

Logan, B. E., Call, D., Cheng, S., Hamelers, H. V. M., Sleutels, T. H. J. A., Jeremiasse, A. W., & Rozendal, R. A. (2008). Microbial electrolysis cells for high yield hydrogen gas production from organic matter. *Environmental Science and Technology*, *42*(23), 8630–8640. https://doi.org/10.1021/es801553z

Logan, B. E., Rossi, R., Ragab, A., & Saikaly, P. E. (2019). Electroactive microorganisms in bioelectrochemical systems. In *Nature Reviews Microbiology* (Vol. 17, Issue 5, pp. 307–319). Nature Publishing Group. https://doi.org/10.1038/s41579-019-0173-x

Lovley, D. R., & Holmes, D. E. (2022). Electromicrobiology: the ecophysiology of phylogenetically diverse electroactive microorganisms. In *Nature Reviews Microbiology* (Vol. 20, Issue 1, pp. 5–19). Nature Research. https://doi.org/10.1038/s41579-021-00597-6

Lu, L., Xing, D., & Ren, N. (2012). Pyrosequencing reveals highly diverse microbial communities in microbial electrolysis cells involved in enhanced H2 production

from waste activated sludge. *Water Research*, *46*(7), 2425–2434. https://doi.org/10.1016/j.watres.2012.02.005

Łukajtis, R., Hołowacz, I., Kucharska, K., Glinka, M., Rybarczyk, P., Przyjazny, A., & Kamiński, M. (2018). Hydrogen production from biomass using dark fermentation. In *Renewable and Sustainable Energy Reviews* (Vol. 91, pp. 665–694). Elsevier Ltd. https://doi.org/10.1016/j.rser.2018.04.043

Lusk, B. G., Badalamenti, J. P., Parameswaran, P., Bond, D. R., & Torres, C. I. (2015). Draft genome sequence of the Gram-positive thermophilic iron reducer Thermincola ferriacetica strain Z-0001T. *Genome Announcements*. https://doi.org/10.1128/genomeA.01072-15

Lusk, B. G., Khan, Q. F., Parameswaran, P., Hameed, A., Ali, N., Rittmann, B. E., & Torres, C. I. (2015). Characterization of Electrical Current-Generation Capabilities from Thermophilic Bacterium Thermoanaerobacter pseudethanolicus Using Xylose, Glucose, Cellobiose, or Acetate with Fixed Anode Potentials. *Environmental Science and Technology*, *49*(24), 14725–14731. https://doi.org/10.1021/acs.est.5b04036

Lusk, B. G., Parameswaran, P., Popat, S. C., Rittmann, B. E., & Torres, C. I. (2016). The effect of pH and buffer concentration on anode biofilms of Thermincola ferriacetica. *Bioelectrochemistry*, *112*, 47–52. https://doi.org/10.1016/j.bioelechem.2016.07.007

Lusk, B. G., Peraza, I., Albal, G., Marcus, A. K., Popat, S. C., & Torres, C. I. (2018). PH Dependency in Anode Biofilms of Thermincola ferriacetica Suggests a Proton-Dependent Electrochemical Response. *Journal of the American Chemical Society*, *140*(16), 5527–5534. https://doi.org/10.1021/jacs.8b01734

Mäkinen, A. E., Nissilä, M. E., & Puhakka, J. A. (2012). Dark fermentative hydrogen production from xylose by a hot spring enrichment culture. *International Journal of Hydrogen Energy*, *37*(17), 12234–12240. https://doi.org/10.1016/j.ijhydene.2012.05.158

Malki, M., De Lacey, A. L., Rodríguez, N., Amils, R., & Fernandez, V. M. (2008). Preferential use of an anode as an electron acceptor by an acidophilic bacterium in the presence of oxygen. *Applied and Environmental Microbiology*, *74*(14), 4472–4476. https://doi.org/10.1128/AEM.00209-08

Mankar, A. R., Pandey, A., Modak, A., & Pant, K. K. (2021). Pretreatment of lignocellulosic biomass: A review on recent advances. *Bioresource Technology*, *334*(April), 125235. https://doi.org/10.1016/j.biortech.2021.125235

Manzella, M. P., Holmes, D. E., Rocheleau, J. M., Chung, A., Reguera, G., & Kashefi, K. (2015). The complete genome sequence and emendation of the hyperthermophilic, obligate iron-reducing archaeon "Geoglobus ahangari" strain 234T. *Standards in Genomic Sciences*, *10*(1). https://doi.org/10.1186/s40793-015-0035-8

Mardanov, A. V., Slododkina, G. B., Slobodkin, A. I., Beletsky, A. V., Gavrilov, S. N., Kublanov, I. V., Bonch-Osmolovskaya, E. A., Skryabin, K. G., & Ravin, N. V. (2015). The Geoglobus acetivorans genome: Fe(III) reduction, acetate utilization, autotrophic growth, and degradation of aromatic compounds in a hyperthermophilic archaeon. *Applied and Environmental Microbiology*. https://doi.org/10.1128/AEM.02705-14

Mars, A. E., Veuskens, T., Budde, M. A. W., Van Doeveren, P. F. N. M., Lips, S. J., Bakker, R. R., De Vrije, T., & Claassen, P. A. M. (2010). Biohydrogen production from untreated and hydrolyzed potato steam peels by the extreme thermophiles Caldicellulosiruptor saccharolyticus and Thermotoga neapolitana. *International Journal of Hydrogen Energy*, *35*(15), 7730–7737. https://doi.org/10.1016/j.ijhydene.2010.05.063

Marshall, C. W., & May, H. D. (2009). Electrochemical evidence of direct electrode reduction by a thermophilic Gram-positive bacterium, Thermincola ferriacetica.

Energy and Environmental Science, *2*(6), 699–705. https://doi.org/10.1039/b823237g

Mathis, B. J., Marshall, C. W., Milliken, C. E., Makkar, R. S., Creager, S. E., & May, H. D. (2008). Electricity generation by thermophilic microorganisms from marine sediment. *Applied Microbiology and Biotechnology*, *78*(1), 147–155. https://doi.org/10.1007/s00253-007-1266-4

Matsunaga, T., & Nakajima, T. (1985). Electrochemical classification of gram-negative and gram-positive bacteria. *Applied and Environmental Microbiology*, *50*(2), 238–242. https://doi.org/10.1128/aem.50.2.238-242.1985

Miroshnichenko, M. L., Kublanov, I. V., Kostrikina, N. A., Tourova, T. P., Kolganova, T. V., Birkeland, N. K., & Bonch-Osmolovskaya, E. A. (2008). Caldicellulosiruptor kronotskyensis sp. nov. and Caldicellulosiruptor hydrothermalis sp. nov., two extremely thermophilic, cellulolytic, anaerobic bacteria from Kamchatka thermal springs. *International Journal of Systematic and Evolutionary Microbiology*, *58*(6), 1492–1496. https://doi.org/10.1099/ijs.0.65236-0

Mladenovska -Indra, Z., Mathrani, M., & Ahring, B. K. (1995). Isolation and characterization of Caldicellulosiruptor lactoaceticus sp. nov., an extremely thermophilic, cellulolytic, anaerobic bacterium. In *Arch Microbiol* (Vol. 163). Springer-Verlag.

Modestra, J. A., & Mohan, S. V. (2014). Bio-electrocatalyzed electron efflux in Gram positive and Gram negative bacteria: An insight into disparity in electron transfer kinetics. *RSC Advances*. https://doi.org/10.1039/c4ra03489a

Muddasar, M., Liaquat, R., Aslam, A., Ur Rahman, M. Z., Abdullah, A., Khoja, A. H., Latif, K., & Bahadar, A. (2022). Performance efficiency comparison of microbial electrolysis cells for sustainable production of biohydrogen—A comprehensive review. In *International Journal of Energy Research* (Vol. 46,

Issue 5, pp. 5625–5645). John Wiley and Sons Ltd. https://doi.org/10.1002/er.7606

Munro, S. A., Zinder, S. H., & Walker, L. P. (2009). The Fermentation Stoichiometry of Thermotoga neapolitana and Influence of Temperature, Oxygen, and pH on Hydrogen Production. *Biotechnol. Prog*, *25*, 1035–1042. https://doi.org/10.1021/bp.201

Murugaiyan, J., Narayanan, A., & Naina Mohamed, S. (2022). An overview of microbial electrolysis cell configuration: Challenges and prospects on biohydrogen production. In *International Journal of Energy Research* (Vol. 46, Issue 14, pp. 20811–20827). John Wiley and Sons Ltd. https://doi.org/10.1002/er.8494

Myers, C. R., & Myers, J. M. (1992). Localization of cytochromes to the outer membrane of anaerobically grown Shewanella putrefaciens MR-1. *Journal of Bacteriology*, *174*(11), 3429–3438. https://doi.org/10.1128/jb.174.11.3429-3438.1992

Ndayisenga, F., Yu, Z., Zheng, J., Wang, B., Liang, H., Phulpoto, I. A., Habiyakare, T., & Zhou, D. (2021). Microbial electrohydrogenesis cell and dark fermentation integrated system enhances biohydrogen production from lignocellulosic agricultural wastes: Substrate pretreatment towards optimization. In *Renewable and Sustainable Energy Reviews* (Vol. 145). Elsevier Ltd. https://doi.org/10.1016/j.rser.2021.111078

Nielsen, S. S. (2013). *Food Analysis Laboratory Manual*.

Nikkanen, L., Solymosi, D., Jokel, M., & Allahverdiyeva, Y. (2021). Regulatory electron transport pathways of photosynthesis in cyanobacteria and microalgae: Recent advances and biotechnological prospects. *Physiologia Plantarum*, *173*(2), 514–525. https://doi.org/10.1111/ppl.13404

Onyenwoke, R. U., Lee, Y. J., Dabrowski, S., Ahring, B. K., & Wiegel, J. (2006). Reclassification of Thermoanaerobium acetigenum as Caldicellulosiruptor

acetigenus comb. nov. and emendation of the genus description. *International Journal of Systematic and Evolutionary Microbiology*, *56*(6), 1391–1395. https://doi.org/10.1099/ijs.0.63723-0

Osman, A. I., Deka, T. J., Baruah, D. C., & Rooney, D. W. (2020). Critical challenges in biohydrogen production processes from the organic feedstocks. *Biomass Conversion and Biorefinery*, 1–19. https://doi.org/10.1007/S13399-020-00965-X/TABLES/6

Osman, A. I., Mehta, N., Elgarahy, A. M., Hefny, M., Al-Hinai, A., Ala', ·, Al-Muhtaseb, H., David, ·, & Rooney, W. (2022). Hydrogen production, storage, utilisation and environmental impacts: a review. *Environmental Chemistry Letters*, *20*, 153–188. https://doi.org/10.1007/s10311-021-01322-8

Parameswaran, P., Bry, T., Popat, S. C., Lusk, B. G., Rittmann, B. E., & Torres, C. I. (2013). Kinetic, electrochemical, and microscopic characterization of the thermophilic, anode-respiring bacterium Thermincola ferriacetica. *Environmental Science and Technology*, *47*(9), 4934–4940. https://doi.org/10.1021/es400321c

Park, S. G., Rajesh, P. P., Sim, Y. U., Jadhav, D. A., Noori, M. T., Kim, D. H., Al-Qaradawi, S. Y., Yang, E., Jang, J. K., & Chae, K. J. (2022). Addressing scale-up challenges and enhancement in performance of hydrogen-producing microbial electrolysis cell through electrode modifications. In *Energy Reports* (Vol. 8, pp. 2726–2746). Elsevier Ltd. https://doi.org/10.1016/j.egyr.2022.01.198

Parkhey, P., & Gupta, P. (2017). Improvisations in structural features of microbial electrolytic cell and process parameters of electrohydrogenesis for efficient biohydrogen production: a review. In *Renewable and Sustainable Energy Reviews* (Vol. 69, pp. 1085–1099). Elsevier Ltd. https://doi.org/10.1016/j.rser.2016.09.101

Pawar, S. S. (2014). *Caldicellulosiruptor saccharolyticus : an ideal hydrogen producer ?* [Doctoral Thesis, Lund University]. https://lucris.lub.lu.se/ws/portalfiles/portal/6011531/4690523.pdf

Pawar, S. S., & Van Niel, E. W. J. (2013). Thermophilic biohydrogen production: How far are we? In *Applied Microbiology and Biotechnology* (Vol. 97, Issue 18, pp. 7999–8009). https://doi.org/10.1007/s00253-013-5141-1

Pillot, G., Davidson, S., Auria, R., Combet-Blanc, Y., Godfroy, A., & Liebgott, P. P. (2020). Production of Current by Syntrophy Between Exoelectrogenic and Fermentative Hyperthermophilic Microorganisms in Heterotrophic Biofilm from a Deep-Sea Hydrothermal Chimney. *Microbial Ecology*, *79*(1), 38–49. https://doi.org/10.1007/s00248-019-01381-z

Pillot, G., Frouin, E., Pasero, E., Godfroy, A., Combet-Blanc, Y., Davidson, S., & Liebgott, P. P. (2018a). Specific enrichment of hyperthermophilic electroactive Archaea from deep-sea hydrothermal vent on electrically conductive support. *Bioresource Technology*, *259*, 304–311. https://doi.org/10.1016/j.biortech.2018.03.053

Rabaey, K., Rodríguez, J., Blackall, L. L., Keller, J., Gross, P., Batstone, D., Verstraete, W., & Nealson, K. H. (2007). Microbial ecology meets electrochemistry: Electricity-driven and driving communities. In *ISME Journal* (Vol. 1, Issue 1, pp. 9–18). https://doi.org/10.1038/ismej.2007.4

Rabaey, K., & Verstraete, W. (2005). Microbial fuel cells: Novel biotechnology for energy generation. In *Trends in Biotechnology* (Vol. 23, Issue 6, pp. 291–298). https://doi.org/10.1016/j.tibtech.2005.04.008

Rainey, F. A., Donnison, A. M., Janssen, P. H., Saul, D., Rodrigo, A., Bergquist, P. L., Daniel, R. M., Stackebrandt, E., & Morgan, H. W. (1994). Description of Caldicellulosiruptor saccharolyticus gen. nov., sp. nov: An obligately anaerobic, extremely thermophilic, cellulolytic bacterium. *FEMS Microbiology Letters*, *120*(3), 263–266. https://doi.org/10.1111/j.1574-6968.1994.tb07043.x

142

Rathinam, N. K., Bibra, M., Salem, D. R., & Sani, R. K. (2019). Thermophiles for biohydrogen production in microbial electrolytic cells. In *Bioresource Technology* (Vol. 277, pp. 171–178). Elsevier Ltd. https://doi.org/10.1016/j.biortech.2019.01.020

Reguera, G., McCarthy, K. D., Mehta, T., Nicoll, J. S., Tuominen, M. T., & Lovley, D. R. (2005). Extracellular electron transfer via microbial nanowires. *Nature*, *435*(7045), 1098–1101. https://doi.org/10.1038/nature03661

Renslow, R. S., Babauta, J. T., Dohnalkova, A. C., Boyanov, M. I., Kemner, K. M., Majors, P. D., Fredrickson, J. K., & Beyenal, H. (2013). Metabolic spatial variability in electrode-respiring Geobacter sulfurreducens biofilms. *Energy and Environmental Science*, *6*(6), 1827–1836. https://doi.org/10.1039/c3ee40203g

Rodríguez, A., Hernández-Herreros, N., García, J. L., & Auxiliadora Prieto, M. (2021). Enhancement of biohydrogen production rate in Rhodospirillum rubrum by a dynamic CO-feeding strategy using dark fermentation. *Biotechnology for Biofuels*, *14*(1). https://doi.org/10.1186/s13068-021-02017-6

Rozendal, R. A., Hamelers, H. V. M., Euverink, G. J. W., Metz, S. J., & Buisman, C. J. N. (2006). Principle and perspectives of hydrogen production through biocatalyzed electrolysis. *International Journal of Hydrogen Energy*, *31*(12), 1632–1640. https://doi.org/10.1016/j.ijhydene.2005.12.006

Rozendal, R. A., Hamelers, H. V. M., Molenkamp, R. J., & Buisman, C. J. N. (2007). Performance of single chamber biocatalyzed electrolysis with different types of ion exchange membranes. *Water Research*, *41*(9), 1984–1994. https://doi.org/10.1016/j.watres.2007.01.019

Saha, R., Bhattacharya, D., & Mukhopadhyay, M. (2022). Enhanced production of biohydrogen from lignocellulosic feedstocks using microorganisms: A

comprehensive review. *Energy Conversion and Management: X, 13.* https://doi.org/10.1016/j.ecmx.2021.100153

Sandberg, T. E., Salazar, M. J., Weng, L. L., Palsson, B. O., & Feist, A. M. (2019). The emergence of adaptive laboratory evolution as an efficient tool for biological discovery and industrial biotechnology. In *Metabolic Engineering* (Vol. 56, pp. 1–16). Academic Press Inc. https://doi.org/10.1016/j.ymben.2019.08.004

Sapireddy, V., Katuri, K. P., Muhammad, A., & Saikaly, P. E. (2021). Competition of two highly specialized and efficient acetoclastic electroactive bacteria for acetate in biofilm anode of microbial electrolysis cell. *Npj Biofilms and Microbiomes*, *7*(1). https://doi.org/10.1038/s41522-021-00218-3

Saravanan, A., Karishma, S., Kumar, P. S., Yaashikaa, P. R., Jeevanantham, S., & Gayathri, B. (2020). Microbial electrolysis cells and microbial fuel cells for biohydrogen production: current advances and emerging challenges. In *Biomass Conversion and Biorefinery*. Springer. https://doi.org/10.1007/s13399-020-00973-x

Sayed, E. T., Saito, Y., Tsujiguchi, T., & Nakagawa, N. (2012). Catalytic activity of yeast extract in biofuel cell. *Journal of Bioscience and Bioengineering*. https://doi.org/10.1016/j.jbiosc.2012.05.021

Schröder, C., Selig, M., & Schönheit, P. (1994). Glucose fermentation to acetate, CO2 and H 2 in the anaerobic hyperthermophilic eubacterium Thermotoga maritima: involvement of the Embden-Meyerhof pathway. In *Arch Microbiol* (Vol. 161).

Schrott, G. D., Ordoñez, M. V., Robuschi, L., & Busalmen, J. P. (2014). Physiological stratification in electricity-producing biofilms of geobacter sulfurreducens. *ChemSusChem*, *7*(2), 598–603. https://doi.org/10.1002/cssc.201300605

Schwarz, W. H. (2001). The cellulosome and cellulose degradation by anaerobic bacteria. *Applied Microbiology and Biotechnology*, *56*(5–6), 634–649. https://doi.org/10.1007/s002530100710

Sekar, N., Wu, C. H., Adams, M. W. W., & Ramasamy, R. P. (2017). Electricity generation by Pyrococcus furiosus in microbial fuel cells operated at 90°C. *Biotechnology and Bioengineering*, *114*(7), 1419–1427. https://doi.org/10.1002/bit.26271

Sekar, N., Wu, C.-H., Adams, M. W. W., & Ramasamy, R. P. (2016). Exploring Extracellular Electron Transfer in Hyperthermophiles for Electrochemical Energy Conversion. *ECS Transactions*, *72*(30), 1–7. https://doi.org/10.1149/07230.0001ecst

Sekoai, P. T., Yoro, K. O., Bodunrin, M. O., Ayeni, A. O., & Daramola, M. O. (2018). Integrated system approach to dark fermentative biohydrogen production for enhanced yield, energy efficiency and substrate recovery. In *Reviews in Environmental Science and Biotechnology* (Vol. 17, Issue 3, pp. 501–529). Springer Netherlands. https://doi.org/10.1007/s11157-018-9474-1

Selembo, P. A., Merrill, M. D., & Logan, B. E. (2009). The use of stainless steel and nickel alloys as low-cost cathodes in microbial electrolysis cells. *Journal of Power Sources*, *190*(2), 271–278. https://doi.org/10.1016/j.jpowsour.2008.12.144

Shi, X. C., Tremblay, P. L., Wan, L., & Zhang, T. (2021). Improved robustness of microbial electrosynthesis by adaptation of a strict anaerobic microbial catalyst to molecular oxygen. *Science of the Total Environment*, *754*. https://doi.org/10.1016/j.scitotenv.2020.142440

Slobodkina, G. B., Kolganova, T. V., Querellou, J., Bonch-Osmolovskaya, E. A., & Slobodkin, A. I. (2009a). Geoglobus acetivorans sp. nov., an iron(III)-reducing archaeon from a deep-sea hydrothermal vent. *International Journal of*

Systematic and Evolutionary Microbiology. https://doi.org/10.1099/ijs.0.011080-0

Smith, J. A., Aklujkar, M., Risso, C., Leang, C., Giloteaux, L., & Holmes, D. E. (2015). Mechanisms involved in Fe(III) respiration by the hyperthermophilic archaeon Ferroglobus placidus. *Applied and Environmental Microbiology*, *81*(8), 2735–2744. https://doi.org/10.1128/AEM.04038-14

Soares, J. F., Confortin, T. C., Todero, I., Mayer, F. D., & Mazutti, M. A. (2020). Dark fermentative biohydrogen production from lignocellulosic biomass: Technological challenges and future prospects. *Renewable and Sustainable Energy Reviews*, *117*(January 2019). https://doi.org/10.1016/j.rser.2019.109484

Sreelekshmy, B. R., Rajappan, A. J., Basheer, R., Vasudevan, V., Ratheesh, A., Meera, M. S., Geethanjali, C. V., & Shibli, S. M. A. (2020). Tuning of Surface Characteristics of Anodes for Efficient and Sustained Power Generation in Microbial Fuel Cells. *ACS Applied Bio Materials*, *3*(9), 6224–6236. https://doi.org/10.1021/acsabm.0c00753

Straub, C. T., Khatibi, P. A., Otten, J. K., Adams, M. W. W., & Kelly, R. M. (2019). Lignocellulose solubilization and conversion by extremely thermophilic Caldicellulosiruptor bescii improves by maintaining metabolic activity. *Biotechnology and Bioengineering*, *116*(8), 1901–1908. https://doi.org/10.1002/bit.26993

Sun, D., Cheng, S., Zhang, F., & Logan, B. E. (2017). Current density reversibly alters metabolic spatial structure of exoelectrogenic anode biofilms. *Journal of Power Sources*, *356*, 566–571. https://doi.org/10.1016/j.jpowsour.2016.11.115

Talluri, S., Mohan, S., & Paul, L. (2013). Consolidated bioprocessing of untreated switchgrass to hydrogen by the extreme thermophile Caldicellulosiruptor saccharolyticus DSM 8903. *Bioresource Technology*, *139*, 272–279. https://doi.org/10.1016/j.biortech.2013.04.005

Tanisho, S., Suzuki, Y., & Wakao, N. (1987). FERMENTATIVE HYDROGEN EVOLUTION BY ENTER OBACTER A EROGENES STRAIN E. 82005. In *Int. J. Hydrogen Energy* (Vol. 12, Issue 9).

Taya, M., Hinoki, H., Yagi, T., & Kobayashi, T. (1988). Isolation and characterization of an extremely thermophilic, cellulolytic, anaerobic bacterium. In *Appl Microbiol Biotechnol* (Vol. 29).

Thapa, B. Sen, Kim, T., Pandit, S., Song, Y. E., Afsharian, Y. P., Rahimnejad, M., Kim, J. R., & Oh, S. E. (2022). Overview of electroactive microorganisms and electron transfer mechanisms in microbial electrochemistry. In *Bioresource Technology* (Vol. 347). Elsevier Ltd. https://doi.org/10.1016/j.biortech.2021.126579

Thauer, R. K., Jungermann, K., & Decker, K. (1977). Energy conservation in chemotrophic anaerobic bacteria. *Bacteriological Reviews*, *41*(1), 100–180. https://doi.org/10.1128/mmbr.41.1.100-180.1977

Urbaniec, K., & Bakker, R. R. (2015). Biomass residues as raw material for dark hydrogen fermentation e A review. *International Journal of Hydrogen Energy*, *40*(9), 3648–3658. https://doi.org/10.1016/j.ijhydene.2015.01.073

Van Niel, E. W. J., Budde, M. A. W., De Haas, G. G., Van Der Wal, F. J., Claassen, P. A. M., & Stams, A. J. M. (2002). Distinctive properties of high hydrogen producing extreme thermophiles, Caldicellulosiruptor saccharolyticus and Thermotoga elÿi. In *International Journal of Hydrogen Energy* (Vol. 27). www.elsevier.com/locate/ijhydene

Wang, H., & Ren, Z. J. (2013). A comprehensive review of microbial electrochemical systems as a platform technology. *Biotechnology Advances*, *31*(8), 1796–1807. https://doi.org/10.1016/j.biotechadv.2013.10.001

Wang, Y., Byrd, C. S., & Barlaz, M. A. (1994). Anaerobic biodegradability of cellulose and hemicellulose in excavated refuse samples using a biochemical methane potential assay. *Journal of Industrial Microbiology*, *13*, 147–153.

Wrighton, K. C., Agbo, P., Warnecke, F., Weber, K. A., Brodie, E. L., DeSantis, T. Z., Hugenholtz, P., Andersen, G. L., & Coates, J. D. (2008). A novel ecological role of the Firmicutes identified in thermophilic microbial fuel cells. *ISME Journal*, *2*(11), 1146–1156. https://doi.org/10.1038/ismej.2008.48

Xing, Y., Li, Z., Fan, Y., & Hou, H. (2010). Biohydrogen production from dairy manures with acidification pretreatment by anaerobic fermentation. *Environmental Science and Pollution Research*, *17*(2), 392–399. https://doi.org/10.1007/s11356-009-0187-4

Yang, S. J., Kataeva, I., Wiegel, J., Yin, Y., Dam, P., Xu, Y., Westpheling, J., & Adams, M. W. W. (2010). Classification of "Anaerocellum thermophilum" strain DSM 6725 as Caldicellulosiruptor bescii sp. nov. *International Journal of Systematic and Evolutionary Microbiology*, *60*(9), 2011–2015. https://doi.org/10.1099/ijs.0.017731-0

Yilmazel, Y. D., & Duran, M. (2021). Biohydrogen production from cattle manure and its mixtures with renewable feedstock by hyperthermophilic Caldicellulosiruptor bescii. *Journal of Cleaner Production*, *292*, 125969. https://doi.org/10.1016/j.jclepro.2021.125969

Yilmazel, Y. D., Johnston, D., & Duran, M. (2015). Hyperthermophilic hydrogen production from wastewater biosolids by Caldicellulosiruptor bescii. *International Journal of Hydrogen Energy*, *40*(36), 12177–12186. https://doi.org/10.1016/j.ijhydene.2015.06.140

Yilmazel, Y. D., Zhu, X., Kim, K. Y., Holmes, D. E., & Logan, B. E. (2018). Electrical current generation in microbial electrolysis cells by hyperthermophilic archaea Ferroglobus placidus and Geoglobus ahangari. *Bioelectrochemistry*, *119*, 142–149. https://doi.org/10.1016/j.bioelechem.2017.09.012

Ying, Y., Meng, D., Chen, X., & Li, F. (2013). An extremely thermophilic anaerobic bacterium Caldicellulosiruptor sp. F32 exhibits distinctive properties in growth

and xylanases during xylan hydrolysis. *Enzyme and Microbial Technology*, *53*(3), 194–199. https://doi.org/10.1016/j.enzmictec.2013.04.004

Yoshida, A., Nishimura, T., Kawaguchi, H., Inui, M., & Yukawa, H. (2005). Enhanced hydrogen production from formic acid by formate hydrogen lyase-overexpressing Escherichia coli strains. *Applied and Environmental Microbiology*, *71*(11), 6762–6768. https://doi.org/10.1128/AEM.71.11.6762-6768.2005

Yu, L., Yuan, Y., Tang, J., & Zhou, S. (2017). Thermophilic Moorella thermoautotrophica-immobilized cathode enhanced microbial electrosynthesis of acetate and formate from CO2. *Bioelectrochemistry*, *117*, 23–28. https://doi.org/10.1016/j.bioelechem.2017.05.001

Zeidan, A. A., & Van Niel, E. W. J. (2009). Developing a thermophilic hydrogen-producing co-culture for efficient utilization of mixed sugars. *International Journal of Hydrogen Energy*, *34*(10), 4524–4528. https://doi.org/10.1016/j.ijhydene.2008.07.092

Zeidan, A. A., & van Niel, E. W. J. (2010). A quantitative analysis of hydrogen production efficiency of the extreme thermophile Caldicellulosiruptor owensensis OLT. *International Journal of Hydrogen Energy*, *35*(3), 1128–1137. https://doi.org/10.1016/j.ijhydene.2009.11.082

Zikmund, E., Kim, K. Y., & Logan, B. E. (2018). Hydrogen production rates with closely-spaced felt anodes and cathodes compared to brush anodes in two-chamber microbial electrolysis cells. *International Journal of Hydrogen Energy*, *43*(20), 9599–9606. https://doi.org/10.1016/j.ijhydene.2018.04.059

Zurawski, J. V., Conway, J. M., Lee, L. L., Simpson, H. J., Izquierdo, J. A., Blumer-Schuette, S., Nookaew, I., Adams, M. W. W., & Kelly, R. M. (2015). Comparative analysis of extremely thermophilic Caldicellulosiruptor species reveals common and unique cellular strategies for plant biomass utilization.

Applied and Environmental Microbiology, *81*(20), 7159–7170. https://doi.org/10.1128/AEM.01622-15

APPENDICES

A. Supplementary information for hydrogen partial pressure calculation

The total biogas production was measured by liquid displacement and the composition was analyzed by gas chromatograph. Since the reactors were operated at elevated temperatures, water vapor pressure should be considered in calculation. Based on Neubert et al. (2021), absolute humidity (AH) to calculate water vapor pressure is calculated as following:

$$AH = \frac{m_{H2O}}{V_{biogas}} = \frac{P_{H2O,sat}}{T_{biogas} \cdot R_{H2O}}$$

where R_{H2O} = 461.52 J/kg.K being the individual gas constant of water.

To calculate water vapor pressure in the range of 0 °C < t < 100 °C:

$$P_s = \frac{\exp\left(34.494 - \frac{4924.99}{t+237.1}\right)}{(t+105)^{1.57}} \quad \text{(unit of Pa)}$$

The water vapor pressures are calculated 38595.5 Pa at 75 °C. Then, m_{H2O} is calculated using the volume of water vapor in the headspace:

$$AH = \frac{m_{H2O}}{V_{biogas}} = \frac{P_{H2O,sat}}{T_{biogas} \cdot R_{H2O}}$$

For Day 27 of Control – 25 g VS/L:

$$\frac{m_{H2O}}{87.4 \times 10^{-3} L} = \frac{38595.5 \text{ Pa}}{348.15 \text{ °C} \cdot 461.52 \frac{J}{kg.K}}$$

m_{H2O} = 0.021 mg

To calculate the volume of water vapor in the headspace, we use the ideal gas law:

$$p.v = n.R.T$$

$$v = \frac{n.R.T}{p}$$

n is equal to $\frac{m}{M}$, where m is the mass of water vapor (m_{H2O}) and M is the molecular weight of water (18.02 g/mol). Therefore,

$$v = \frac{m.R.T}{p.M} = \frac{(0.021 \text{ mg})\left(8.314\frac{J}{mol.K}\right)(348.15 \text{ °C})\text{x}1000\frac{m3}{L}}{(99000 \text{ Pa})(18.02\frac{g}{mol})} = 0.034 \text{ mL}$$

Then, to find the v_{biogas}^{dry}:

$$v_{biogas}^{total} = v_{biogas}^{dry} + v_{H2O}$$

$$v_{biogas}^{dry} = 87.4 \text{ mL-0.034 mL} = 87.37 \text{ mL}$$

After that, the real composition of measured H_2 was calculated based on the v_{biogas}^{dry}.

$$\frac{v_{H2}}{v_{total\ biogas}} = 0.35$$

$$\frac{P_{H2}}{P_{total\ biogas}} = \frac{P_{H2}}{101.325 \text{ kPa}} = 0.35$$

$P_{H2} = 35.5$ kPa